AD-A084 787 ILLINOIS UNIV AT URBANA-CHAMPAIGN DEPT OF [illegible] F/G 20/4
A THEORETICAL AND EXPERIMENTAL INVESTIGATION OF TRANSONIC FLOW --ETC(U)
JAN 80 J C DUTTON, A L ADDY DAAG29-79-C-0184
UNCLASSIFIED UILU-ENG-80-4001 ARO-13737.1-EX NL

1 OF 2
AD A084787

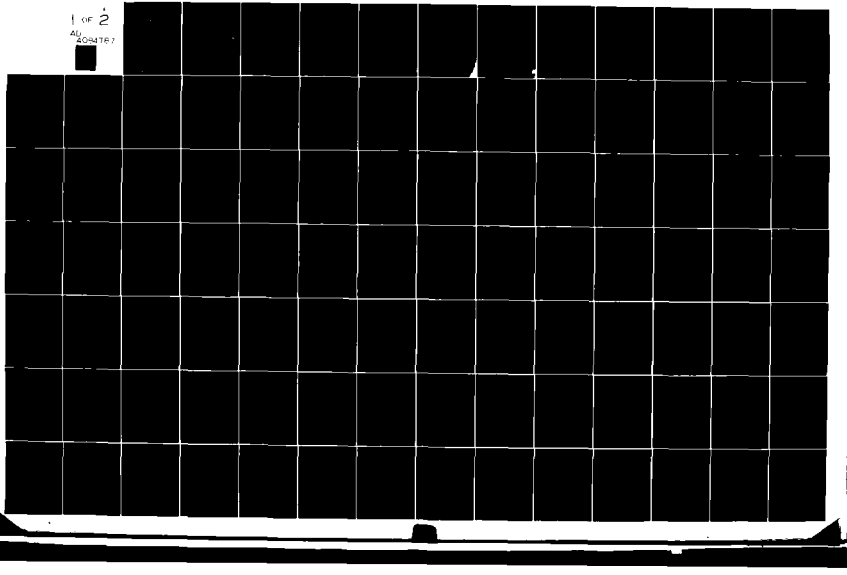

ARO 13737.1-EX and
16719.1-E

MECHANICAL ENGINEERING LABORATORY
UILU-ENG-80-4001
DEPARTMENT OF MECHANICAL
AND INDUSTRIAL ENGINEERING
UNIVERSITY OF ILLINOIS AT URBANA-CHAMPAIGN
URBANA, ILLINOIS 61801

LEVEL II

12

SC

A THEORETICAL AND EXPERIMENTAL INVESTIGATION OF TRANSONIC FLOW IN THE THROAT REGION OF ANNULAR AXISYMMETRIC, SUPERSONIC NOZZLES

by
J. C. DUTTON
A. L. ADDY

JANUARY 1980

Supported by
U.S. Army Research Office
Research Grant DAAG 29-76-G-0200
and
Research Contract DAAG 29-79-C-0184
and the
Department of Mechanical and Industrial Engineering

Unclassified

SECURITY CLASSIFICATION OF THIS PAGE (When Data Entered)

REPORT DOCUMENTATION PAGE

READ INSTRUCTIONS BEFORE COMPLETING FORM

1. REPORT NUMBER: UILU-ENG-80-4001 (14)
2. GOVT ACCESSION NO.: AD A084 787
3. RECIPIENT'S CATALOG NUMBER: ----

4. TITLE (and Subtitle): A THEORETICAL AND EXPERIMENTAL INVESTIGATION OF TRANSONIC FLOW IN THE THROAT REGION OF ANNULAR AXISYMMETRIC, SUPERSONIC NOZZLES. (1)
5. TYPE OF REPORT & PERIOD COVERED: Technical Report (9)
6. PERFORMING ORG. REPORT NUMBER: UILU-ENG-80-4001

7. AUTHOR(s): J. C. Dutton, A. L. Addy (10)
8. CONTRACT OR GRANT NUMBER(s): ~~DAAG 29-76-G-0200~~ DAAG 29-79-C-0184 (15)

9. PERFORMING ORGANIZATION NAME AND ADDRESS: Dept. of Mechanical and Industrial Engineering, University of Illinois at Urbana-Champaign, Urbana, Illinois 61801
10. PROGRAM ELEMENT, PROJECT, TASK AREA & WORK UNIT NUMBERS: DAAG-29-76-G-0200 AF

11. CONTROLLING OFFICE NAME AND ADDRESS: U.S. Army Research Office, Post Office Box 12211, Research Triangle Park, NC 27709
12. REPORT DATE: Jan[illegible]80 (11)
NUMBER OF PAGES: 183

14. MONITORING AGENCY NAME & ADDRESS (if different from Controlling Office): (12) 181
15. SECURITY CLASS. (of this report): Unclassified
15a. DECLASSIFICATION/DOWNGRADING SCHEDULE: NA

16. DISTRIBUTION STATEMENT (of this Report): Approved for public release; distribution unlimited.

(12) ARO AF

DTIC ELECTE MAY 2 8 1980

17. DISTRIBUTION STATEMENT (of the abstract entered in Block 20, if different from Report)

(19) 15737.1-EX, 16719.1-E

18. SUPPLEMENTARY NOTES: The findings of this report are not to be construed as an official Department of the Army position, unless so designated by other authorized documents.

19. KEY WORDS (Continue on reverse side if necessary and identify by block number):
Transonic Flow
Annular Nozzle
Supersonic Nozzle

20. ABSTRACT (Continue on reverse side if necessary and identify by block number):
An integrated theoretical and experimental investigation of flow in the throat region of unconventional, annular, supersonic nozzles was conducted. The theoretical analysis consists of the formulation and development of an approximate series expansion solution to the inviscid, irrotational governing equations. The resulting solution provides a direct means of analyzing the throat flowfields in a variety of two-dimensional nozzle configurations including axisymmetric, annular, and planar nozzles. A major advantage of the →

DD FORM 1 JAN 73 1473 EDITION OF 1 NOV 65 IS OBSOLETE

Unclassified

SECURITY CLASSIFICATION OF THIS PAGE (When Data Entered)

400833 Jm

solution is the speed and reliability of its numerical implementation, making feasible parametric studies and iterative calculations.

Flowfield static pressure measurements were obtained for four nozzle configurations including an axisymmetric, Laval nozzle and three annular ones. Half-section cylindrical models were constructed and mounted on a splitter plate whose surface corresponds to a plane of symmetry for the axisymmetric geometries under consideration. Readings from a grid of pressure taps arranged on the splitter plate allowed the determination of the static pressure fields in the nozzle throats. For all four cases tested, it was found that the agreement between the theoretical and experimental results is quite good through a significant region of the throat. Only near the bounding walls in the throat inlet region was there a noticeable discrepancy for some of the cases.

A THEORETICAL AND EXPERIMENTAL INVESTIGATION OF TRANSONIC FLOW IN THE THROAT REGION OF ANNULAR AXISYMMETRIC, SUPERSONIC NOZZLES*

by

J. C. Dutton†

A. L. Addy††

January 1980

Supported by

U.S. Army Research Office
Research Grant DAAG 29-76-G-0200

and

Research Contract DAAG 29-79-C-0184

and the

Department of Mechanical and Industrial Engineering
University of Illinois at Urbana-Champaign
Urbana, Illinois 61801

---

* This report is based on the Ph.D. thesis of J. C. Dutton

† Formerly Graduate Research Assistant; currently employed by Lawrence Livermore Laboratory, Livermore, California 94550

†† Professor of Mechanical Engineering

TABLE OF CONTENTS

LIST OF TABLES

LIST OF FIGURES

NOMENCLATURE

Symbols	Meaning
a	speed of sound
a^*	critical speed of sound
a_i, a_o	x-coordinates of centers of curvature of inner and outer wall contours, Appendix A
A	area
A_0', A_1', A_1	functions of y in first order series expansion solution, Eqs. (III-64), (III-60), and (III-63)
b_i, b_o	y-coordinates of centers of curvature of inner and outer wall contours, Appendix A
$B_0, B_1, B_2, B_3, B_4, B_5$	constants in first order series expansion solution, Eqs. (III-66), (III-62), (III-61), (III-65), (III-67), (III-68)
C_D	discharge or flow coefficient defined in Eq. (III-79)
C_{D1}, C_{D2}, C_{D3}	discharge coefficient constants defined in Eq. (III-80)
$C_0', C_1', C_1, C_2', C_2$	functions of y in second order series expansion solution, Eqs. (III-69) and (III-70)
d	throat half-height, defined as throat radius for conventional axisymmetric nozzles and distance between inner and outer throat wall locations for annular nozzles
d_h	static hole diameter, Fig. IV.16
D_0, D_1, D_2	constants in second order series expansion solution, Eq. (III-70)
$E_0', E_1', E_1, E_2', E_2, E_3, E_3'$	functions of y in third order series expansion solution, Eqs. (III-71) and (III-72)
f_2, f_3	right hand sides of Eq. (III-40) defined in Eqs. (III-41) and (III-42)
F	wall shear force, Eq. (IV-5)
F_0, F_1, F_2, F_3	constants in third order series expansion solution Eq. (III-72)

Symbols	Meaning
g,h	equations of inner and outer nozzle wall contours in the local x-y coordinate system, Fig. III.1
$g_1, h_1, g_2, h_2, g_3, h_3$	dimensionless quantities defined in Eq. (III-35)
G,H	equations of inner and outer nozzle wall contours in the cylindrical R-Z coordinate system, Fig. III.1
j'	average, symmetric throat slope defined in Eq. (A-10)
ℓ	static hole depth, Fig. IV.16
M	Mach number
M^*	dimensionless velocity ratio defined in Eq. (III-75)
N	number of terms to be included from series expansion solution
O	used to denote physical order of magnitude
p	static pressure
p_0	stagnation pressure
R	radial coordinate in cylindrical system
R_c	wall radius of curvature non-dimensionalized with respect to throat half-height
Re^+	Reynolds number based on static hole diameter and friction velocity, Eq. (IV-8)
Re_{2d}	Reynolds number based on sonic conditions and throat height, $Re_{2d} \equiv \rho^* V^* 2d/\mu^*$, where V^* is the magnitude of the velocity vector at $M = 1$
u,v	dimensionless velocity components in x-y coordinate system defined in Eqs. (III-5) and (III-6), Fig. III.1
$\tilde{u},\tilde{v}$	transonic perturbation velocity components defined in Eqs. (III-10) and (III-11)
$(u_1,v_1), (u_2,v_2), (u_3,v_3)$	transonic perturbation velocity components defined by expansions in Eqs. (III-36) and (III-37)

Symbols	Meaning
U,V	velocity components in cylindrical R-Z coordinate system, Fig. III.1
U(F)	uncertainty of the function F, defined in Eq. (IV-1)
x,y	local coordinates non-dimensionalized with respect to throat half-height and oriented such that y-axis lies along minimum area cross-section and origin is on the axis of symmetry, Fig. III.1
y_i ,y_c	y-coordinates of inner and outer throat wall locations
z	stretched axial coordinate defined by Eq. (III-35)
Z	axial coordinate in cylindrical system
Z*	Z-coordinate of origin of x-y coordinate system, Fig. III.1

Greek symbol	Meaning
α	inclination of x-axis from Z axis of symmetry, positive counterclockwise, Fig. III.1
β_1	dimensionless quantity defined in Eq. (III-35)
γ	specific heat ratio
Δ	grid spacing in finite difference approximations
ϵ	expansion parameter defined in Eq. (III-22)
η	parameter in expansion variable definition, Eq. (III-22)
θ	angle of inclination of velocity vector from x-axis, positive counterclockwise
μ	absolute viscosity
ν	kinematic viscosity, $\nu \equiv \mu/\rho$
ρ	density
τ_0	wall shear stress
ω	parameter equal to zero for planar configurations and one for axisymmetric configurations

Subscripts	Meaning
c	curvature
i, o	pertaining to inner and outer wall

Superscripts	Meaning
′ ″ ‴ ⁗	used to denote order of differentiation
¯	average
*	evaluated at sonic conditions

I. INTRODUCTION

There are a number of practical applications for which annular, supersonic nozzles are used. Among these are turbofan bypass nozzles, as well as unconventional propulsion nozzles such as the spike, plug, and expansion-deflection designs. The purpose of the latter group of nozzles, which all contain centerbodies, is to obtain improved thrust performance over the conventional converging-diverging configuration at off-design operating conditions. Another application of annular supersonic nozzles which has recently been proposed [1]†, is the use of coaxial, coflowing supersonic streams in order to obtain jet noise suppression. The advantage of this configuration is that the complex, interacting two-stream flowfield allows the suppression of noise-generation mechanisms with a minimal thrust penalty, as opposed to the insertion of mechanical devices into the exhaust flow.

However, the primary motivation for this work is the supersonic-supersonic ejector, Fig. I.1, whereby an energetic, coflowing, supersonic, primary stream is used to pump a low pressure, supersonic, secondary stream. This device has applications, for example, in establishing and maintaining supersonic flow conditions in the cavity region of chemical lasers [2,3] or as a means of augmenting the pressure recovery for supersonic wind tunnel applications [4-7].

From previous experience with the subsonic-supersonic ejector [8,9], for which the secondary stream is subsonic, it is known that the overall ejector

---

† Numbers in brackets refer to entries in REFERENCES.

operating characteristics are controlled to a great extent by the interaction of the primary and secondary streams immediately downstream from their point of confluence. Thus, any detailed investigation of the supersonic-supersonic ejector flowfield should naturally concentrate on this "initial interaction region." For example, in the preliminary investigation of Guile, et al. [10], a two-dimensional, inviscid, rotational method of characteristics technique was used to analyze the flow in this region starting at the ejector inlet station. However, in this adverse pressure gradient situation, it is recognized that the boundary layer and viscous shear layer flows near the primary-secondary confluence should be investigated. The experiments of Mikkelsen, et al. [2] showed severe pressure recovery losses for the constant area supersonic-supersonic ejector due to separation of the secondary stream as the static pressure of the primary was increased above that of the secondary at their confluence point. It is also known that in the hot-flow, chemical laser application the boundary layers of the secondary, laser flow are extremely thick at the ejector station. Therefore, any detailed calculations of the primary-secondary flowfield interactions should include these viscous effects and preferably should be initiated upstream of the ejector inlet so that the characteristics of the boundary layers along the walls of the primary and secondary streams can be well established before the confluence point is reached.

One natural place to start these calculations, particularly for the primary stream, is in the throat region of the supply nozzles using an appropriate transonic throat analysis. Since the Reynolds number of the primary stream is generally quite large and since the streamwise wall

pressure gradient in the throat region is favorable, the inviscid assumption may be made in the development of the throat analyses. The results can then be used as initial conditions to start the coupled inviscid/boundary layer computations which proceed downstream through the remainder of the ejector flowfield.

For both the chemical laser and wind tunnel applications of the supersonic-supersonic ejector, the geometry at the ejector may be either two-dimensional plane or axisymmetric. Hence, transonic analyses for nozzles with plane, axisymmetric-no centerbody, or annular configurations may be required to initialize the ejector flowfield calculations. In particular, if the ejector sketched in Fig. I.1 is taken as axisymmetric, the primary supply nozzle is an annular one with a small relative distance from the axis of symmetry to the nozzle when non-dimensionalized with respect to the throat height. However, if the primary stream is somehow centrally submerged in the supersonic secondary, for example by a strut support arrangement, its supply nozzle is a conventional axisymmetric one. Plane configurations for the supersonic-supersonic ejector have also been proposed and studied [10].

The objective of this study is twofold. First it is desired to develop an analytical technique which provides an accurate description of the transonic throat flowfield for a wide variety of two-dimensional nozzle configurations including those mentioned previously. Although the analysis is to be applicable to as wide a region as possible in the nozzle throat, its main intent is to establish an initial value line for starting the marching-type computations, e.g., method of characteristics, for the

supersonic portion of the flowfield. Also, since the implementation of such transonic analyses is invariably numerical, it is desired that the solution be numerically fast and reliable so that parametric studies or iterative calculations, as might occur in nozzle design situations, can be made in an efficient and low-cost manner. The second objective is to provide further insight into the characteristics of transonic throat flows by an experimental investigation of a number of configurations including conventional axisymmetric and annular ones. Comparison of the theoretical and experimental results then allows conclusions to be drawn regarding the limits of applicability of the analysis and suggests possible refinements of it.

As will be discussed further in the next chapter, no analytical techniques are known to exist which contain all of the desired features just outlined. In addition, experimental information concerning transonic throat flows is extremely sparse, particularly for axisymmetric geometries. This investigation is intended to provide additional information in these areas.

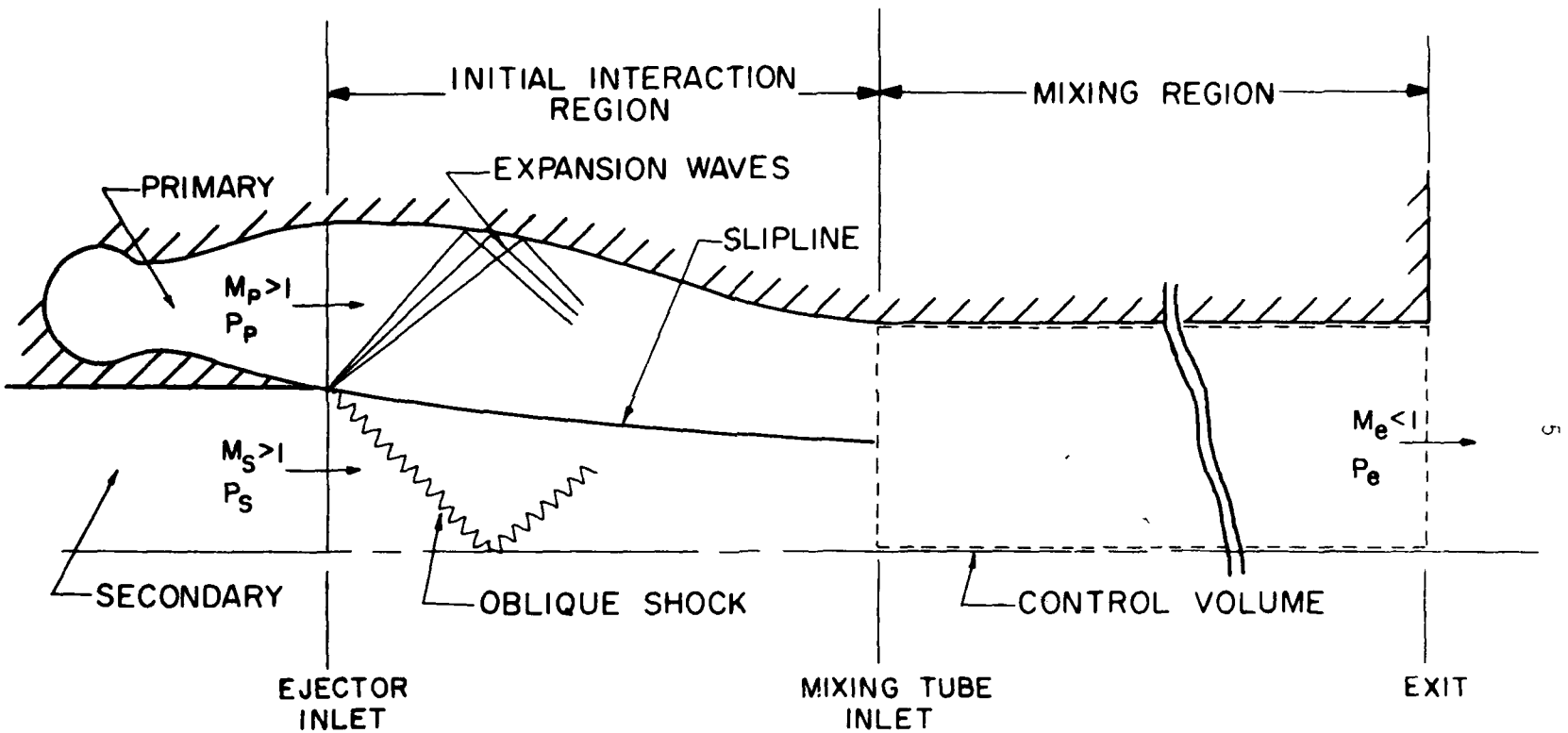

Figure I.1 Schematic diagram of proposed supersonic-supersonic ejector-diffuser configuration

II. LITERATURE REVIEW

The subject of transonic flow in nozzles and ducts has been studied for well over a hundred years, dating from the converging nozzle studies of Navier [11] in 1829 and St. Venant and Wantzel [12] in 1839. During this period, many techniques have been developed for investigating nozzle throat flows as the state of understanding of this topic has been advanced. The large majority of the contributions in this area are theoretical in nature and apply to the conventional two-dimensional plane and axisymmetric configurations, since study of annular nozzles has been motivated by the relatively recent development of devices such as the plug and expansion-deflection nozzles, the supersonic-supersonic ejector, etc. Because the annular configuration is of prime importance in this investigation, the purpose of the present chapter is to review those papers dealing explicitly with this configuration and to summarize the major contributions to the general methods which have been developed for throat flow analysis. The survey of Hall and Sutton [13] provides a useful review of early work while the more recent surveys of Flack and Thompson [14] and Brown and Hamilton [15] consider newer developments in this area.

A. ANALYTICAL

One of the fundamental difficulties involved with the theoretical solution of most fluid flow problems is the basic nonlinear nature of the governing equations. Further complicating the analysis of steady transonic flows is the fact that in the subsonic portions of the flowfield the equations are of elliptic type while in the supersonic portions they are of hyperbolic

type. The mixed, nonlinear nature of the equations describing transonic nozzle throat flows makes the solution of these problems by both analytical and numerical techniques difficult at best. However, several methods of varying degrees of accuracy and usability have been developed. Those to be reviewed in this section have been divided into the following categories: indirect techniques, series expansion methods, time dependent numerical techniques, and other methods.

1. Indirect Techniques

In the indirect or inverse methods, the velocity distribution is assumed along a reference streamline, such as the nozzle centerline, the flowfield is calculated by some, usually approximate, technique, and then in the inviscid approximation, any other streamline can be taken as a nozzle wall. Therefore, indirect techniques can be applied only to the nozzle design problem and cannot, without iteration, be applied to the direct problem of calculating the flowfield in a nozzle with given wall contours.

Among the earliest attempts at analyzing the flow in the throat of a plane converging-diverging nozzle was that of Meyer [16]. He assumed that the velocity along the axis increased linearly and substituted a double power series expansion in the coordinates into the perturbation potential equation. The coefficients up to and including the sixth order terms were obtained from which the characteristics of the flowfield were deduced.

Another early solution technique which was applied to nozzle flow analyses is the hodograph method developed successively by Lighthill [17,18],

Frankl [19], and Cherry [20-22]. In this method the hodograph equations, which employ the velocity components as independent variables, are used. These equations are linear, but the solution is complicated by the fact that over a portion of the supersonic flowfield the mapping from the hodograph plane to the physical plane is not one-to-one. Cherry [20] was able to devise a transformation which provides a single-valued solution over the entire plane and later [21,22] showed how superposition could be used to obtain solutions for realistic nozzle flows. Major drawbacks of the hodograph method are that it is applicable only to the planar case and that practical calculations appear to be quite complicated.

An early publication dealing with annular nozzles is that of Lord [23] who considered a supersonic nozzle with a cylindrical centerbody. In his inverse technique, two orders of solution were obtained by assuming that the velocity along the cylinder surface increases linearly in the streamwise direction for the first order solution and quadratically for the second order. As noted by Lord, the solutions for the annular case are much more complicated than for the limiting cases of axisymmetric and plane nozzles for which the centerbody diameter approaches zero and the throat diameter, respectively. Lord used his throat flowfield results to obtain a starting line for method of characteristics nozzle design computations.

One of the more well known indirect techniques was developed by Hopkins and Hill [24] who used the Friedrichs formulation to obtain the flowfields in axisymmetric nozzles with a small wall radius of curvature at the throat. The dependent variables were expanded as power series in the stream function so that the flowfield could be found from the prescribed velocity

distribution along the axis by solving for the series coefficients. A correlation was developed between a one-dimensional "reference boundary" and the computed boundary to facilitate the solution of the direct problem of analyzing nozzles with specified wall contours. The authors found that the most significant geometric parameter affecting the flow in the throat is the wall radius of curvature at the throat and that the inlet angle of the convergent section is not important unless this radius of curvature is less than the throat radius. In a later publication [25], Hopkins and Hill extended their method, with corrections by Morden and Farquhar [26], to the case of unconventional, annular nozzles inclined at arbitrary angles to the axis of symmetry. Their method assumes, however, the existence of a straight reference streamline along which the velocity is specified; this is not necessarily the case in the direct problem. Also, because of the asymmetry of the streamlines about the reference streamline, no correlations were obtained between reference and computed boundaries. For analysis of given nozzles, iterations on a computer are suggested.

Norton [27] developed a somewhat different inverse technique for conventional axisymmetric nozzles. In his method, the Euler equations, including the effects of rotationality and swirl, are first transformed by introducing the stream function and a stretched axial coordinate; these transformed equations are then numerically integrated outward from the given velocity distribution along the axis. Norton presents some calculated results, which required approximately two minutes of Univac 1108 time, but emphasizes that the method is not suited to the problem of analyzing given nozzle contours.

In a novel application of the indirect method, Van Tuyl [28] has obtained solutions for both axisymmetric and planar nozzles. The stream function and density are expanded as Taylor series in the neighborhood of a point on the nozzle axis along which the velocity distribution is specified. The coefficients of these series are found by substitution into the governing irrotationality and Bernoulli equations, and series for other quantities of interest are also determined. Padé fractions are then used to obtain convergence when the resulting power series diverge and to accelerate convergence when they converge. Van Tuyl carried out sample calculations for a specific axisymmetric nozzle using a digital computer both to obtain the terms of the series and to form the Padé approximants. The computations took 21 seconds on a CDC 6400 when 25 terms in the power series were retained.

An inverse scheme for analyzing the flow in conventional plane and axisymmetric nozzles has been reported by Klopfer and Holt [29]. In their formulation, the von Mises transformation is applied to the continuity and Euler equations so that the dependent variables are taken as the pressure, the transverse coordinate, and the ratio of the transverse to streamwise velocity components. The resulting equations are numerically integrated using the prescribed pressure distribution along the nozzle axis. Results for both plane inverse and axisymmetric direct problems are presented, and good agreement is obtained with the data of Cuffel, et. al. [30] in the axisymmetric case. The direct problem is solved iteratively as a sequence of inverse problems.

Ishii [31] has recently proposed an inverse method for nozzle design. In this technique, the governing equations for inviscid flow are transformed

so as to use the streamline and orthogonal trajectories as independent variables. The flowfield is divided into streamtubes and integration of the equations is carried out numerically starting from the prescribed velocity distribution along the nozzle axis.

As should be clear from the preceding discussion, the major disadvantage of the indirect methods is their inability to deal with the problem of analyzing the flow in a nozzle of a given configuration. Only Hopkins and Hill [24] have devised a scheme for avoiding the iterations which are inevitable when applying an inverse technique to the direct problem. As discussed by Brown and Hamilton [15] and Klopfer and Holt [29], another objection to these methods is the potentially poorly posed nature of the problem resulting from the specification of the velocity along the centerline in the subsonic region. When the governing equations are solved numerically, this specification is known to have a destabilizing effect on the computations (Hadamard instability).

2. Series Expansion Methods

The series expansion techniques have proven to be very popular for obtaining the flowfields in the throats of supersonic nozzles. In these methods, the dependent variables are expanded in series, and the unknown constants and functions are then determined by substitution into the governing equations and boundary conditions. These techniques can generally be considered to provide approximate solutions for the problem of analyzing the flow in a nozzle of a given configuration.

One of the first attempts at solving the direct problem of flow in a planar nozzle was made by Taylor [32] in 1930. He expanded the compressible

perturbation potential in a double power series in the coordinates and substituted it into the corresponding potential equation. By using the boundary condition that the nozzle wall is a streamline in the inviscid sense, the coefficients in the series were obtained. Taylor calculated an example for a nozzle with circular walls and a dimensionless radius of curvature[†], R_c, of 4.

Somewhat later, Sauer [33] presented series solutions for the flow in both axisymmetric and planar supersonic nozzles. In this well known technique, the compressible potential equation was first simplified by retaining only the dominant terms, and the perturbation potential function was then expanded as a power series in the transverse coordinate, y, with unknown coefficient functions of the streamwise coordinate, x. By substituting the expansion into the simplified potential equation and relating the resulting flowfield to the curvature of the nozzle walls, the unknown functions and constants were obtained. However, since the series was terminated after the first two terms, the results are applicable only to nozzles with small wall curvature, i.e., large R_c.

At about the same time, a somewhat different solution technique for the conventional configurations was proposed by Oswatitsch and Rothstein [34]. Rather than obtaining solutions for nozzles whose centerline velocity distribution is approximated to be linear as in Sauer's method, any centerline distribution is, in principle, possible in Oswatitsch and Rothstein's method.

[†]Throughout this investigation, the dimensionless radius of curvature, R_c, is defined as the throat wall radius of curvature divided by the throat half-height. For conventional axisymmetric nozzles the half-height is taken as the throat radius, while for annular nozzles it is taken as the distance between the inner and outer throat wall locations in the meridional plane.

however, since it is determined by the iterative solution of a differential equation which results from the continuity equation for a given nozzle contour, this technique is much more difficult to use than Sauer's closed form solutions. In addition, Oswatitsch and Rothstein's method gives anomalous results for nozzles which have a small wall radius of curvature.

Hall [35] also carried out an expansion solution for the flow in the throat of axisymmetric and plane nozzles. In this investigation, a careful order of magnitude analysis of the various dependent and independent variables was made, and the transonic perturbation velocity components were expanded in appropriate series using $\epsilon = R_c^{-1}$ as the expansion parameter. By substituting these series into the wall boundary conditions and the governing irrotationality and gas dynamic equations, the formulations for the various orders of solution in the expansion technique were obtained. Closed form expressions for the first three orders were determined by using solution forms suggested by the boundary conditions. The first order solutions are identical to those of Sauer [33], and Hall also found that to the first three orders the approximate solutions for nozzles with circular, parabolic, and hyperbolic arc wall contours coincide. Nozzles for which the wall radius of curvature is less than the throat half-height, $R_c < 1$, cannot be analyzed with this technique since this results in expansion parameters greater than unity. In fact the smallest value of R_c used by Hall in his example calculations is 10/3.

This same solution technique was later extended by Moore and Hall [36] to the case of annular nozzles inclined arbitrarily to the axis of symmetry. However, as pointed out by Thompson and Flack [37], the coordinate system

employed in this study is an overspecified, inconsistent one. In a companion report, Moore [38] used $\epsilon = R_c^{-1/2}$ as the expansion parameter to construct approximate solutions for the flow in asymmetric planar nozzles. The first three terms of the series solution were presented along with the results for two special cases, namely the configurations in which the two nozzle walls have unequal curvature and in which the nozzle wall contour is asymmetric about the throat plane.

In a series of articles [39-42], Szaniawski has investigated transonic flow in nozzle throats. In [39] and [40], the governing equations are derived and the existence and nature of solutions for the flow of a viscous, heat conducting gas in the throat region of two-dimensional plane nozzles are investigated. The two later papers [41,42] are concerned with finding solutions under the usual assumptions of inviscid, irrotational flow. A solution is developed for a particular class of planar nozzle wall contours in [41]. The potential function is expanded as a power series in the transverse coordinate with undetermined coefficient functions of the streamwise coordinate. Recurrence relations for these functions are then determined by substitution into the potential equation and the boundary conditions. A similar method is used in [42] to determine solutions for both plane and axisymmetric conventional nozzles, but an auxiliary system of curvilinear coordinates is employed. Both solution techniques are applicable only to nozzles which have a large throat radius of curvature.

In a somewhat different but closely related area, Sichel [43,44] has studied the flow in two-dimensional nozzle throats at operating conditions near the choking point. The transition from symmetric Taylor flow to

continuously accelerating Meyer flow was investigated by including the effect of longitudinal viscosity in the governing equations. Based on this formulation, a similarity solution was found which provides a smooth transition between the regimes and which shows the initial stages of shock formation.

Kliegel and Quan [45] used a method similar to Hall's for predicting plane and axisymmetric nozzle flows except that a different stretched axial coordinate was employed. The velocity components were expanded as series in $\epsilon = R_c^{-1}$, and two orders of corrections to the one-dimensional solution were obtained. The authors conclude that the resulting solution, which is claimed to be valid throughout the entire nozzle, should be limited to nozzles which have a large wall radius of curvature, $R_c \geq 2$, and that Hall's transonic solution can be obtained from it through a coordinate transformation and reordering of the terms. The cases of unchoked nozzle flows and multistream nozzle expansions, as would occur in film cooled rocket engines, are also discussed.

The expansion solutions presented so far are all limited to nozzles with gentle wall curvatures. In an attempt to analyze the case of small wall radius of curvature for axisymmetric nozzles, Kliegel and Levine [46] presented a solution utilizing $\epsilon = (R_c+1)^{-1}$ as the expansion parameter. Since this parameter is less than unity for all values of the radius of curvature, the resulting series should have superior convergence properties in the limit of small R_c. The authors contend that this solution is the one obtained when the solution in toroidal coordinates, which are convenient for circular arc wall contours, are transformed back to cylindrical

coordinates. However, in a later publication Levine and Coats [47] conclude that this contention is false and also that "the proposed series do not satisfy the differential equations of motion in cylindrical coordinates." In reality, the "solution" proposed in [46] is simply Hall's solution in $\epsilon = R_c^{-1}$ transformed to a series in $\epsilon = (R_c+1)^{-1}$ such that the two are equivalent in the limit of large radius of curvature, $R_c \to \infty$. Kliegel and Levine also corrected some errors which appeared in Hall's third order solution for axisymmetric nozzles, although the present author has found their correction of the discharge coefficient to be in error.

The conclusions of Levine and Coats [47] just mentioned were the result of an extensive investigation of axisymmetric nozzle throat flows. The transonic equations of motion, including the effect of variable specific heat ratio, were solved in toroidal coordinates using a combination of a small parameter expansion and a double series in the coordinates. Although a number of expansion parameters was tried, none of the resulting solutions was found to be convergent for small values of R_c. The authors hypothesized that this is because the expansion solutions assume that the local wall geometry, in particular the throat radius of curvature, completely determines the flowfield in the throat and that this premise breaks down as $R_c \to 0$. In addition, the effect of variable specific heat ratio was found to be negligible in the transonic region.

Taulbee and Boraas [48] have developed a Hall-type series solution for transonic flow in the throat region of axisymmetric nozzles with a nonuniform stagnation temperature distribution at the inlet. The governing continuity and Euler equations were first transformed using the stream function

as an independent variable, and expansions for the dependent variables were then assumed using an order of magnitude analysis. Two orders of solutions were obtained, and the results indicate that the sonic line location is essentially unaffected by the nonuniformity of the stagnation temperature. However, as demonstrated by the calculated example presented in [49], the flowfield details such as the flow angle are sensitive to the total temperature distribution. In a later paper, Boraas [50] included the effects of nonuniform total temperature and composition in an analysis of transonic throat flow in axisymmetric nozzles. First and second order solutions were again found (see Ishii [51] for corrected equations), and it is stated that in this case the sonic line location does depend on the nonuniformities of the properties upstream of the throat although no examples are presented. In both of the rotational analyses just cited the expansion parameter is taken as $\varepsilon = R_c^{-1}$ so that the solutions are not applicable to nozzles with small radius of curvature of the throat wall.

Apparently unaware of the earlier work of Lord [23], Smithey and Naber [52] presented a solution for the sonic line in an axisymmetric nozzle with a concentric inner cylinder. The solution was obtained by hypothesizing a trial form suggested by the Sauer [33] solutions for the limiting cases of axisymmetric and plane nozzles. Substitution into the transonic gas dynamic equation and use of the boundary conditions then allowed determination of the unknown functions and constants. However, since the resulting solution satisfies the irrotationality condition only for the limiting configurations, its applicability to the annular case of interest is questionable.

Thompson and Flack [14,37,53] have performed a very extensive investigation of the flow in the throat region of asymmetric plane and annular axisymmetric supersonic nozzles. In their theoretical analysis, the method of Hall was used with an expansion parameter which reduces to $\cdot = (\bar{R}_c + \cdot)^{-1}$ where $\bar{R}_c$ is an average dimensionless radius of curvature for the two walls and $\cdot$ may be taken as zero or one. Three solution orders were obtained, and the authors noted that significant improvement in the convergence properties of the solution for small radii of curvature resulted from using $\cdot = 1$. However, because of the manner in which the axisymmetric term in the gas dynamic equation was expanded, the annular solutions can be applied only to configurations for which the distance from the axis of symmetry to the nozzle throat is large when non-dimensionalized with respect to the throat half-height, i.e., annular nozzles which approach the plane configuration. Their solution cannot be used for conventional axisymmetric nozzles, and, in addition, it appears that it gives planar results for annular nozzles which are not inclined with respect to the axis of symmetry. Experiments utilizing both static wall pressure and laser doppler velocimeter measurements were performed for a series of plane nozzle throat configurations; good agreement was found between the analytically and experimentally determined sonic lines. These experiments will be discussed in more detail in a later section.

Recently, Ishii has published the results of analytical investigations of the flow in axisymmetric nozzle throats with rotationality effects included. In [54] throat flowfields with rate processes and nonuniform property distributions are considered; see also the comment by Boraas [55]

and the rebuttal by Ishii [51]. The expansion method of Hall was used with the parameter taken as $\varepsilon = R_c^{-1}$, and one term of the series is presented for frozen and equilibrium, uniform flows. The transonic flow of a vibrationally relaxing or chemically reacting gas in a converging-diverging nozzle is investigated in [56]. Again the Hall method was employed, but in this study the expansion parameter was chosen as $\varepsilon = (R_c+1)^{-1}$.

The main disadvantage of the series expansion techniques is that they can generally be applied only to a given class of configurations. In particular, most of the analyses mentioned above have been developed only for the conventional two-dimensional plane and axisymmetric configurations. Also, for all of these analyses, there is a lower limit on the throat wall radius of curvature below which the analyses give unreasonable results. On the other hand, since the series methods generally lead to closed form expressions, the implementation of these solutions is quite straightforward.

3. Time Dependent Numerical Techniques

In order to avoid the mixed nature of the governing equations for steady transonic flow, the time dependent methods utilize the unsteady form of the equations which are hyperbolic for all speed regimes. The resulting initial value problem is solved numerically by continuing the computations in the time domain from an arbitrarily assumed set of initial conditions until the steady state is asymptotically approached.

Saunders [57] apparently was the first to apply this technique to internal transonic flows. In this study the two-step Lax-Wendroff differencing scheme was employed to integrate the equations for flow in axisymmetric

nozzles with uniform inlet conditions assumed. Good agreement was found between the numerical results and the wall static pressure data of Back, et al. [58] for a converging-diverging nozzle. The computation time was reported as approximately 45 minutes on a CDC 3200 computer.

Migdal, Klein, and Moretti [59] utilized a nonconservative form of the basic equations together with a stretching of the axial coordinate to obtain the throat flowfield in axisymmetric Laval nozzles. An example calculation was performed for a configuration with a dimensionless throat wall radius of curvature of 0.625 and inlet and exit angles of 45° and 15°, respectively. The agreement between these results and the wall pressure data of Back, et al. [58] is excellent. The running time for this case was less than five minutes on an IBM 360/75.

By using the two-step Law-Wendroff scheme developed by Saunders [57], Wehofer and Moger [60] investigated the effect of nonuniform inlet conditions on axisymmetric convergent-divergent nozzle flows. These authors also considered the case of an axisymmetric converging nozzle with a conical inlet section including the influence of the operating pressure ratio and the associated free jet structure. The computations were very time consuming, however, taking from two to five hours, depending on the mesh size, on an IBM 360/50.

Brunell [61] used a somewhat different technique to study the transonic flowfields in planar, supersonic nozzles. In his method, a modified upwind differencing scheme was utilized to integrate a conservative form of the governing equations. The results appear to be reasonable for operating conditions in which the nozzle is not choked, but problems were encountered

for the choked conditions which are of primary interest. In the latter case, the constant Mach number lines contain slope discontinuities which Brunell hypothesizes are due to numerical pressure disturbances that are propagated from the supersonic wall region into the subsonic region. Experiments were also conducted using an annular nozzle with a cylindrical centerbody and small throat gap, but in all cases only unchoked operating conditions were studied.

In order to predict the flowfields, and especially the discharge coefficients, for axisymmetric and plane nozzles with small throat radius of curvature, Laval [62,63] used a time dependent method similar to that of Saunders [57]. In this treatment, however, an axial coordinate stretching was employed together with the introduction of a pseudo-viscosity term to avoid stability problems. Calculations were carried out for nozzles with radius of curvature values down to 0.1, and very good agreement between computed and measured values of the flow coefficient was noted. Laval states that the method can be applied to annular configurations, although no such examples are presented in the references cited above. The calculations required approximately two hours of IBM 360/50 time.

Serra [64] has also developed a transient technique for the determination of nozzle flows. In his method, the one-step Law-Wendroff difference scheme is incorporated with a numerical damping term so as to stabilize the numerical procedure in the vicinity of shock waves. Also, since mathematical overspecification of the entrance flow conditions caused accuracy difficulties in earlier numerical studies, the problem was formulated to establish realistic conditions at the entrance. The computed results compare well

with experimental data and previous theories for axisymmetric and planar nozzles. An example is also included of the flow in an annular turbofan passage. The computation time on a Univac 1108 computer was 80 minutes for an axisymmetric nozzle problem.

In an effort to reduce the long computation times associated with time-dependent methods, Cline [65-68] has developed an efficient program for calculating a wide variety of compressible, internal flows. The second-order accurate, MacCormack finite difference method is utilized to solve the governing equations which are left in a nonconservative form. A second-order, reference plane characteristic scheme is used for the boundary points, and an explicit artificial viscosity is included for shock calculations. The most recent version [68] of the code solves the Navier-Stokes rather than the Euler equations so that viscous flows with Reynolds numbers up to about 10^4 can be analyzed. Several examples are presented including inviscid converging, converging-diverging, and annular nozzle flows as well as a viscous converging-diverging nozzle calculation. Good agreement between the computations and experimental data is obtained with computation times ranging from 29 seconds on a CDC 6600 to 7 minutes on a CDC 7600 for the example problems. These times are obtained, however, at the expense of using coarse mesh spacing, particularly in the inviscid cases.

The major advantage of the time-dependent numerical techniques is that if the codes are developed in a sufficiently general manner they may be employed in the analysis of a variety of transonic internal flows. A serious drawback to their use, however, is the long computation times required. This means that parametric studies or iterative calculations, such

as might be necessitated in a design procedure, would be numerically time consuming and expensive.

4. Other Methods

A number of other methods have also been used for nozzle flow analysis. One such technique is the method of integral relations developed originally by Dorodnitsyn [69]. In the application of this method, the flowfield is divided into streamwise strips across which the governing partial differential equations are integrated using assumed profiles for the dependent variables. The resulting ordinary differential equations are then solved to obtain the coefficients. Holt [70] formulated the one strip and two strip approximations for both the inverse and direct problems of flow in planar nozzles. Results of a one strip, inverse calculation are presented and are found to agree well with the hodograph results of Cherry [21] in the supersonic region but to diverge seriously from them in the subsonic region. Liddle and Archer [71] carried out one and two strip computations for the analysis of the flowfield in axisymmetric nozzles of arbitrary shape with particular emphasis on conical nozzles. The two strip solutions gave good agreement with experimental wall and centerline pressure measurements for nozzles with $R_c \geq 2$. Liddle [72] later extended the method to include the cases of annular and asymmetric, plane nozzles. One strip calculations were performed and were found to be in reasonable agreement with wall pressure measurements for an annular configuration and with the numerical method of Katsanis [73] for incompressible flow in a planar nozzle. One of the fundamental difficulties involved with using the method of integral

relations is that to achieve reasonable accuracy for nozzles which have a small throat radius of curvature a large number of strips is required with attendant long computing times and program complexity. Saddle point singularities which arise in the integration of the equations must also be carefully handled.

Numerical techniques other than the time dependent ones discussed previously have also been utilized for throat flowfield analyses. In an early investigation, Emmons [74] developed a method which used a conformal transformation and a relaxation process designed for hand calculations to solve the governing equations. In a later publication [75], an example was calculated for the flow in a two-dimensional nozzle with a hyperbolic wall contour. Interestingly, when this method was programmed on a digital computer convergence problems were encountered [15]. Twenty-five years later Prozan and Kooker [76] investigated axisymmetric nozzle flowfields using an error minimization technique. A sophisticated steepest descent procedure was employed to minimize the residuals in the steady flow conservation equations. The results of this method agree quite well with the flowfield measurements of Cuffel, et al. [30] for a nozzle with small throat radius of curvature. Typical run times ranged from 5 to 10 minutes on an IBM 7094. Recently, Brown, et al. [77] used a type-dependent relaxation technique to study both conventional and annular axisymmetric nozzle flows including the effects of rotationality. In this method, which is quite popular for external transonic flows, the axial derivatives are approximated by centered differences in the subsonic (elliptic) portion of the flowfield and by backward differences in the supersonic (hyperbolic)

region. The results of example calculations for hyperbolic, conically convergent, and annular nozzles indicate that the rotational effects of entrance flow nonuniformities can be significant in evaluating nozzle performance. The example problems required from 3½ to 5 minutes and a region size of approximately 170K on an IBM 370/158 computer. Using a somewhat different numerical scheme, Fanning and Mueller [78] have studied planar nozzle flowfields. The problem was first recast as a Laplace equation with an inhomogeneous term that encompasses the compressibility effects. A successive approximation method was then utilized to converge to a final solution. Flowfield and discharge coefficient results agree well with experimental measurements, but the computing times are extremely long, taking from 45 minutes to 6 hours of IBM 370/155 time.

B. EXPERIMENTAL

Not only are theoretical analyses of transonic nozzle flows quite complicated, but experimental measurement of them is also difficult. This is because disturbances introduced by measurement probes are propagated along characteristics and are reflected from the duct walls back into the region of interest. Thus, most experimental studies have been limited to wall static pressure measurements, although some investigators have attempted to use pitot probes. Recently, non-intrusive optical techniques have also been employed.

The most thorough flowfield experiments have been performed for the two-dimensional planar geometry, primarily because sidewall static taps can be used to obtain both transverse and streamwise pressure distributions. Jacobs [79] utilized this method to determine isobars in six asymmetric plane

nozzles. Later, Flack and Thompson [14,53,80] conducted an extensive series of experiments on a set of 13 two-dimensional nozzles with a number of wall curvature combinations. For each configuration the sonic line location was determined using sidewall static pressure readings and also laser doppler velocimeter (LDV) measurements. It was found that the two data sets and the results of the series solution developed in [37] agreed with each other reasonably well with the LDV measurements being slightly upstream of the static pressure measurements and the theoretical results being still further upstream. These investigators observed that small changes in the boundary geometry caused very large changes in the sonic line location.

Experiments for axisymmetric Laval nozzles have been limited mainly to wall static pressure readings since the nozzle geometry does not provide any means for making flowfield static pressure or LDV measurements. One of the first experimental investigations of transonic nozzle flow was performed by Stanton [81]. The flowfield in an axisymmetric nozzle with $R_c = 4.77$ was studied by determining static pressure distributions along the contour for a number of supply pressures. Pitot pressure distributions were also measured along the axis and along an axial line near the nozzle wall, but the probe certainly disturbed these measurements, particularly those made near the wall. At the Jet Propulsion Laboratory a number of experimental investigations [30,58,82-84] of axisymmetric nozzle flows has been made by Back and his co-workers. Static wall pressure and discharge coefficient measurements for nozzles with a dimensionless throat radius of curvature as small as 0.25 were used to study the effects of contraction section shape, inlet flow direction, wall friction, entrance boundary layer thickness, and

wall cooling. Only for a nozzle with a radius of curvature of R_c = 0.625 and conical inlet and exit angles of 45° and 15°, respectively, were flowfield measurements made [30]. These were obtained by means of a 0.889 mm diameter tube which was supported and held taut between an upstream plenum chamber and a downstream vacuum chamber. The tube had a 0.152 mm diameter hole drilled radially in it, and the pressure distributions along the axis and along five radial locations were found by appropriate axial traverses. At the off-axis positions disturbances were undoubtedly introduced into the flowfield and the velocity vector was inclined to the tube. However, to date this is the only known set of data which considers the flow patterns in the transonic region of an axisymmetric nozzle. Liddle and Archer [71] measured the centerline and wall pressures for four axisymmetric nozzles with radius of curvature values ranging from 0.625 to 4.0. The centerline distributions, however, are reported for only two of the nozzles. In another series of experiments, Masure, et al. [63] measured the discharge coefficients for five nozzles with conical inlet and exit sections and R_c values from 0.25 to 0.8 .

Data for annular configurations is extremely sparse. Bresnahan and Johns [85] measured static pressures along the inner wall of a turbojet plug nozzle. In their experiments the outer wall was straight and parallel to the axis of symmetry and the inner wall had a large radius of curvature, R_c = 7.8 . However, there were only three pressure taps in the transonic region for which the corresponding Mach number was less than 1.5, since the supersonic region was of primary interest in this study. As mentioned previously, Brunell [61] conducted experiments on an annular nozzle with a

cylindrical centerbody, but only operating conditions for which the nozzle was unchoked were considered. Liddle [72] has also obtained wall pressure measurements for an annular, supersonic nozzle. However, the geometry of the experimental setup is not specified in [72], and, in any event, the data are very close to the results of one-dimensional theory.

Obviously, there is a need to expand the data base for flow in the transonic region of nozzles, particularly in terms of flowfield measurements for both conventional and annular axisymmetric configurations. As mentioned in the preceding chapter, this is one of the objectives of the present investigation.

III. THEORETICAL ANALYSIS

The objectives outlined in the introductory chapter for the theoretical investigation are to provide a numerically fast, reliable, and accurate method for describing the throat flowfields in annular, supersonic nozzles. In addition, it is desired that the method be direct and that it be applicable to a wide variety of configurations. Of the few previous analyses which have considered the annular geometry, none are felt to have all of the desired characteristics. Two [23,25] utilize indirect methods; others [36,37,52,72] may be applied only to specialized configurations, and the rest [62,64,68,77] are generally numerically slow and expensive. Only the recent numerical techniques of Cline [68] and Brown, et al. [77] have obtained results with a modest expenditure of computing time. However, both of these methods implicitly assume that the main flow direction in the throat is essentially parallel to the axis of symmetry.

Based on these considerations, the method which has been chosen is a series expansion technique similar to that used by Moore and Hall [36] and Thompson and Flack [37] but more general in terms of the geometries which can be analyzed.

A. FORMULATION

A sketch of the configuration under consideration is shown in Fig. III.1. The R-Z coordinate system is the standard cylindrical system while the x-y coordinate system is rotated such that the y-axis lies along the cross section of minimum area in the throat with the x-axis perpendicular to the y-axis and the origin located on the axis of symmetry. For this general case, the main

flow x-direction is inclined to the axis of symmetry at an angle β, positive in the counterclockwise direction, and d is the throat half-height in the R-Z coordinates. It should be noted that for an inclined, annular nozzle the minimum area cross section does not correspond to the cross section of minimum distance between the contours. The influence of the radial coordinate, R, in computing the annular area results in the minimum area section being nearer the axis of symmetry than the minimum distance section.

It is assumed that the problem to be analyzed is the steady, inviscid, irrotational, adiabatic flow of a perfect gas in an annular nozzle operating in the choked, continuously accelerating, Meyer regime. These are the usual assumptions and operating conditions of interest. The inviscid assumption, in particular, is justified since the Reynolds number based on the throat height is large for most practical applications and the streamwise pressure gradient is favorable. Therefore, the boundary layers in the throat region are very thin and viscous effects may be safely neglected.

Under these assumptions, the governing equations may be taken as the irrotationality condition and the "gas dynamic equation" [86],

$$U_R - V_Z = 0 \qquad \text{(III-1)}$$

$$\left(U^2-a^2\right)U_Z + \left(V^2-a^2\right)V_R + 2UVU_R - \frac{a^2V}{R} = 0 \qquad \text{(III-2)}$$

$a \equiv$ speed of sound ,

where the gas dynamic equation is obtained from the continuity equation, Euler's momentum equation, and the definition of the speed of sound. In these equations, subscripts are used to denote partial differentiation with respect to Z and R. These two governing equations can be combined to form

the well-known compressible potential equation, but since the solution is to be found in terms of the velocity components, the potential function is not introduced into this analysis. Transforming from the R-Z cylindrical coordinates to the x-y system with lengths non-dimensionalized with respect to the throat half-height, d, and velocities with respect to the critical speed of sound, a*,

$$x = \frac{(Z-Z^*)}{d}\cos\beta + \frac{R}{d}\sin\beta \qquad \text{(III-3)}$$

$$y = -\frac{(Z-Z^*)}{d}\sin\beta + \frac{R}{d}\cos\beta \qquad \text{(III-4)}$$

$$u = \frac{U}{a^*}\cos\beta + \frac{V}{a^*}\sin\beta \qquad \text{(III-5)}$$

$$v = -\frac{U}{a^*}\sin\beta + \frac{V}{a^*}\cos\beta \ , \qquad \text{(III-6)}$$

and using the following adiabatic relation for a perfect gas with constant specific heats,

$$\left(\frac{a}{a^*}\right)^2 = \frac{\gamma+1}{2} - \frac{\gamma-1}{2}\left(u^2+v^2\right) \ , \qquad \text{(III-7)}$$

the governing equations take the form

$$u_y - v_x = 0 \qquad \text{(III-8)}$$

$$\left(1-u^2-\frac{\gamma-1}{\gamma+1}v^2\right)u_x - \frac{4}{\gamma+1}uvu_y + \left(1-v^2-\frac{\gamma-1}{\gamma+1}u^2\right)v_y + \frac{\left(1-\frac{\gamma-1}{\gamma+1}u^2-\frac{\gamma-1}{\gamma+1}v^2\right)(v\cos\beta + u\sin\beta)}{y\cos\beta + x\sin\beta} = 0 \ . \qquad \text{(III-9)}$$

The final step in the transformation of the equations is the introduction of the transonic perturbation velocity components by

$$u = 1 + \tilde{u} \qquad \text{(III-10)}$$

$$v = \tilde{v} \ , \tag{III-11}$$

where $\tilde{u}$ and $\tilde{v}$ are assumed to be small compared to unity, $|\tilde{u}|, |\tilde{v}| \ll 1$. This results in

$$\tilde{u}_y - \tilde{v}_x = 0 \tag{III-12}$$

$$\left(-2\tilde{u}-\tilde{u}^2-\frac{\gamma-1}{\gamma+1}\tilde{v}^2\right)\tilde{u}_x - \frac{4}{\gamma+1}(1+\tilde{u})\tilde{v}\,\tilde{u}_y + \left(\frac{2}{\gamma+1}-\tilde{v}^2-2\frac{\gamma-1}{\gamma+1}\tilde{u}-\frac{\gamma-1}{\gamma+1}\tilde{u}^2\right)\tilde{v}_y$$

$$+\frac{\left(\frac{2}{\gamma+1}-2\frac{\gamma-1}{\gamma+1}\tilde{u}-\frac{\gamma-1}{\gamma+1}\tilde{u}^2-\frac{\gamma-1}{\gamma+1}\tilde{v}^2\right)\left[\tilde{v}\cos\beta+(1+\tilde{u})\sin\beta\right]}{y\cos\beta + x\sin\beta} = 0 \ . \tag{III-13}$$

The boundary conditions in this inviscid analysis are that the bounding walls must be streamlines. Using $y = g(x)$ and $y = h(x)$ as the functional forms of the equations for the inner and outer wall contours, respectively, the boundary conditions can be stated as

$$\tilde{v}(x,g(x)) = [1+\tilde{u}(x,g(x))]g'(x) \tag{III-14}$$

$$\tilde{v}(x,h(x)) = [1+\tilde{u}(x,h(x))]h'(x) \ , \tag{III-15}$$

where primed quantities represent differentiation with respect to x, $(\ )' \equiv \frac{d}{dx}$. Expanding the equations for the boundaries in Maclaurin series about the throat,

$$y = g(x) = y_i + g'(0)x + g''(0)\frac{x^2}{2!} + g'''(0)\frac{x^3}{3!} + \ldots \tag{III-16}$$

$$y = h(x) = y_0 + h'(0)x + h''(0)\frac{x^2}{2!} + h'''(0)\frac{x^3}{3!} + \ldots \ , \tag{III-17}$$

the boundary conditions can be rewritten as

$$\tilde{v}(x,g(x)) = [1+\tilde{u}(x,g(x))]\left[g'(0)+g''(0)x+g'''(0)\frac{x^2}{2!}+\ldots\right] \tag{III-18}$$

$$\tilde{v}(x,h(x)) = [1+\tilde{u}(x,h(x))]\left[h'(0)+h''(0)x+h'''(0)\frac{x^2}{2!}+\ldots\right] \ . \tag{III-19}$$

The solution technique involves expanding the perturbation velocity components in appropriate series and substituting them into the governing equations and boundary conditions. However, before this can be done an expansion parameter, ε, must be chosen and various order of magnitude estimates made. Both Kliegel and Levine [46] and Thompson and Flack [37] found that improved convergence properties of their series solutions were attained for nozzles with a small wall radius of curvature by using $\varepsilon = (R_c+1)^{-1}$ rather than the Hall [35] parameter $\varepsilon = R_c^{-1}$. Based on their experience, the expansion parameter which has been used in this investigation is

$$\varepsilon = (\bar{R}_c+\eta)^{-1} , \tag{III-20}$$

where $\bar{R}_c$ is an average dimensionless radius of curvature for the two bounding walls and η is arbitrary. For $\eta > 1$, ε is therefore less than unity regardless of how small $\bar{R}_c$ may be. Defining $\bar{R}_c$ in terms of the second derivatives of the equations for the wall contours,

$$\bar{R}_c \equiv \frac{2}{h''(0) - g''(0)} , \tag{III-21}$$

ε becomes

$$\varepsilon = \frac{h''(0) - g''(0)}{2 + \eta[h''(0) - g''(0)]} . \tag{III-22}$$

This is identical to the parameter used in [37] except that η may have any value here and is not restricted to the values zero or one.

From one-dimensional considerations, it is well known [13] that the acceleration at the throat of a supersonic nozzle is given by

$$\left.\frac{du}{dx}\right|_{x=0} = \left[\frac{\omega+1}{(\gamma+1)R_c}\right]^{1/2} , \tag{III-23}$$

where $\omega = 0$ for plane two-dimensional nozzles

$= 1$ for axisymmetric nozzles

Using Eq. (III-10), the definition of transonic perturbation velocity component $\tilde{u}$, and Eq. (III-20), the definition of the expansion parameter ε, Eq. (III-23) yields the following order of magnitude estimate for the transonic throat region,

$$\tilde{u}_x = O\left(\varepsilon^{1/2}\right) . \qquad \text{(III-24)}$$

Also from the dominant terms in boundary conditions (III-18) and (III-19), it is known that

$$\tilde{v}_x\big|_{y=g} = g''(0) + g'''(0)x + \ldots \qquad \text{(III-25)}$$

$$\tilde{v}_x\big|_{y=h} = h''(0) + h'''(0)x + \ldots . \qquad \text{(III-26)}$$

It is shown in Appendix A that the terms $g''(0)$ and $h''(0)$ dominate the right hand sides of the two preceding equations for nozzles with circular arc wall contours. Combining this information with the definition of ε in Eq. (III-22) allows the estimate

$$\tilde{v}_x = O(\varepsilon) \qquad \text{(III-27)}$$

for the transonic region.

Requiring that both terms in the irrotationality condition (III-12) be of the same order of magnitude and using this last estimate for $\tilde{v}_x$ results in the conclusion that $\tilde{u}_y$ must also be $O(\varepsilon)$ in the throat. Since all lengths have been non-dimensionalized with respect to the throat half-height, d, Δy is $O(1)$ across the throat and therefore $\tilde{u}$ must be $O(\varepsilon)$ in the transonic region of interest. Utilizing the estimates expressed in Eqs. (III-24) and (III-27), it is concluded that $\tilde{v}/\tilde{u} = O\left(\varepsilon^{1/2}\right)$ or $\tilde{v} = O\left(\varepsilon^{3/2}\right)$. Taking this estimation for

the magnitude of $\tilde{v}$ together with Eq. (III-27), or alternately the irrotationality governing equation (III-12), results in the requirement that x be of $\mathcal{O}\left(\varepsilon^{1/2}\right)$ for consistency. Thus, the solution developed here is restricted to the narrow transonic region about the throat plane, x = 0.

To complete the order of magnitude analysis the gas dynamic equation (III-13) must be investigated. Dividing the numerator and denominator of the last term of this equation by cosβ, it may be restated as,

$$\left(-2\tilde{u}-\tilde{u}^2-\frac{\gamma-1}{\gamma+1}\tilde{v}^2\right)\tilde{u}_x-\frac{4}{\gamma+1}(1+\tilde{u})\tilde{v}\tilde{u}_y+\left(\frac{2}{\gamma+1}-\tilde{v}^2-2\frac{\gamma-1}{\gamma+1}\tilde{u}-\frac{\gamma-1}{\gamma+1}\tilde{u}^2\right)\tilde{v}_y$$

$$+\frac{\left(\frac{2}{\gamma+1}-2\frac{\gamma-1}{\gamma+1}\tilde{u}-\frac{\gamma-1}{\gamma+1}\tilde{u}^2-\frac{\gamma-1}{\gamma+1}\tilde{v}^2\right)[\tilde{v}+(1+\tilde{u})\tan\beta]}{y+x\tan\beta}=0,$$

$$\cos\beta\neq 0\ . \qquad \text{(III-28)}$$

Disregarding their numerical coefficients, the dominant factors in each of the first three terms are $\tilde{u}\tilde{u}_x$, $\tilde{v}\tilde{u}_y$, and $\tilde{v}_y$ which are $\mathcal{O}\left(\varepsilon^{3/2}\right)$, $\mathcal{O}\left(\varepsilon^{5/2}\right)$, and $\mathcal{O}\left(\varepsilon^{3/2}\right)$, respectively. Likewise, the dominant factors in the last term are,

$$\frac{\tilde{v}+\tan\beta}{y+x\tan\beta}\ .$$

Assuming for the moment that tanβ is at most $\mathcal{O}(1)$, i.e., disallowing configurations with radial or nearly radial main flow directions for which $\tan\beta\to\infty$[†], this term can further be reduced to

$$\frac{\tilde{v}+\tan\beta}{y}\ ,$$

since x has been restricted to the throat region, $x=\mathcal{O}\left(\varepsilon^{1/2}\right)$. Since $y=\mathcal{O}(1)$ or larger, depending on the dimensionless distance from the axis of

---

[†] This restriction is consistent with the previous one that $\cos\beta\neq 0$ in Eq. (III-28).

symmetry to the annular nozzle throat, and using the previous estimate for the magnitude of $\tilde{v}$, it is known that,

$$\frac{\tilde{v}}{y} = O\left(\varepsilon^{3/2}\right) \tag{III-29}$$

or smaller. Therefore, in order that the dominant terms in Eq. (III-28) all be of the same order, it is required that

$$\frac{\tan\beta}{y} = O\left(\varepsilon^{3/2}\right) \tag{III-30}$$

or smaller. This means that for annular nozzles with throats that are near the axis of symmetry in a dimensionless sense, $y = O(1)$, only small angles of inclination, β, may be considered. However, this would seem to be the only physically realistic case anyway, since one would not expect to encounter an annular configuration for which the throat is very close to the symmetry axis while the main flow x-direction is highly inclined to it. For nozzles whose throats are large distances from the axis, $y >> 1$, the restriction to small angles of inclination may be relaxed as long as the estimate of Eq. (III-30) is satisfied. In the limit as $y \to \infty$, the last term in the governing gas dynamic equation (III-28) vanishes as it takes the correct planar form.

The expansion parameter, ε, as defined in Eq. (III-22), is related to the average wall curvature of the bounding walls at the throat and enters the formulation through the second derivative terms in the Maclaurin series expansions for the boundary conditions, Eqs. (III-18) and (III-19). However, because of the complication that the definition of ε involves both $g''(0)$ and $h''(0)$ while each boundary condition contains only one or the other, a method must be devised such that when expansions are assumed for the dependent

variables, appropriate series occur in the expression of the boundary conditions. This is done in the following manner. Solving Eq. (III-20) for $\bar{R}_c^{-1}$,

$$\bar{R}_c^{-1} = \frac{\varepsilon}{1 - \eta\varepsilon} , \tag{III-31}$$

and using the identity $g''(0) = g''(0)\bar{R}_c \bar{R}_c^{-1}$ along with Eq. (III-21) for $\bar{R}_c$ and Eq. (III-31) for $\bar{R}_c^{-1}$ yields

$$g''(0) = \frac{2g''(0)}{h''(0) - g''(0)} \frac{\varepsilon}{1 - \eta\varepsilon} = \frac{2g''(0)}{h''(0) - g''(0)} \left\{\varepsilon+\eta\varepsilon^2+\eta^2\varepsilon^3+ \ldots\right\}, \tag{III-32}$$

for $|\eta\varepsilon| < 1$.

Similarly,

$$h''(0) = \frac{2h''(0)}{h''(0) - g''(0)} \frac{\varepsilon}{1 - \eta\varepsilon} = \frac{2h''(0)}{h''(0) - g''(0)} \left\{\varepsilon+\eta\varepsilon^2+\eta^2\varepsilon^3+ \ldots\right\}, \tag{III-33}$$

for $|\eta\varepsilon| < 1$.

The requirement that $|\eta\varepsilon| < 1$ in the expansions above is always met since $h''(0) - g''(0) > 0$ for an area *minimum* at the throat and only non-negative values of η are considered (see Eq. (III-22)). In this way power series in ε are obtained in the boundary condition evaluations, although it is clear that the second derivatives are exactly matched only for $\eta = 0$. The coefficients multiplying the parentheses in Eqs. (III-32) and (III-33) are $O(1)$, and as shown in Appendix A, the first few derivatives in the Maclaurin series expansions for circular arc wall contours are of the following orders of magnitude,

$$g'(0),\ h'(0) = O\left(\varepsilon^{3/2}\right) \qquad g''(0),\ h''(0) = O(\varepsilon)$$

$$g'''(0),\ h'''(0) = O\left(\varepsilon^{7/2}\right) \qquad g^{iv}(0),\ h^{iv}(0) = O\left(\varepsilon^3\right) \tag{III-34}$$

$$\vdots$$

Using the estimates obtained thus far, various $\mathcal{O}(1)$ independent variables and parameters are defined as shown below,

$$z \equiv \left[\frac{\gamma+1}{2}\,\varepsilon\right]^{-1/2} x \qquad\qquad y \equiv y$$

$$\beta_1 \equiv \left[\frac{\gamma+1}{2}\right]^{-1/2} \varepsilon^{-3/2} \tan\beta$$

$$g_1 \equiv \left[\frac{\gamma+1}{2}\right]^{-1/2} \varepsilon^{-3/2} g'(0) \qquad h_1 \equiv \left[\frac{\gamma+1}{2}\right]^{-1/2} \varepsilon^{-3/2} h'(0) \qquad \text{(III-35)}$$

$$g_2 \equiv \frac{2g''(0)}{h''(0) - g''(0)} \qquad h_2 \equiv \frac{2h''(0)}{h''(0) - g''(0)}$$

$$g_3 \equiv \left[\frac{\gamma+1}{2}\right]^{-1/2} \varepsilon^{-7/2} g'''(0) \qquad h_3 \equiv \left[\frac{\gamma+1}{2}\right]^{-1/2} \varepsilon^{-7/2} h'''(0) \; .$$

$$\vdots \qquad\qquad \vdots$$

Note particularly the transformation from coordinate x to the $\mathcal{O}(1)$, stretched coordinate z. It is also seen that the estimates $y = \mathcal{O}(1)$ and $\tan\beta = \mathcal{O}\left(\varepsilon^{3/2}\right)$ have been used in the definitions of y and β_1, although as previously discussed, nozzles with larger inclinations may be analyzed if the requirement expressed in Eq. (III-30) is satisfied.

With these definitions and order of magnitude estimates the next step is to expand the perturbation velocity components in appropriate series. Assuming expansions in half-powers of ε starting with $\tilde{u} = \mathcal{O}(\varepsilon)$ and $\tilde{v} = \mathcal{O}\left(\varepsilon^{3/2}\right)$, it has been found that the following series are sufficient,

$$\tilde{u}(z,y) = u_1(z,y)\varepsilon + u_2(z,y)\varepsilon^2 + u_3(z,y)\varepsilon^3 + \ldots \qquad \text{(III-36)}$$

$$\tilde{v}(z,y) = \left[\frac{\gamma+1}{2}\,\varepsilon\right]^{1/2}\left[v_1(z,y)\varepsilon + v_2(z,y)\varepsilon^2 + v_3(z,y)\varepsilon^3 + \ldots\right] , \qquad \text{(III-37)}$$

i.e., terms involving odd half-powers of ε in the $\tilde{u}$ expansion and even half-powers of ε in the $\tilde{v}$ expansion vanish.

Substituting definitions (III-35) and expansions (III-36) and (III-37) into the governing irrotationality equation (III-12) and gas dynamic equation (III-28) and gathering coefficients of like powers of ϵ results in the following two sets of equations,

$$\frac{\partial u_n}{\partial y} - \frac{\partial v_n}{\partial z} = 0 \qquad (n = 1,2,3, \ldots) \tag{III-38}$$

and

$$-2u_1 \frac{\partial u_1}{\partial z} + \frac{\partial v_1}{\partial y} + \frac{\beta_1 + v_1}{y} = 0 \qquad (n = 1) \tag{III-39}$$

$$-2u_1 \frac{\partial u_n}{\partial z} - 2u_n \frac{\partial u_1}{\partial z} + \frac{\partial v_n}{\partial y} + \frac{v_n}{y} = f_n\left(u_1, v_1, \ldots, u_{n-1}, v_{n-1}\right) \quad (n = 2,3, \ldots), \tag{III-40}$$

where the functions, f_n, on the right hand side of Eq. (III-40) are always known from the lower order solutions. The first two are given by

$$f_2 = u_1^2 \frac{\partial u_1}{\partial z} + 2v_1 \frac{\partial u_1}{\partial y} + (\gamma-1)u_1 \frac{\partial v_1}{\partial y} + (\gamma-1)\frac{u_1 v_1}{y} + (\gamma-2)\frac{\beta_1 u_1}{y} \tag{III-41}$$

and

$$\begin{aligned} f_3 = {} & 2u_2 \frac{\partial u_2}{\partial z} + u_1^2 \frac{\partial u_2}{\partial z} + 2u_1 u_2 \frac{\partial u_1}{\partial z} + \left(\frac{\gamma-1}{2}\right) v_1^2 \frac{\partial u_1}{\partial z} + 2v_2 \frac{\partial u_1}{\partial y} + 2u_1 v_1 \frac{\partial u_1}{\partial y} \\ & + 2v_1 \frac{\partial u_2}{\partial y} + (\gamma-1)u_1 \frac{\partial v_2}{\partial y} + (\gamma-1)u_2 \frac{\partial v_1}{\partial y} + \left(\frac{\gamma-1}{2}\right) u_1^2 \frac{\partial v_1}{\partial y} + (\gamma-1)\frac{u_1 v_2}{y} \\ & + (\gamma-1)\frac{u_2 v_1}{y} + \left(\frac{\gamma-1}{2}\right)\frac{u_1^2 v_1}{y} + (\gamma-2)\frac{\beta_1 u_2}{y} + \frac{3}{2}(\gamma-1)\frac{\beta_1 u_1^2}{y} + \left(\frac{\gamma+1}{2}\right)\frac{\beta_1^2 z}{y^2} \\ & + \left(\frac{\gamma+1}{2}\right)\frac{\beta_1 v_1 z}{y^2} . \end{aligned} \tag{III-42}$$

In the last term of gas dynamic equation (III-28), the binomial expansion of the factor $(y+x\tan\beta)^{-1}$ has been used which assumes that $|x\tan\beta/y| < 1$.

This requirement is certainly met if the one stated in Eq. (III-30) is. Of interest is the fact that the irrotationality condition retains its simple, linear form through all orders and that the only nonlinear equation among the set of gas dynamic governing equations is the first order one. This behavior is typical of expansion solution techniques.

The boundary conditions which apply to each solution order must also be obtained in an appropriate form. Only the details for the boundary condition at the inner wall will be given since the procedure for the outer wall boundary condition is identical. Transforming from coordinate x to coordinate z, Eq. (III-14) for the inner wall condition becomes,

$$\tilde{v}(z,g(z)) = \left[1 + \tilde{u}(z,g(z))\right] \frac{dg}{dz} \frac{dz}{dx} \tag{III-43}$$

where the Maclaurin series expansion for the inner contour, Eq. (III-16), is

$$y = g(z) = y_i + \frac{\gamma+1}{2}\left(g_1 z + \frac{1}{2} g_2 z^2\right)\varepsilon^2 + \frac{\gamma+1}{2}\left(\frac{1}{2} g_2 \eta z^2\right)\varepsilon^3 + \frac{\gamma+1}{2}\left(\frac{1}{2} g_2 \eta^2 z^2\right)\varepsilon^4 + \ldots , \tag{III-44}$$

when the definitions and expansions in Eqs. (III-32), (III-33), and (III-35) are introduced. The derivative dg/dz needed in Eq. (III-43) is,

$$\frac{dg}{dz} = \frac{\gamma+1}{2}\left(g_1 + g_2 z\right)\varepsilon^2 + \frac{\gamma+1}{2}\left(g_2 \eta z\right)\varepsilon^3 + \frac{\gamma+1}{2}\left(g_2 \eta^2 z\right)\varepsilon^4 + \ldots . \tag{III-45}$$

Expansion of the perturbation velocity components at the inner wall in Taylor series about $y = y_i$ yields,

$$\tilde{u}(z,g(z)) = \tilde{u}\left(z,y_i\right) + \left.\frac{\partial \tilde{u}}{\partial y}\right|_{y=y_i}\left(g(z)-y_i\right) + \left.\frac{\partial^2 \tilde{u}}{\partial y^2}\right|_{y=y_i}\frac{\left(g(z)-y_i\right)^2}{2!} + \ldots \tag{III-46}$$

and

$$\tilde{v}(z,g(z)) = \tilde{v}\left(z,y_i\right) + \left.\frac{\partial \tilde{v}}{\partial y}\right|_{y=y_i}\left(g(z)-y_i\right) + \left.\frac{\partial^2 \tilde{v}}{\partial y^2}\right|_{y=y_i}\frac{\left(g(z)-y_i\right)^2}{2!} + \ldots \quad . \tag{III-47}$$

The procedure then is to substitute these expansions into boundary condition (III-43) using the series for $\tilde{u}$ and $\tilde{v}$, Eqs. (III-36) and (III-37), and the wall contour information, Eqs. (III-44) and (III-45). Gathering and equating coefficients of powers of ε leads to the following set of inner wall boundary conditions,

$$v_1\left(z,y_i\right) = g_1 + g_2 z \tag{III-48}$$

$$v_2\left(z,y_i\right) = g_2 \eta z + \left(g_1+g_2 z\right) u_1\left(z,y_i\right) \tag{III-49}$$

$$v_3\left(z,y_i\right) = g_2 \eta^2 z + g_2 \eta z u_1\left(z,y_i\right) + \left(g_1+g_2 z\right) u_2\left(z,y_i\right) - \left(\frac{\gamma+1}{2}\right)\left(g_1 z + \frac{1}{2} g_2 z^2\right) \left.\frac{\partial v_1}{\partial y}\right|_{y=y_i} \quad . \tag{III-50}$$

$$\vdots$$

The boundary conditions along the outer contour are exactly analogous,

$$v_1\left(z,y_o\right) = h_1 + h_2 z \tag{III-51}$$

$$v_2\left(z,y_o\right) = h_2 \eta z + \left(h_1+h_2 z\right) u_1\left(z,y_o\right) \tag{III-52}$$

$$v_3\left(z,y_o\right) = h_2 \eta^2 z + h_2 \eta z u_1\left(z,y_o\right) + \left(h_1+h_2 z\right) u_2\left(z,y_o\right) - \left(\frac{\gamma+1}{2}\right)\left(h_1 z + \frac{1}{2} h_2 z^2\right) \left.\frac{\partial v_1}{\partial y}\right|_{y=y_o} \quad . \tag{III-53}$$

$$\vdots$$

In performing these Taylor series expansions about the inner and outer throat wall locations, it is clear that the boundary conditions are satisfied exactly only at these points.

The formulations for the various orders of solution in the expansion technique are now complete. For the first order, n = 1, irrotationality condition (III-38), gas dynamic equation (III-39), and boundary conditions (III-48) and (III-51) comprise the formulation. Likewise, Eqs. (III-38), (III-40), (III-49), and (III-52) are the ones of importance for the second order, etc. . Once the solutions for the various orders in the expansion technique have been obtained, the flowfields in the throat region of annular, supersonic nozzles may be characterized.

B. SOLUTION

The solution technique is similar to that used originally by Hall [35] and proceeds by first considering the formulation for the first order problem and then moving to the second and higher order problems. As just mentioned, the governing equations and boundary conditions for the first order are

$$\frac{\partial u_1}{\partial y} - \frac{\partial v_1}{\partial z} = 0 \qquad \text{(III-38)}$$

$$- 2u_1 \frac{\partial u_1}{\partial z} + \frac{\partial v_1}{\partial y} + \frac{\beta_1 + v_1}{y} = 0 \qquad \text{(III-39)}$$

and

$$v_1\left(z, y_i\right) = g_1 + g_2 z \qquad \text{(III-48)}$$

$$v_1\left(z, y_o\right) = h_1 + h_2 z \ . \qquad \text{(III-51)}$$

Inspection of boundary conditions (III-48) and (III-51) suggests the following solution form for v_1,

$$v_1(z,y) = A_0'(y) + A_1'(y) z \ , \qquad \text{(III-54)}$$

where

$$A_1'(y_1) = g_2 \qquad A_1'(y_0) = h_2 \qquad \text{(III-55)}$$

$$A_0'(y_1) = g_1 \qquad A_0'(y_0) = h_1 \ , \qquad \text{(III-56)}$$

and the prime is now used to denote differentiation with respect to y. Substitution of the v_1 solution form into irrotationality equation (III-38) and integration with respect to y results in

$$u_1(z,y) = A_1(y) + B_0 + B_1 z \ , \qquad \text{(III-57)}$$

where B_0 and B_1 are constants and the form of the integrating function is suggested by Eq. (III-54) for v_1. The assumption of terms involving higher powers of z in either Eqs. (III-54) or (III-57) is unnecessary since these terms would vanish by boundary conditions (III-48) and (III-51) anyway.

The unknown A functions and B constants must still be determined. This is accomplished by first substituting the expressions for u_1 and v_1, into the gas dynamic governing equation, (III-39), and gathering coefficients of similar powers of z. Since the resulting equation is to be satisfied for all z, these coefficients must vanish which leads to the following two equations,

$$z^1: \quad A_1''(y) + \frac{A_1'(y)}{y} = 2B_1^2 \qquad \text{(III-58)}$$

$$\text{and} \quad z^0: \quad A_0''(y) + \frac{A_0'(y)}{y} = 2B_1 A_1(y) + 2B_0 B_1 - \frac{B_1}{y} \ . \qquad \text{(III-59)}$$

In this manner the problem has been reduced from the solution of the original set of partial differential equations and boundary conditions to the solution of the two preceding ordinary differential equations with conditions (III-55) and (III-56). Equation (III-58) can be integrated once to give

$$A_1'(y) = B_1^2 y + \frac{B_2}{y} \ , \qquad \text{(III-60)}$$

where the constants B_2 and B_1 are determined from the conditions in Eq. (III-55) as

$$B_2 = \frac{-\left(h_2 y_i - g_2 y_o\right) y_i y_o}{y_o^2 - y_i^2} \qquad \text{(III-61)}$$

and

$$B_1 = \frac{\left(h_2 y_o - B_2\right)^{1/2}}{y_o} . \qquad \text{(III-62)}$$

The positive root is chosen in the expression for B_1 since $\partial u/\partial z$, which is identically $B_1 \varepsilon$ for the first order solution, must be positive for an accelerating nozzle flow. Investigation of the radicand reveals that it also is always positive for the nozzle configurations considered here, $h_2 > 0$ and $g_2 < 0$. Integration of Eq. (III-60) yields

$$A_1(y) = \frac{1}{2} B_1^2 y^2 + B_2 y \ln y , \qquad \text{(III-63)}$$

where an integration constant is unnecessary since it can be considered as being included with the still undetermined constant B_0 in Eq. (III-57) for u_1.

Substituting this relation for $A_1(y)$ into Eq. (III-59) and integrating once yields

$$A_0'(y) = \frac{1}{4} B_1^3 y^3 + B_1 B_2 y \ln y + \left(B_0 B_1 - \frac{1}{2} B_1 B_2\right) y - \beta_1 + \frac{B_3}{y} . \qquad \text{(III-64)}$$

The conditions listed in (III-56) may then be used to determine B_3 and B_0 as,

$$B_3 = \frac{-\left(h_1 y_i - g_1 y_o - B_4 y_i + B_5 y_o\right) y_i y_o}{y_o^2 - y_i^2} \qquad \text{(III-65)}$$

and

$$B_0 = \frac{h_1 y_o - B_4 y_o - B_3}{B_1 y_o^2} , \qquad \text{(III-66)}$$

where B_4 and B_5 have been defined as,

$$B_4 = \frac{1}{4} B_1^3 y_o^3 + B_1 B_2 y_o \ln y_o - \frac{1}{2} B_1 B_2 y_o - B_1 \qquad \text{(III-67)}$$

and

$$B_5 = \frac{1}{4} B_1^3 y_i^3 + B_1 B_2 y_i \ln y_i - \frac{1}{2} B_1 B_2 y_i - B_1 . \qquad \text{(III-68)}$$

The first order solution is complete. The B constants are evaluated in the following order: B_2, Eq. (III-61); B_1, Eq. (III-62); B_4, Eq. (III-67); B_5, Eq. (III-68); B_3, Eq. (III-65); and B_0, Eq. (III-66). With these constants determined, the functions $A_1'(y)$, $A_1(y)$, and $A_0'(y)$ are then known from Eqs. (III-60), (III-63), and (III-64), and u_1 and v_1 may be evaluated from Eqs. (III-57) and (III-54), respectively.

The higher order solutions are obtained in a very similar manner starting from the formulations developed in the preceding section. Solutions through the first three orders have been found, and as might be guessed from the form of the gas dynamic governing equations, Eqs. (III-39)-(III-42), the effort required to obtain them increases dramatically as one moves to the higher order problems. For the second order, v_2 and u_2 are of the form,

$$v_2(z,y) = C_0'(y) + C_1'(y)z + C_2'(y)z^2 \qquad \text{(III-69)}$$

$$u_2(z,y) = \left[C_1(y)+D_0\right] + \left[2C_2(y)+D_1\right]z + D_2 z^2 , \qquad \text{(III-70)}$$

requiring the solution of three ordinary differential equations, while the third order problem requires solving four ordinary differential equations with v_3 and u_3 given by,

$$v_3(z,y) = E_0'(y) + E_1'(y)z + E_2'(y)z^2 + E_3'(y)z^3 \qquad \text{(III-71)}$$

$$u_3(z,y) = \left[E_1(y)+F_0\right] + \left[2E_2(y)+F_1\right]z + \left[3E_3(y)+F_2\right]z^2 + F_3 z^3 \quad . \qquad \text{(III-72)}$$

Lengthy algebraic manipulations are involved, but the form of the differential equations to be solved is very similar to Eqs. (III-58) and (III-59). As in the integration of the equations for the first order problem, a large number of intermediate constants are defined and used, but because of space limitations the details of the second and third order solutions will not be presented here. However, a complete solution summary is included in Appendix B.

With the expressions for the $\left(u_1,v_1\right)$, $\left(u_2,v_2\right)$, and $\left(u_3,v_3\right)$ perturbation velocity components determined, other quantities of interest may also be found. These include: the velocities components u and v in the x-y coordinate system; M*, the ratio of the local speed to the critical speed of sound; θ, the angle of inclination of the velocity vector from the x-axis; the Mach number, M; and the local static to stagnation pressure ratio, p/p_0. The series expansions for these quantities in terms of the perturbation velocity components are given below,

$$u(z,y) = 1 + \tilde{u} = 1 + u_1\varepsilon + u_2\varepsilon^2 + u_3\varepsilon^3 + \ldots \qquad \text{(III-73)}$$

$$v(z,y) = \tilde{v} = \left[\frac{\gamma+1}{2}\,\varepsilon\right]^{1/2}\left[v_1\varepsilon + v_2\varepsilon^2 + v_3\varepsilon^3 + \ldots\right] \qquad \text{(III-74)}$$

$$M^*(z,y) = \left(u^2+v^2\right)^{1/2} = 1 + u_1\varepsilon + u_2\varepsilon^2 + \left(u_3 + \frac{\gamma+1}{4}\,v_1^2\right)\varepsilon^3 + \ldots \qquad \text{(III-75)}$$

$$\theta(z,y) = \tan^{-1}(v/u) = \left[\frac{\gamma+1}{2}\,\varepsilon\right]^{1/2}\left[v_1\varepsilon + \left(v_2-u_1v_1\right)\varepsilon^2 + \left(v_3-u_1v_2-u_2v_1+u_1^2v_1\right)\varepsilon^3 + \ldots\right] \qquad \text{(III-76)}$$

$$M(z,y) = \left[\frac{\frac{2}{\gamma+1} M^{*2}}{1 - \frac{\gamma-1}{\gamma+1} M^{*2}}\right]^{1/2} = 1 + \left(\frac{\gamma+1}{2}\right)\left[u_1 \varepsilon + u_2 \varepsilon^2 + \frac{3}{4}(\gamma-1)u_1^2 \varepsilon^2\right.$$

$$\left. + \left[u_3 + \frac{\gamma+1}{4} v_1^2 + \frac{3}{2}(\gamma-1)u_1 u_2 + \frac{(5\gamma^2-8\gamma+3)}{8} u_1^3\right]\varepsilon^3 + \ldots\right] \qquad \text{(III-77)}$$

$$\frac{p}{p_0}(z,y) = \left[1 - \frac{\gamma-1}{\gamma+1} M^{*2}\right]^{\gamma/(\gamma-1)} = \left(\frac{2}{\gamma+1}\right)^{\gamma/(\gamma-1)}\left[1 - \gamma\left[u_1 \varepsilon + u_2 \varepsilon^2\right.\right.$$

$$\left.\left. + \left(u_3 + \frac{\gamma+1}{4} v_1^2 - \frac{\gamma+1}{6} u_1^3\right)\varepsilon^3 + \ldots\right]\right] . \qquad \text{(III-78)}$$

The reason that these expansions should be employed is so that the only terms included are those for which the coefficients of the various powers of ε are completely known. For example, if u and v are first calculated from Eqs. (III-73) and (III-74) and then M* is determined from the definition $M^* = \left(u^2+v^2\right)^{1/2}$, information from just one of the many sixth order terms, $v_3^2 \varepsilon^6$, will be included.

Another quantity of importance is the discharge or flow coefficient, C_D, defined as the ratio of the actual nozzle mass flow to that obtained from the ideal one-dimensional approximation of uniform, sonic flow at the throat, i.e.,

$$C_D = \int_{y_i}^{y_o} \left[\frac{\rho}{\rho^*} u \frac{dA}{A^*}\right]_{x=0} , \qquad \text{(III-79)}$$

where in the present notation u has been non-dimensionalized with respect to the critical speed of sound, a*. Substituting the series expansions for ρ/ρ^* and u and the expression for dA/A* into the integrand, the relation for C_D becomes

$$C_D = 1 - \frac{(\gamma+1)\varepsilon^2}{\left(y_o^2 - y_i^2\right)}\left[C_{D1} + C_{D2}\varepsilon + C_{D3}\varepsilon^2 + \ldots\right] \qquad \text{(III-80)}$$

after integration, where the constants C_{D1}, C_{D2}, and C_{D3} are evaluated as shown in Appendix B. The reduction in mass flow due to the two-dimensional, nonuniform nature of the flowfield is generally small and the value of the discharge coefficient is therefore very close to unity for the configurations which may be analyzed with the expansion solution developed here.

Thus, with the $\left(u_1, v_1\right)$, $\left(u_2, v_2\right)$, and $\left(u_3, v_3\right)$ transonic perturbation velocity components and the C_{D1}, C_{D2}, and C_{D3} discharge coefficient constants determined, all of the flow variables of interest, including those just presented, are known to the third order in the present series approximations.

C. SOLUTION CHECKS

Because the development of the solutions described in the preceding section requires lengthy algebraic manipulations, particularly for the third order solution, they must be thoroughly checked to ensure their validity. To accomplish this task two groups of tests have been carried out as shown in Table III.1.

The first set of tests involves reducing the solution obtained here for the general annular configuration to previous solutions for simpler geometries. The results for the conventional axisymmetric configuration are found by passing to the limit $y_i \to 0$ for a nozzle with a straight inner boundary, i.e., as the inner wall approaches the axis of symmetry. The limiting value, $y_i = 0$, *cannot* be used in the numerical implementation of the annular solution since this leads to division by zero. However, an arbitrarily small value, e.g., $y_i = 10^{-10}$, may be employed to approximate the axisymmetric configuration. In a similar manner, the planar symmetric

geometry may be investigated by considering the limit $y_i \to \infty$, since the transverse curvature effect becomes negligible in that limit. In this situation there are two possible wall configurations of interest. Both the case in which the bounding walls have equal and opposite curvatures and that in which one of the walls is straight approach the symmetric plane limit as $y_i \to \infty$; in the latter case, the straight wall may be considered as the centerline of a symmetric nozzle. Using $\eta = 0$ in the expansion parameter definition, (Eq. III-22), the results of the present solution reduce to those of Hall [35], with corrections by Kliegel and Levine [46], in both the axisymmetric and plane symmetric limits. Likewise, for $\eta = 2$ the solution developed here is identical to previous, unpublished solutions [87] by the present author for both the conventional axisymmetric and plane configurations, where $\varepsilon = \left(R_c+1\right)^{-1}$ was employed as the expansion parameter. It should be emphasized that neither of these $\varepsilon = \left(R_c+1\right)^{-1}$ solutions for the axisymmetric case coincide with that of Kliegel and Levine [46] because, as pointed out in Chapter II, their result is not a solution since it doesn't satisfy the equations of motion. Rather, it is simply a transformation from the Hall series in $\varepsilon = R_c^{-1}$ to a series in $\varepsilon = \left(R_c+1\right)^{-1}$ such that the two are equivalent as $R_c \to \infty$. Except for errors in the third order discharge coefficient constants, the analysis of Thompson and Flack [37] for plane nozzles can also be reduced to the $\varepsilon = \left(R_c+1\right)^{-1}$ solutions mentioned above for the symmetric, planar case. Another configuration which provides a limit check on the solution for the general annular nozzle is the specialized case for which either the inner or outer boundary is straight and parallel to the axis of symmetry. Results of the two term solutions developed in [87] using $\varepsilon = \left(R_c+1\right)^{-1}$ agree with those of the present solution for $\eta = 2$.

It is to be noted that when one of the bounding walls is straight, e.g., $g''(0) = 0$, the expression for ε, Eq. (III-22), simplifies to

$$\varepsilon = \frac{h''(0)}{2 + \eta h''(0)} , \qquad \text{(III-81)}$$

which is equivalent to

$$\varepsilon = \left(2R_c + \eta\right)^{-1} , \qquad \text{(III-82)}$$

since $h''(0) = R_c^{-1}$ if $h'(0) = 0$. Because of the presence of the factor 2 in Eq. (III-82) it might be expected that for cases with one straight boundary, different results would be obtained with the present analysis than with previous analyses which use either $\varepsilon = R_c^{-1}$ or $\varepsilon = \left(R_c + 1\right)^{-1}$ as the expansion parameter. However, if the formulation of the present investigation is carefully studied, it is found that η enters the problem only as the product $\eta\varepsilon$ through the boundary conditions, Eqs. (III-32) and (III-33). As long as this product is the same for two solutions, the results obtained with them will be identical regardless of the numerical coefficient of R_c in the expansion parameter. Therefore, no generality is lost by employing the definitions given in Eqs. (III-20)-(III-22) for ε. This explains why all of the $\eta = 0$ solutions produce identical results independent of the ε definition and also why the $\eta = 2$ case in the present technique corresponds with the previous $\varepsilon = \left(R_c + 1\right)^{-1}$ analyses.

The reduction tests just discussed were generally carried out numerically by comparing the discharge coefficient constants C_{D1}, C_{D2}, and C_{D3} and the transonic perturbation velocity components $\left(u_1, v_1\right)$, $\left(u_2, v_2\right)$, and $\left(u_3, v_3\right)$ obtained with the present solution to those obtained from earlier solutions for the specialized configurations. As demonstrated by the expansions given

in Eqs. (III-73)-(III-78) and (III-80), these parameters completely specify the quantities of interest. The perturbation velocity comparisons were made by evaluating the components at a number of y locations on planes of constant x through the throat region. Only for the limiting case of the conventional axisymmetric nozzle is it convenient to simplify the general solution analytically. Since this is a special case of great practical importance, the resulting solution is summarized in Appendix C, where the expansion parameter has been taken as $\varepsilon = \left(R_c + \eta\right)^{-1}$. For $\eta \neq 0$ this is a new and very useful result.

The second group of tests involves numerically back substituting the solutions for the various orders into the corresponding governing equations, (III-38)-(III-42), and boundary conditions, (III-48)-(III-53) and evaluating the residuals. The partial derivatives in these equations are approximated by using second order, central, finite differences for all z-derivatives and for y-derivatives at interior points and either forward or backward, second order differences for the y-derivatives at boundary points. This scheme provides a powerful means of checking the solution given its formulation and can be used to verify it in this sense.

The satisfaction of the governing equations, (III-38)-(III-42), as measured by the size of the residuals, was tested at a number of y-locations ranging from the inner to the outer boundary on planes of constant x through the throat region. The boundary conditions were also checked at various x stations through this region. In addition, the tests were carried out for a large number of geometrical configurations and specific heat ratios for the gas so that all of the significant parameters were varied. In all cases it

was found that the residuals for the equations and boundary conditions were $O(10^{-8})$ or smaller when a grid spacing of $\Delta x = \Delta y = 10^{-4}$ was used for the differencing.

The results of the two sets of tests described above provide strong evidence of the correctness of the solution developed in the preceding section. It is felt, therefore, that the results of this analysis can be used with confidence to predict the flowfields in the throat regions of annular, supersonic nozzles.

D. PARAMETRIC STUDY OF SOLUTION BEHAVIOR

So far no mention has been made either of the convergence properties of the series solution which has been developed or its range of applicability to various geometrical configurations, etc. . The purpose of this section is to present the results of a comprehensive, numerical study whose objective was to parametrically investigate these questions.

As mentioned in the first section of this chapter, the order of magnitude estimate, $y = O(1)$ or larger, was made, and the origin of the x-y coordinate system was taken to lie on the axis of symmetry so that annular configurations whose throats are near the axis can be analyzed. These geometries are of prime importance for the supersonic-supersonic ejector application, and use of this estimate also means that the solution may be applied to conventional axisymmetric nozzles. However, for annular axisymmetric, or in the limiting case, planar configurations for which the dimensionless distance from the symmetry axis to the throat region is large, $y \gg 1$, the evaluation of the transonic series solution involves sums and

differences of very large terms since the constants and functions are proportional to powers of y_i, y_o, and y. This situation, of course, can lead to roundoff errors in the numerical implementation; the appearance of these errors depends on the precision of the machine being used. Therefore, the first set of studies which was carried out simply determined the y-distance from the axis of symmetry at which roundoff errors began to significantly affect the solution when evaluated on the University of Illinois CDC Cyber 175 digital computer. Both single precision (14 digit accuracy) and double precision (29 digit accuracy) versions of the subroutine which performs all of the constant and function evaluations for the series solution were tested. As expected, it was found that the only significant parameter in these tests was y_i, the dimensionless distance from the axis of symmetry to the inner nozzle wall. This quantity may be used to characterize the axis-to-throat distance since $y_i \leq y \leq y_o$ and $y_o - y_i = 1$ in the region of interest. Other parameters such as β, the angle between the throat axis and the symmetry axis, η, the parameter in the expansion variable definition, R_{ci} and R_{co}, the wall radii of curvature, etc., were found not to affect the appearance of roundoff errors.

The results for the upper limits on y_i for avoiding roundoff errors in the determination of the various orders of perturbation velocity components, (u_1, v_1), (u_2, v_2), and (u_3, v_3), are shown in part (a) of Table III.2. The single precision limits were found by noting the y_i value at which the single precision results for the velocity components in the throat plane deviate significantly [$O(0.1\%)$] from the double precision values, while the double precision limits were found by observing the value of y_i at which the

double precision values deviate significantly [(0.1%)] from those of the planar limit which is asymptotically approached as $y_i \to \infty$. If all three orders in the series solution are employed, the limit for single precision is approximately $y_i = 15$; this includes the axisymmetric-no centerbody case and most annular geometries of interest. The double precision limit is $y_i = 1000$, which provides a very good approximation to the plane configuration. If only two terms of the solution are used, the limits are $y_i = 60$ and $y_i = 30{,}000$, respectively, for single and double precision, etc. . The reason that the limits are relaxed for the lower orders is that their solutions involve lower powers of y than does the third order solution.

Since the derivation of the discharge coefficient, C_D, requires the integration of the density-u velocity component product across the throat plane, the constants involved in its evaluation contain higher powers of y_i and y_o than do the velocity components themselves. Thus, the upper limits on y_i for avoiding roundoff errors are more restrictive for C_D as shown in part (b) of Table III.2. The technique used to determine these limits was similar to that previously discussed for the perturbation velocity components except that in this case it was the flow coefficient constants, C_{D1}, C_{D2}, and C_{D3} that were monitored. For solutions involving all three orders, the limit on y_i is approximately 10 for single precision and 250 for double precision. However, since the value of the discharge coefficient is so close to 1.0 for all of the configurations for which the analysis applies, i.e., for $R_e \geq O(1)$: $.98 \leq C_D \leq 1.0$, the discharge coefficient, with its more stringent limits, is of less interest than the velocity components. This is particularly true since one of the primary purposes of the nozzle

throat analysis is to establish an accurate initial value line for analyzing the supersonic portion of the flowfield using, e.g., the method of characteristics.

At this point it should be mentioned that the numerical implementation of the series solution is extremely fast on the Cyber 175. A typical problem requires less than a second of execution time when the single precision version of the constant-evaluating subroutine is used and less than two seconds when the double precision version is employed. For this reason the double precision form is routinely used, and as can be deduced from the preceding discussion, it provides throat flowfield information for a wide variety of configurations. Conventional axisymmetric, annular, and planar geometries can all be analyzed as the distance from the axis to the inner boundary is increased from zero to the limiting value for avoiding roundoff errors.

Once these limits on the axis-to-throat distance were established, a second series of studies was performed to observe the behavior of the transonic series solution over a wide range of parameters for nozzles with circular arc contours. The parameters involved in the analysis are: γ, the specific heat ratio of the flowing gas; η, the parameter in the expansion variable definition, Eq. (III-22); the geometrical configuration of the nozzle including y_i, R_{ci}, R_{co}, and β; and the number of terms of the expansion solution to be included, i.e., first, second, or third order solutions. There are an infinite number of possible geometries and values of γ and η as well as the three possible solution orders which can be investigated. Obviously, then, these must be limited in a significant and useful way in

order to effectively study the solution behavior. First, it was found that the solutions are not strongly dependent on γ so that only the usual diatomic value of 1.4 was used. Hence, it is assumed that the analysis correctly predicts the weak parametric dependence upon this physical property. Five values of n were employed, n = 0, 0.5, 1, 2, and 4, and each of the three solution orders was considered. In addition, twelve total configurations were analyzed with three values of the radius of curvature, R_c = 0.625, 2, and 5, utilized in each of four groups of geometries. These configurations are defined and shown in Fig. III.2: (1) conventional axisymmetric; (2) annular axisymmetric with the outer boundary straight and parallel to the axis of symmetry, y_i = 2; (3) annular with the inner radius of curvature twice that of the outer and the x-axis inclined at roughly + 20° to the axis of symmetry, $y_i \cong 5.3$; and (4) an approximately plane symmetric *configuration* with y_i = 100. The value R_c = 0.625 was chosen since a dimensionless wall radius of curvature less than unity was desired and this was the radius of curvature value for the axisymmetric nozzle tested by Cuffel, et al. [30]. As mentioned in Chapter II, this is the only experimental investigation to date in which flowfield measurements have been obtained for an axisymmetric configuration.

With these 60 combinations of nozzle geometry and n, the following studies were performed. For each case, the M = 0.8, 1.0, and 1.2 constant Mach number contours were first found and plotted as one, two, and three terms of the expansion solution were included. These plots provide graphical information concerning the convergence properties of the solution over the range of parameters investigated. The convergence was further studied

by printing the quantities $u_1\varepsilon$, $v_1\varepsilon$, $u_2\varepsilon^2$, $v_2\varepsilon^2$, $u_3\varepsilon^3$, and $v_3\varepsilon^3$ at a number of points along the loci of the third order iso-Mach curves and noting whether the following inequalities were satisfied: $|u_2\varepsilon| < |u_1|$, $|u_3\varepsilon| < |u_2|$, etc. . In a similar manner, the discharge coefficient inequalities, $|C_{D2}\varepsilon| < |C_{D1}|$ and $|C_{D3}\varepsilon| < |C_{D2}|$, were also investigated for each configuration. Satisfaction of these inequalities indicates that the series solution is convergent for the combination of parameters under consideration.

The final set of tests in this series involved evaluating the u and v velocity components from the first, second, and third order solutions at a number of points along the third order M = 0.8, 1.0, and 1.2 constant Mach number curves and substituting these values into the exact governing equations. In this context "exact" is used to denote a form of the equations in which no order of magnitude simplifications have been made or expansions assumed. The equations which were utilized in this study are irrotationality condition (III-8) and gas dynamic equation (III-9), repeated here for convenience,

$$u_y - v_x = 0 \tag{III-8}$$

$$\left(1-u^2 - \frac{\gamma-1}{\gamma+1} v^2\right)u_x - \frac{4}{\gamma+1} uvu_y + \left(1-v^2 - \frac{\gamma-1}{\gamma+1} u^2\right)v_y + \frac{\left(1 - \frac{\gamma-1}{\gamma+1} u^2 - \frac{\gamma-1}{\gamma+1} v^2\right)(v\cos\beta + u\sin\beta)}{y\cos\beta + x\sin\beta} = 0 . \tag{III-9}$$

Whereas the identical satisfaction of the equations and boundary conditions in the expansion formulation, Eqs. (III-38)-(III-42) and (III-48)-(III-53), verifies the details of the solution development as discussed in the preceding section, the size of the residuals in the exact equations above provides a

measure of the validity of the approximations made during the course of the formulation. Comparison of the residuals among the various cases studied also allows conclusions to be drawn concerning the effects of the parameters on the various assumptions and approximations which have been made. As in the solution verification studies, the derivatives in the exact governing equations have been approximated by second order, finite differences with a grid spacing of $\Delta x = \Delta y = 10^{-4}$.

The exact boundary conditions that the velocity vector be tangent to the bounding walls was also checked along each contour from the M = 0.8 location to the M = 1.2 location. This interval was widened in order to include the throat station for those cases in which it was not already included. The exact boundary conditions were investigated in the form,

$$\left[\frac{dR}{dZ} - \tan(\theta+\beta)\right]_{G(R,Z)=0} = 0 \qquad \text{(III-83)}$$

$$\left[\frac{dR}{dZ} - \tan(\theta+\beta)\right]_{H(R,Z)=0} = 0 \ , \qquad \text{(III-84)}$$

where G(R,Z) = 0 and H(R,Z) = 0 are the equations of the inner and outer contours and $(\theta+\beta)$ is the inclination angle of the velocity vector in the cylindrical R-Z coordinate system.

The basic purpose of these studies was to investigate in an organized and rational manner the convergence properties of the solution and to determine if an optimum value of the parameter η could be found that provided improved solution convergence and simultaneously minimized the residuals in the exact governing equations and boundary conditions. The main conclusions of this investigation are discussed below.

(1) As expected from the problem formulation, all orders of the expansion solution identically satisfy both the exact irrotationality condition and the boundary conditions for straight walls. Therefore, the significant tests are the residuals for the exact gas dynamic equation and for the boundary conditions at curved contours, as well as the convergence properties of the series solution.

(2) For the smallest wall radius of curvature tested in each of the groups of geometries, $R_c = 0.625$, the solutions are highly divergent for $\eta = 0$, Fig. III.3. This behavior is also expected since for $\eta = 0$ the solutions correspond to those of Hall [35] who used the expansion parameter $\varepsilon = R_c^{-1}$, and for $R_c < 1$ this expansion parameter exceeds unity. As η is increased for these configurations, the convergence of the solutions is dramatically improved, Fig. III.4, although for the highest value tested here, $\eta = 4$, the solutions tend to be only slowly convergent, especially away from the sonic line. Interestingly, as η is increased from zero for these small radius of curvature geometries, the convergence of the higher Mach number contours is improved first.

(3) For configurations with large radius of curvature boundaries, the high subsonic, i.e., $M = 0.8$, constant Mach number contours are less convergent than the low supersonic, i.e., $M = 1.2$, ones for $\eta = 0$, Fig. III.5. For larger values of η, improved convergence of the high subsonic iso-Mach curves is obtained somewhat at the expense of the convergence of the low supersonic ones, Fig. III.6. It should also be mentioned that for nozzles with a large throat wall radius of curvature, there is little difference between the third order constant Mach number contours for various values of η.

(4) For $\eta = 0$, the expansion solution is generally an alternating series, such that the third order iso-Mach curve for a particular Mach number lies between those of the first and second order, Fig. III.7. As η is increased, the nature of the solution gradually changes until at $\eta = 4$ it is a slowly convergent, non-alternating type series, Fig. III.8.

(5) For geometries and values of η for which the solutions are convergent, the residuals in the gas dynamic equation are generally reduced as the order of the solution is increased from the first to the second to the third order. The residuals in the boundary conditions for the circular arc boundaries are also generally reduced as the higher order solutions are utilized with this trend becoming very strong as η is increased from zero.

(6) It appears that the dependence of the residuals in the gas dynamic equation upon η is directly related to the convergence of the series solution. Thus, those values of η which result in improved convergence properties for the expansion solution also generally result in reduced residuals in the gas dynamic equation.

(7) The residuals in the exact boundary conditions for the circular boundaries are *increased* near the throat location as η is increased from zero, particularly for the larger values of η. This behavior is consistent with the observations from Eqs. (III-32) and (III-33) that the second derivatives in the Maclaurin series expansions for the wall contours are exactly matched only for $\eta = 0$ and that the approximations deteriorate progressively as η is increased.

(8) As found by previous investigators, the geometrical parameter which is by far the most influential is the radius of curvature of the

bounding walls. For nozzles having a large radius of curvature, the solution behavior is generally improved over that for nozzles with sharp throat curvature, i.e., the residuals in the gas dynamic equation and boundary conditions are reduced and the solutions are more convergent. This behavior is, of course, expected since the expansion parameter has been defined as $\varepsilon = \left(R_c + \eta\right)^{-1}$. The parametric effects on the solution behavior of the distance of the nozzle throat from the axis of symmetry and the inclination of the main flow x-direction from the axis are generally negligible so that the dependence of the solution on η, the solution order, and the wall radius of curvature discussed previously are repeated in each of the four groups of geometries sketched in Fig. III.2. Two exceptions to this statement are:

(a) For cases in which both boundaries are curved it appears that the shift in solution nature from an alternating type series to a non-alternating one occurs at lower values of η than for those cases in which one boundary is straight.

(b) For the smallest radius of curvature cases tested in each of the four geometrical groups, the solution for the conventional axisymmetric configuration, $y_i = 0$, appears to be the best behaved. For the other three sharp curvature cases, the M = 0.8, and in two cases, the M = 1.0 contours were found not to intersect the highly curved wall, Fig. III.9.

Based on the preceding observations, it is concluded that third order solutions should generally be used. Also, for configurations with a large

wall radius of curvature, the expansion solution is essentially independent of η. However, for geometries with small radius of curvature walls, two competing effects appear: as η is increased from zero the convergence of the series solution is improved significantly, but the satisfaction of the exact boundary conditions in the throat region is compromised, especially for the largest value tested, $\eta = 4$. Ideally, then, the smallest value of η for which the convergence properties in the region of interest are deemed satisfactory should be employed. For general use $\eta = 2$ is recommended.[†]

Third order, $\eta = 2$ solutions are compared to two existing data sets in Figs. III.10 and III.11. In the first figure comparison is made to the data of Cuffel, et al. [30] for an axisymmetric nozzle with a dimensionless wall radius of curvature of $R_c = 0.625$. As mentioned in Chapter II, this data was obtained by means of a small diameter, hollow tube which was stretched between an upstream stagnation chamber and a downstream vacuum chamber. This small value or R_c provides a severe test for the expansion solution, and as can be seen in the figure, the results are in reasonably good agreement with the data through the throat region except for the high subsonic Mach numbers, $M = 0.6$ and $M = 0.8$. In particular, the $M = 1.2$ contour appears to provide an accurate starting line for initiating the hyperbolic computations for the supersonic region. In Fig. III.11 the results of the series solution are compared to the sonic line data of Flack and Thompson [14] for a planar, symmetric nozzle with a wall curvature of $R_c = 2$. The experimental information was determined by using static pressure measurements obtained from

---

[†]The equivalent recommended value for the simplified, conventional axisymmetric solution, Appendix C, is $\eta = 1$.

pressure taps located in the sidewalls of the nozzle. For the theoretical results, the plane, two-dimensional geometry has been approximated by an annular configuration located a very large dimensionless distance from the axis of symmetry, $y_i = 1000$. As shown in the figure, the analytical and experimental sonic lines are of the same shape with the measurements lying somewhat downstream of the series results. The agreement is within approximately 3 percent, however, since calculation of the Mach numbers along the experimental sonic line using the expansion solution results in values of about 1.03.

As a result of the parametric studies and comparisons presented in this section, it is felt that the approximate solution which has been developed is applicable to a wide variety of nozzle configurations including axisymmetric, annular, and planar ones. As long as the radius of curvature of the bounding walls is of the order of the throat half-height or larger, and as long as attention is restricted to the transonic throat region, $x = O\left(\epsilon^{1/2}\right)$, with the inclination angle satisfying the restriction, $\beta_1/y = O(1)$, satisfactory results are expected. Further comparisons between the theoretical solution and experimental measurements obtained during the course of this investigation are presented in the next chapter.

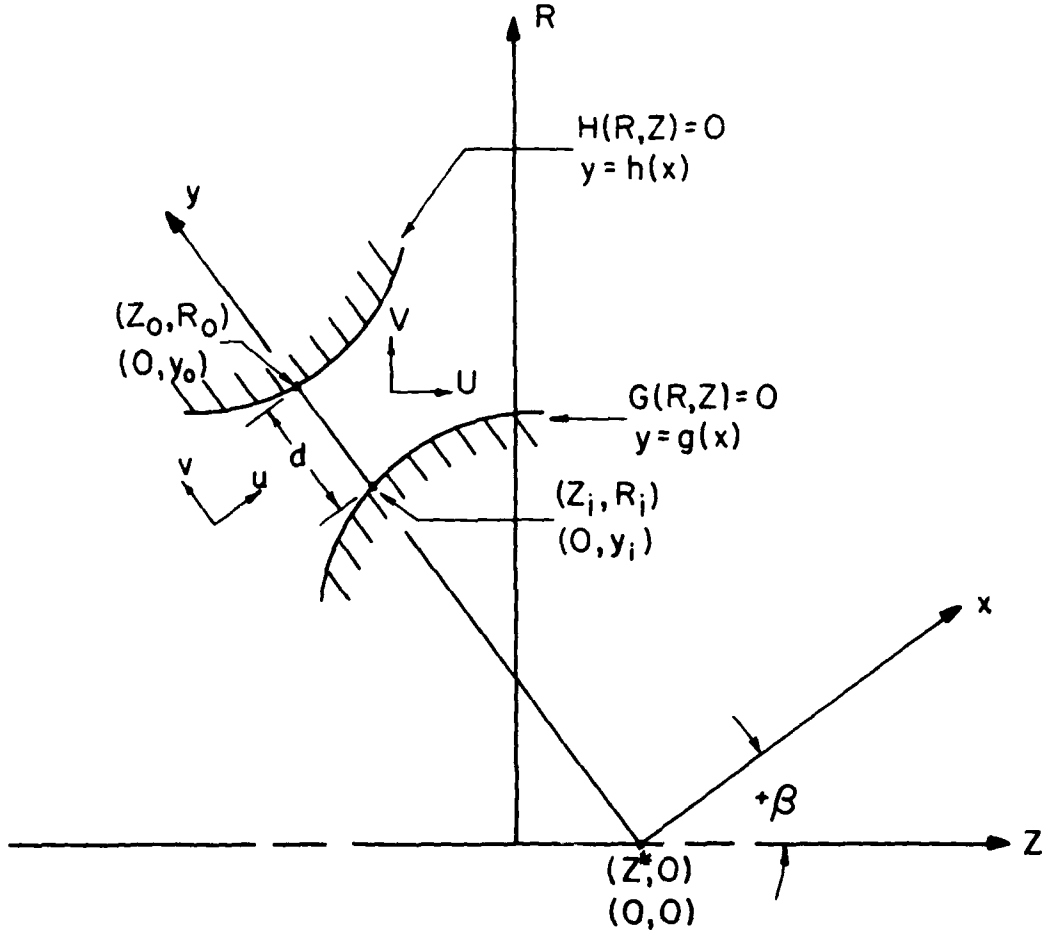

Figure III.1 Configuration for throat flowfield analysis of annular supersonic nozzles

Table III.1 Solution Tests

I. Reduction to Previous Solutions for Simpler Geometries

A. Reduction to Conventional Axisymmetric Configuration as $y_i \to 0$

1. $\eta = 0$ -- Hall [35], with corrections by Kliegel and Levine [46].
2. $\eta = 2$ -- Dutton [87].

B. Reduction to Planar Symmetric Configuration as $y_i \to \infty$

1. $\eta = 0$ -- Hall [35].
2. $\eta = 2$ -- Dutton [87] and Thompson and Flack [37].

C. Reduction to Annular Axisymmetric Configuration with One Boundary Straight and Parallel to the Axis of Symmetry.

1. $\eta = 2$, $g''(0) = 0$ -- Dutton [87].
2. $\eta = 2$, $h''(0) = 0$ -- Dutton [87].

II. Independent Numerical Back Substitution into the Governing Equations and Boundary Conditions (Derivatives approximated with finite differences)

Table III.2 Roundoff Error Investigation

(a) Approximate values of y_i at which roundoff error† affects solutions for perturbation velocity components:

	Single Precision	Double Precision
First Order (u_1, v_1)	3000	10^7
Second Order (u_2, v_2)	60	30,000
Third Order (u_3, v_3)	15	1000

(b) Approximate values of y_i at which roundoff error† affects solutions for discharge coefficient constants:

	Single Precision	Double Precision
First Order (C_{D1})	120	50,000
Second Order (C_{D2})	20	1500
Third Order (C_{D3})	10	250

†On the University of Illinois CDC Cyber 175 digital computer

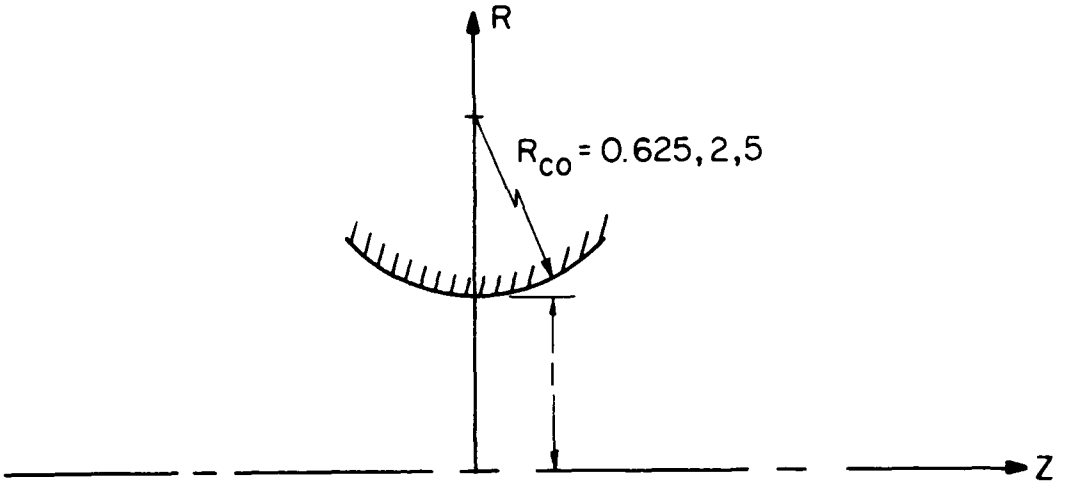

(a) Conventional axisymmetric

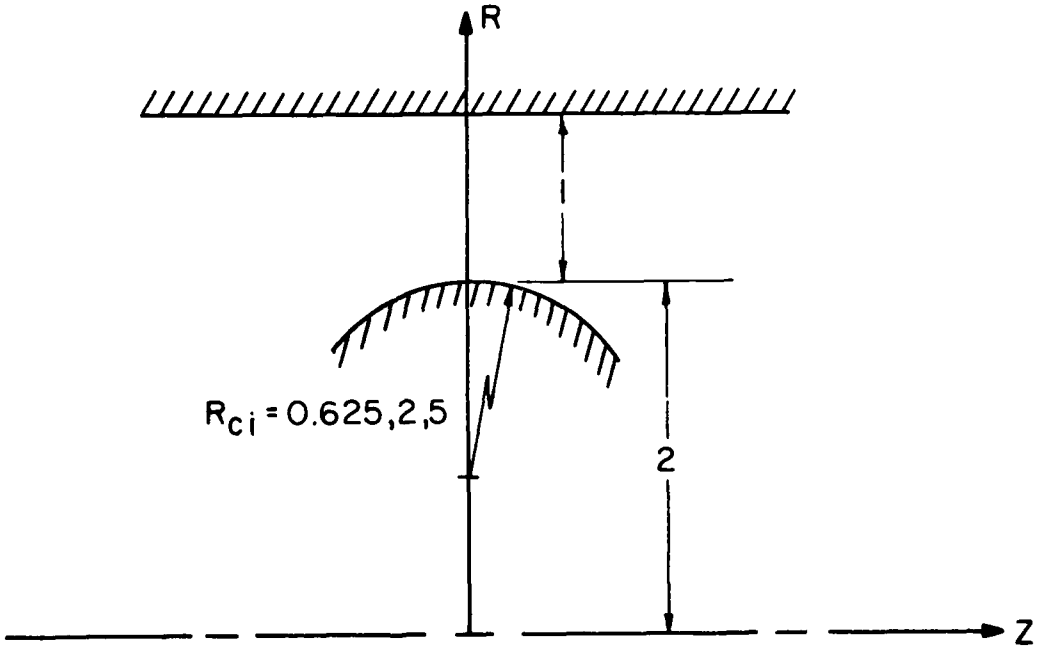

(b) Annular axisymmetric with straight outer boundary, $y_i = 2$

Figure III.2 Configurations for parametric study of solution behavior

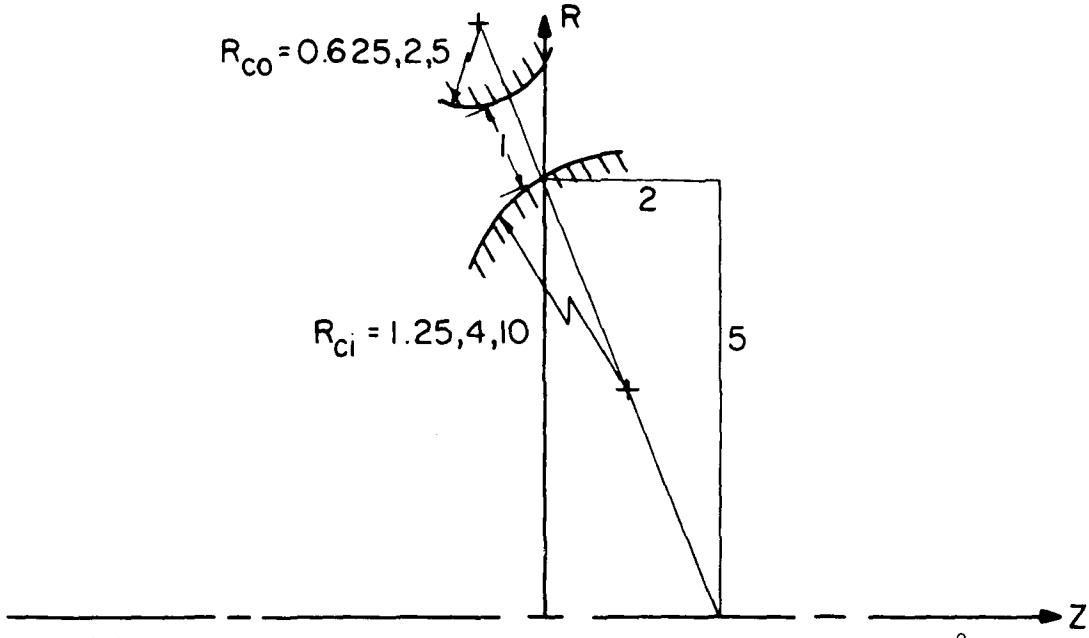

(c) Inclined, annular axisymmetric with $R_{ci} = 2R_{co}$, $\beta \cong +20^{\circ}$, $y_i \cong 5.3$

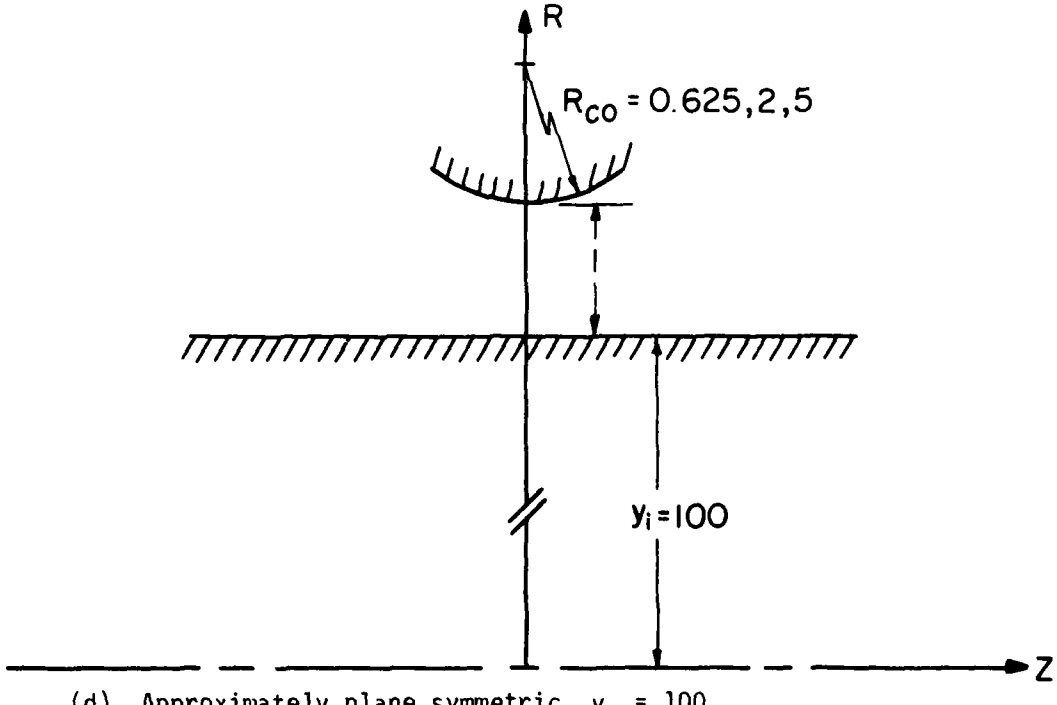

(d) Approximately plane symmetric, $y_i = 100$

Figure III.2 (cont.) Configurations for parametric study of solution behavior

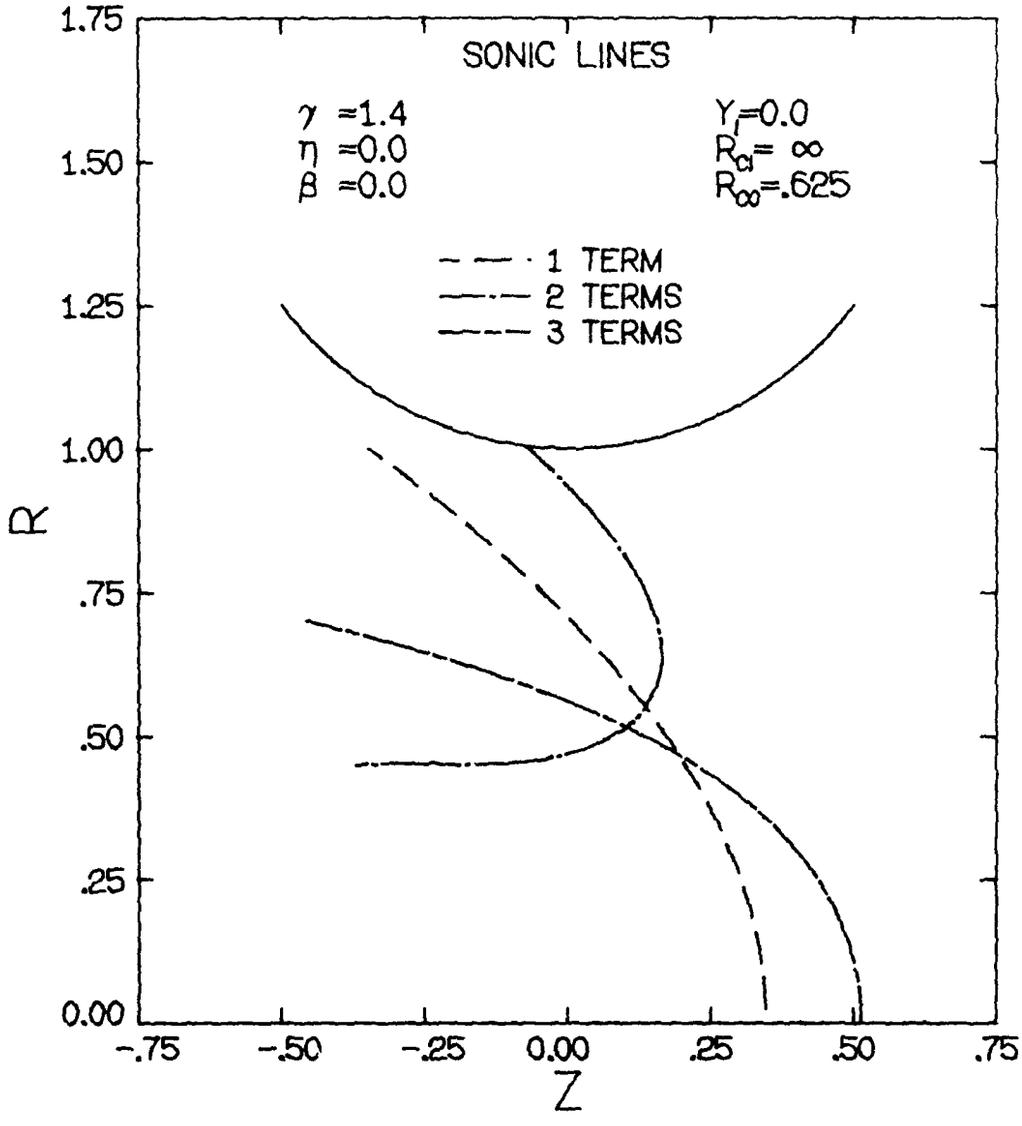

Figure III.3 Sonic lines for axisymmetric configuration, R_{co} = 0.625, η = 0

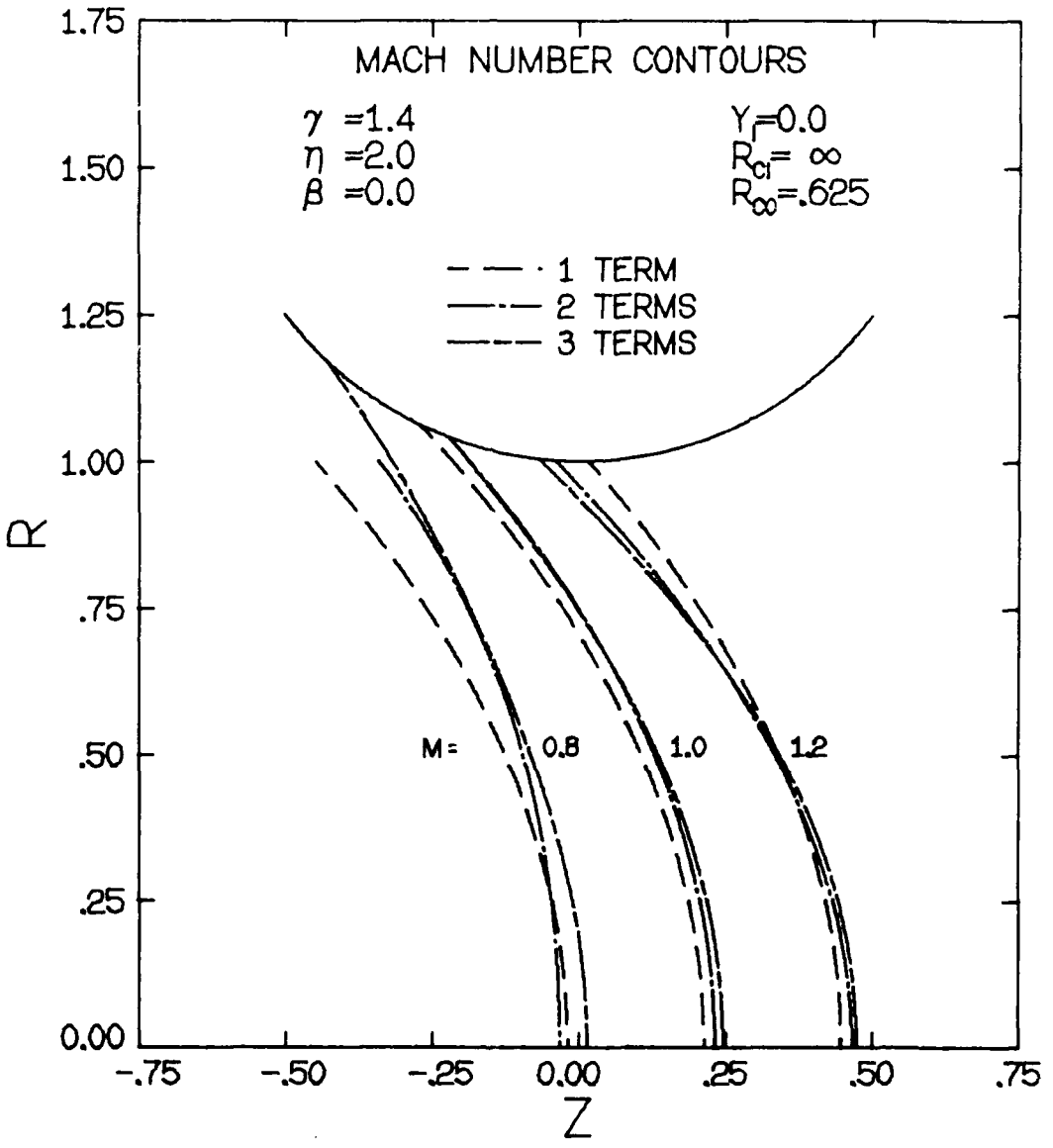

Figure III.4 M = 0.8, 1.0, and 1.2 contours for axisymmetric configuration, R_{co} = 0.625, n = 2

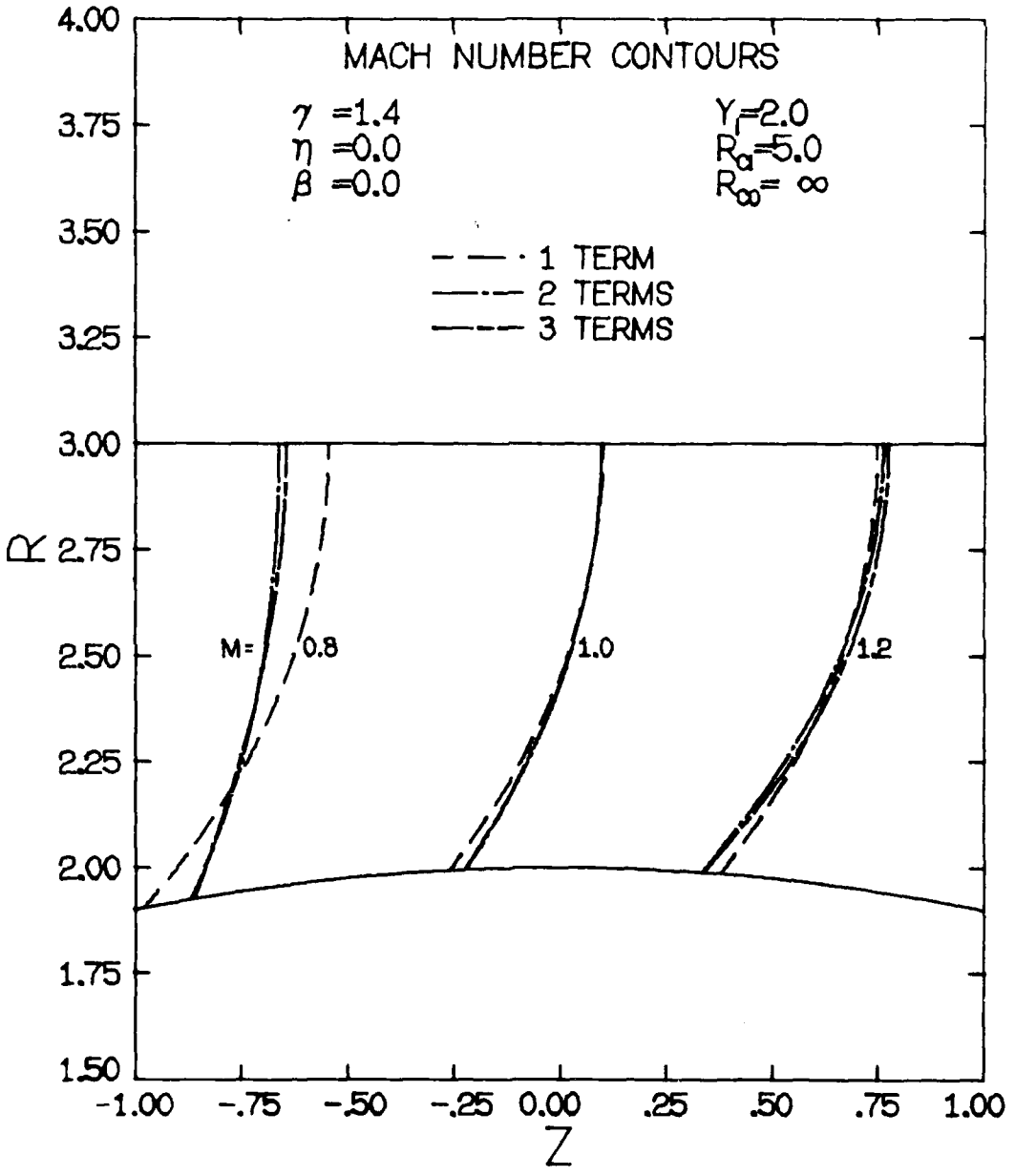

...urs for annular configuration.

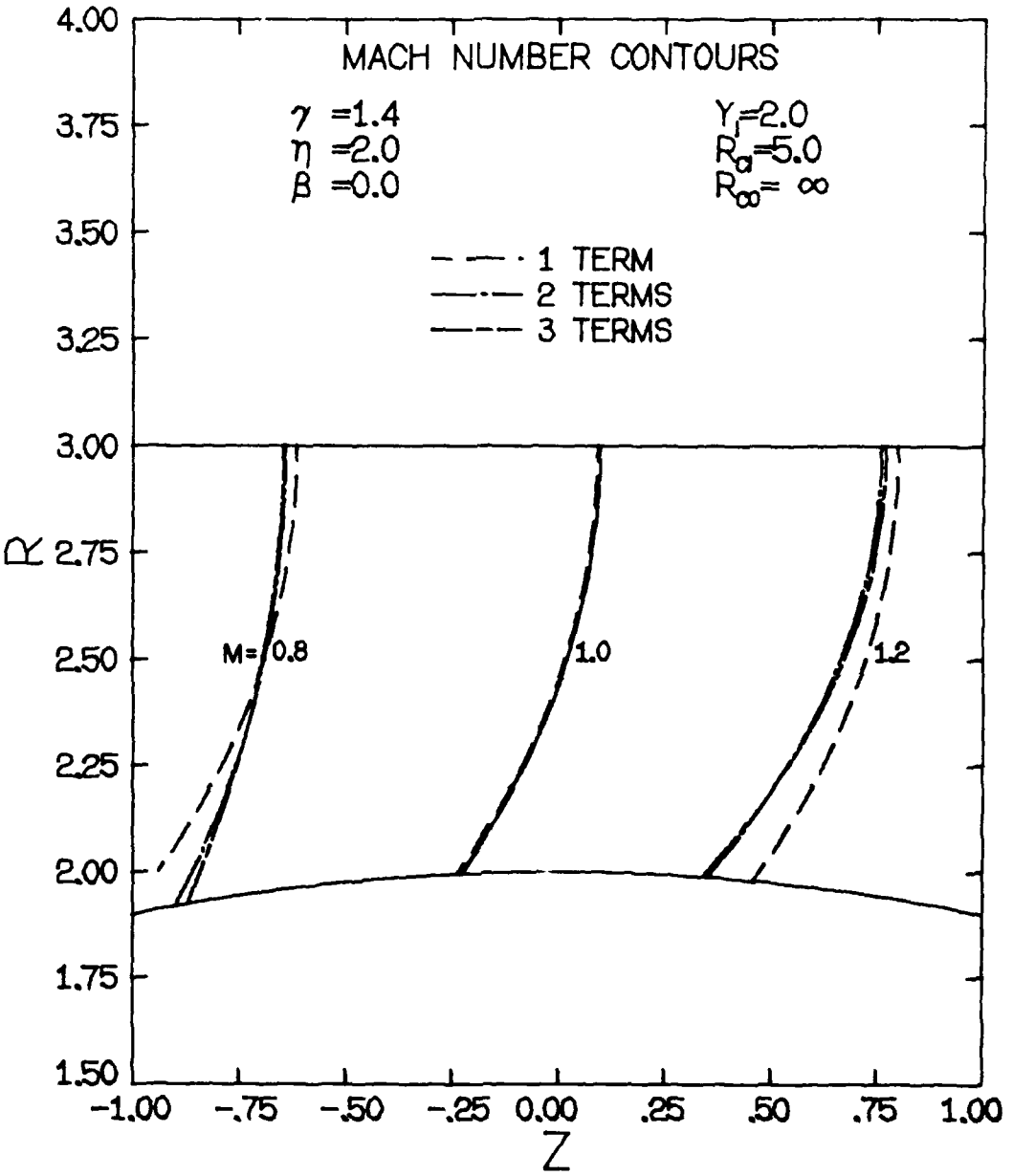

Figure III.6 M = 0.8, 1.0, and 1.2 contours for annular configuration, $R_{ci} = 5$, $y_i = 2$, $\eta = 2$

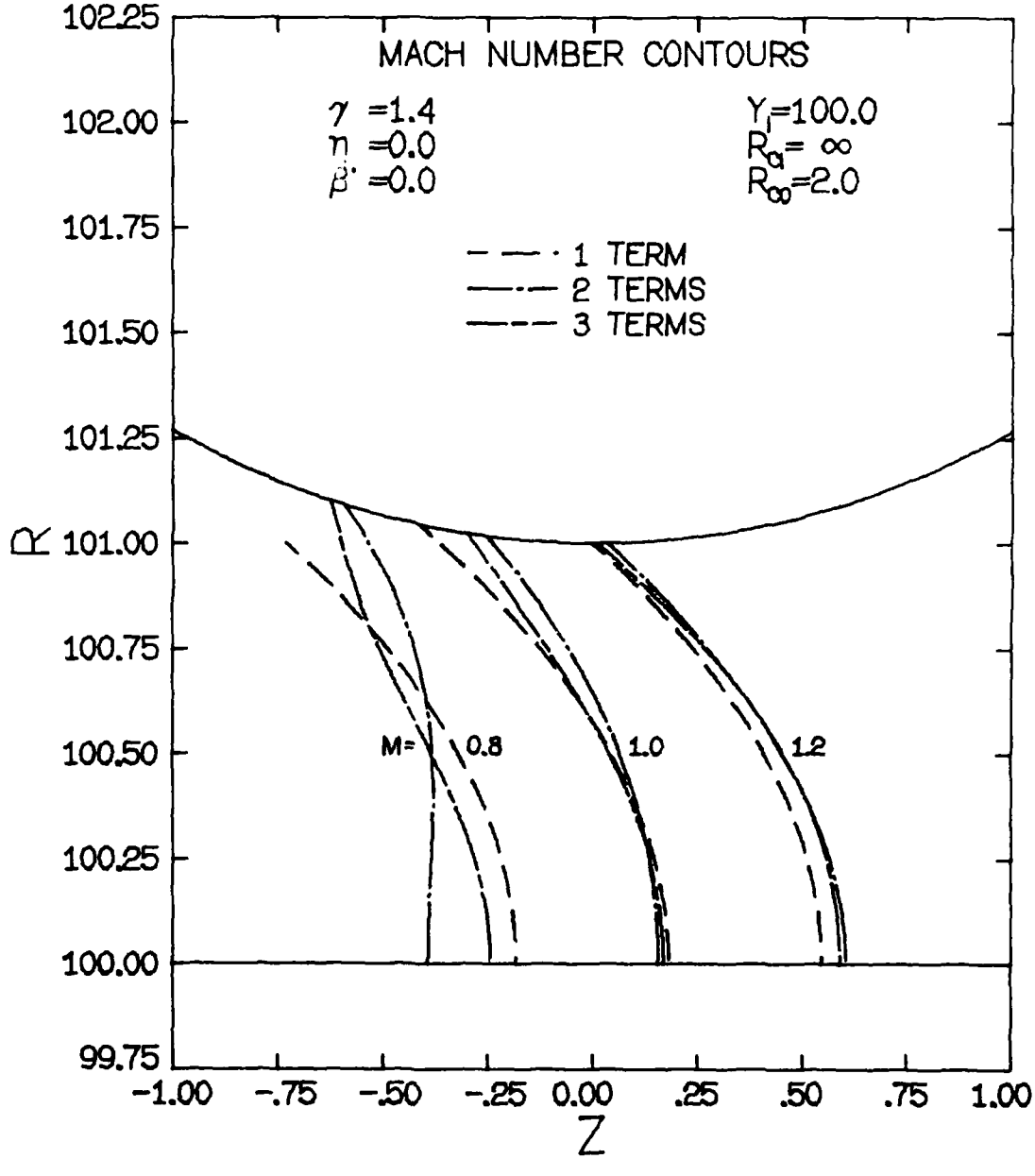

Figure III.7 M = 0.8, 1.0, and 1.2 contours for approximately planar configuration, R_{co} = 2, y_i = 100, η = 0

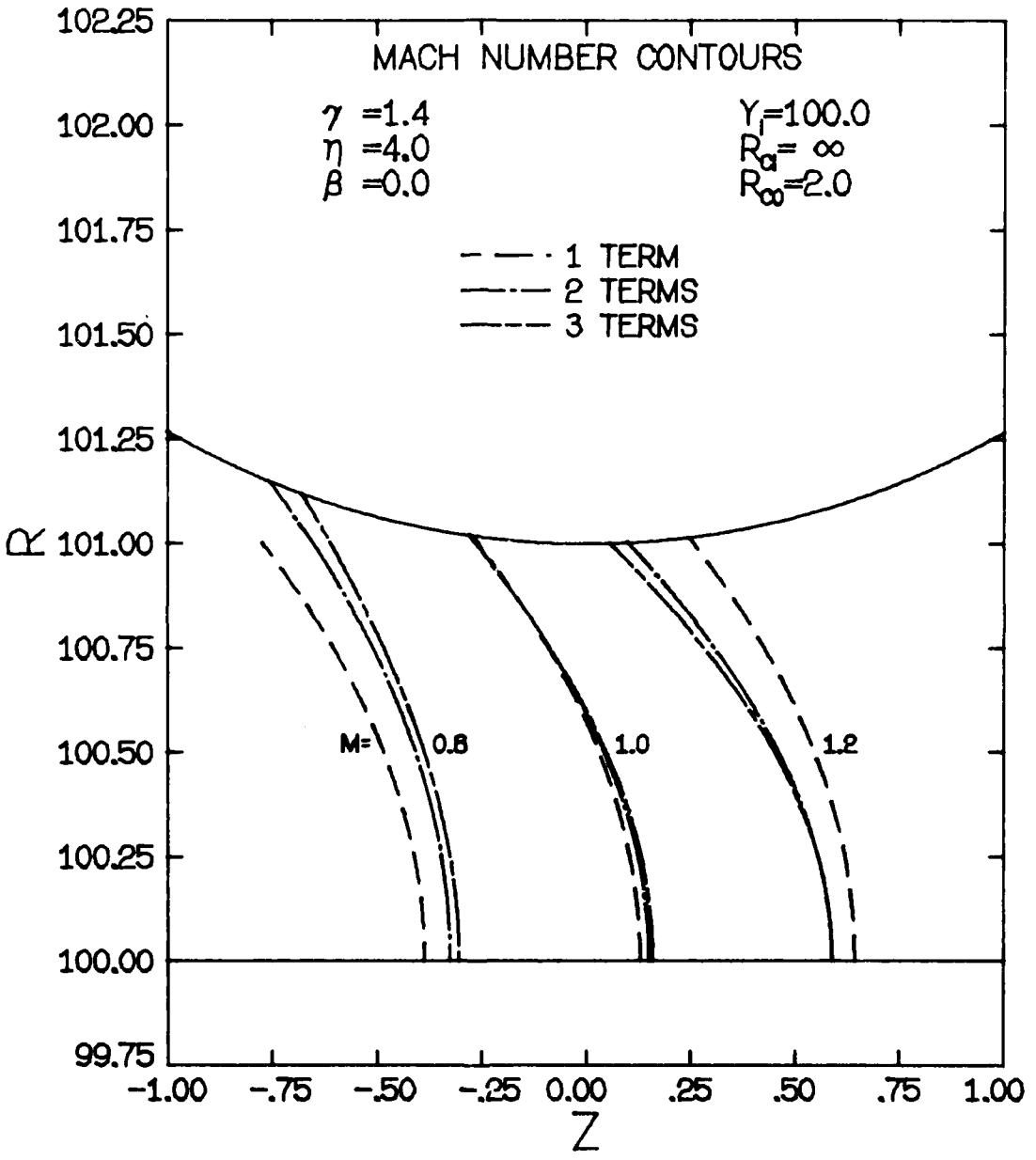

Figure III.8 M = 0.8, 1.0, and 1.2 contours for approximately planar configuration, R_{co} = 2, y_i = 100, η = 4

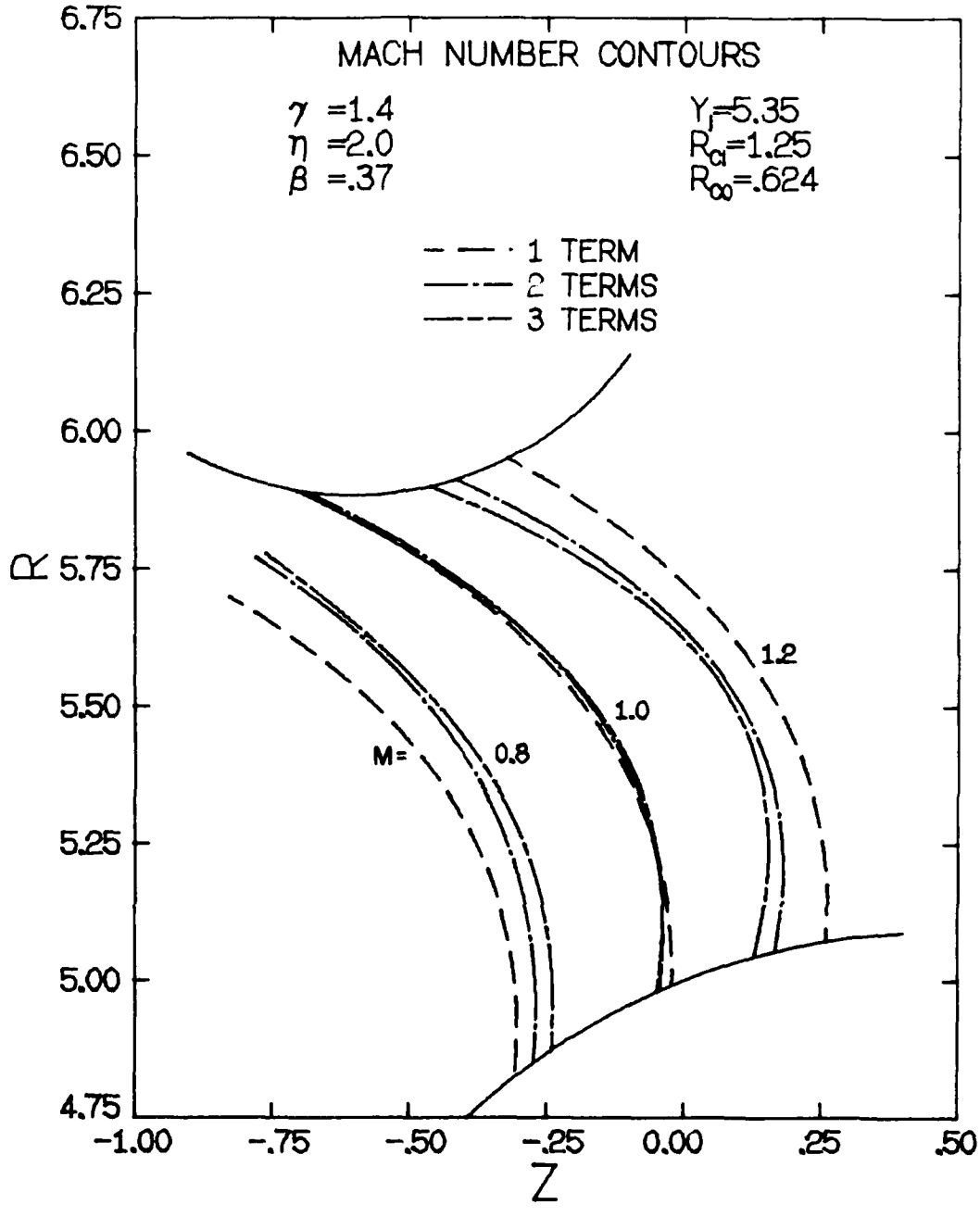

Figure III.9 M = 0.8, 1.0, and 1.2 contours for annular configuration, R_{co} = 0.625, R_{ci} = 1.25, $\beta \cong +20^{\circ}$, $y_i \cong 5.3$, $\eta = 2$

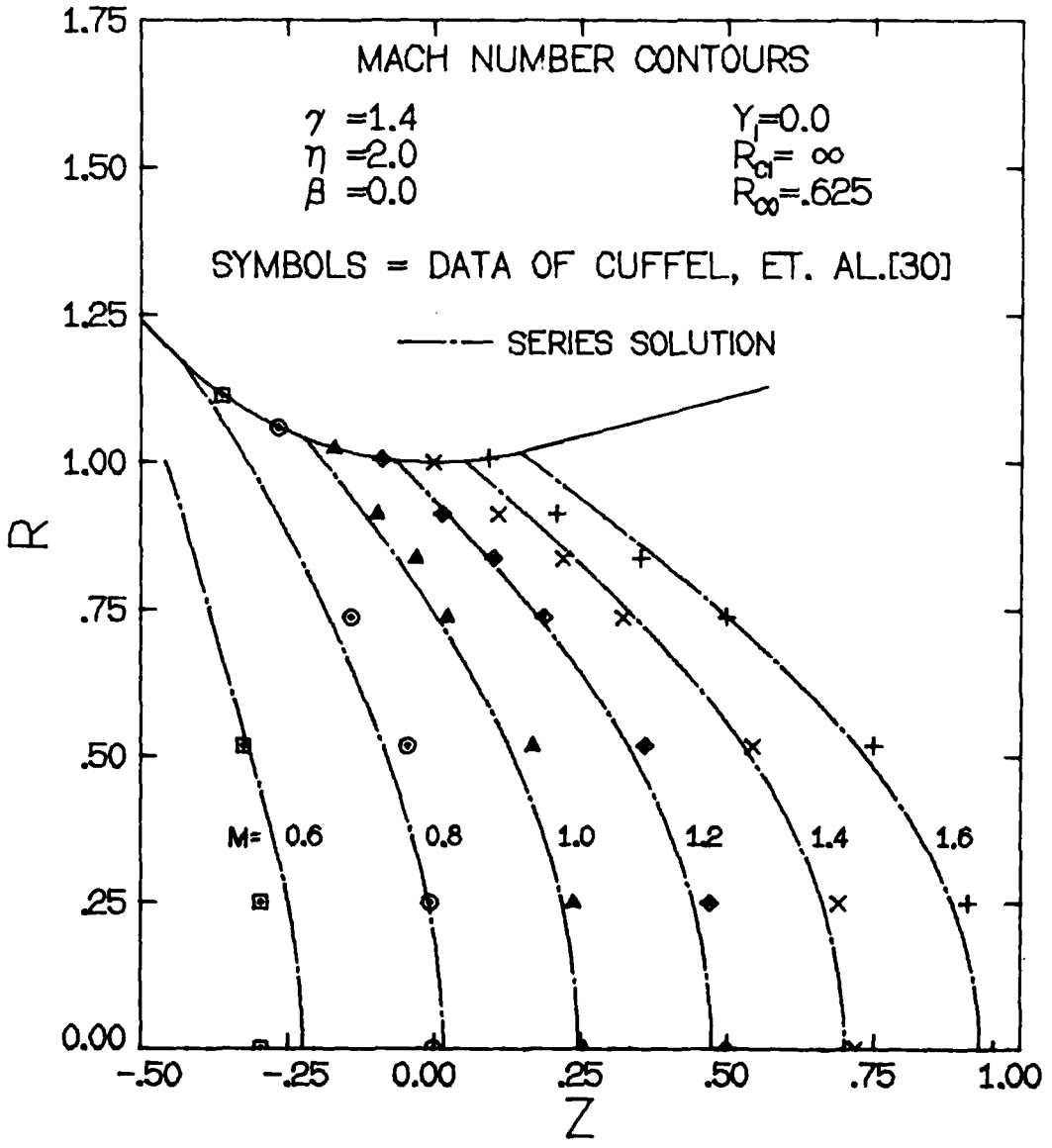

Figure III.10 Comparison of third order, $\eta = 2$ solutions to data of Cuffel, et al. [30] for an axisymmetric nozzle with $R_{co} = 0.625$; $Re_{2d} = 2.8 \times 10^6$ for experiments

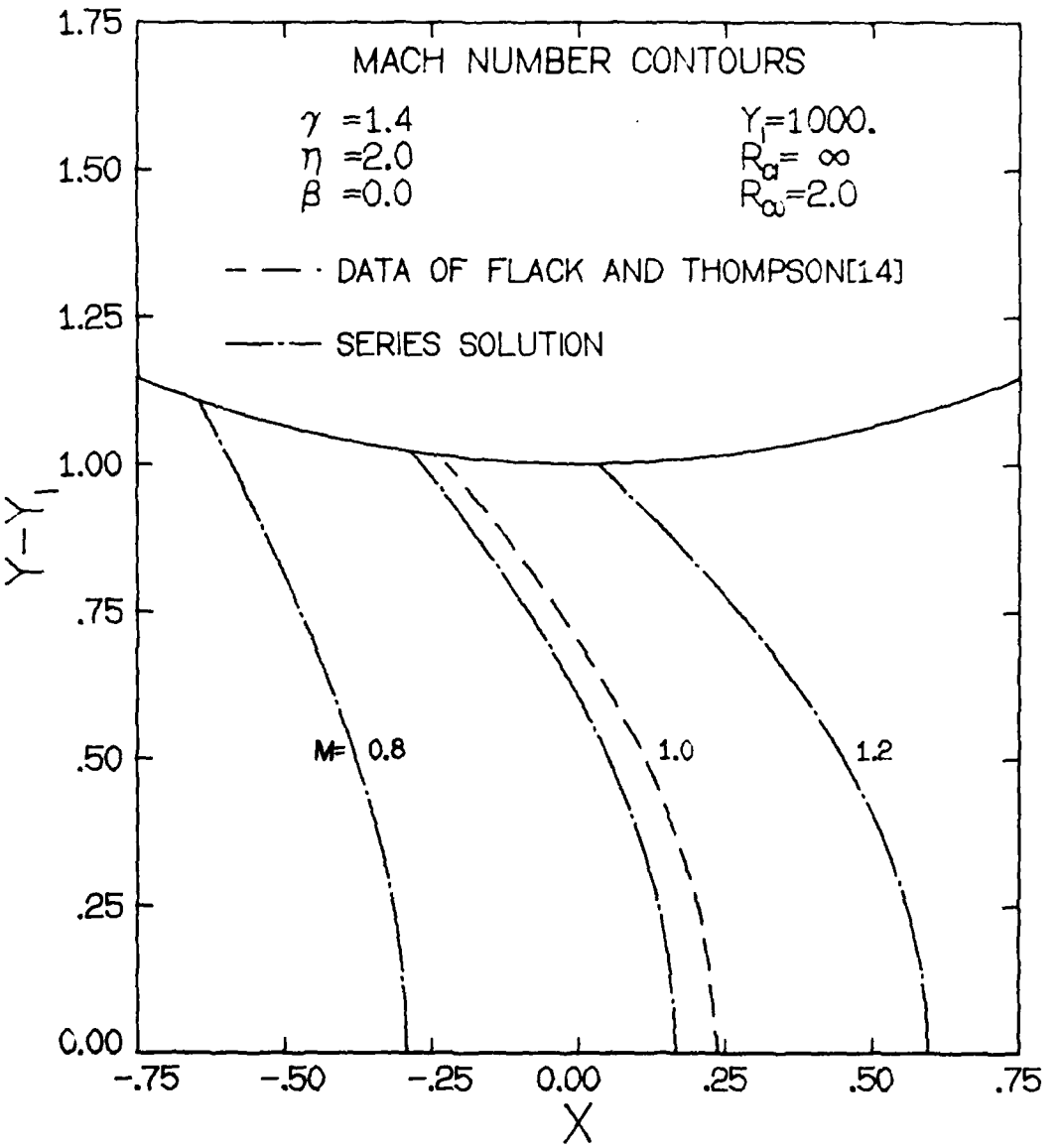

Figure III.11 Comparison of third order, $\eta = 2$ solutions to data of Flack and Thompson [14] for a planar nozzle with $R_{co} = 2.0$; average $Re_{2d} = 8.6 \times 10^6$ for experiments

IV. EXPERIMENTAL INVESTIGATION

As discussed in the literature survey, there have been few experimental studies of supersonic nozzle throat flows, particularly in terms of flowfield measurements for axisymmetric configurations. For this reason, an experimental investigation was performed to obtain flowfield pressure distributions for a number of annular nozzle geometries including a conventional axisymmetric nozzle. For the annular configurations, these measurements are the first ones known to consider more than just the wall pressure distribution along one of the bounding walls, while the data of Cuffel, et al. [30] is the only other set of flowfield data for the axisymmetric, no-centerbody case. The resulting measurements provide a basis of comparison in order both to verify the theoretical solution developed in the preceding chapter and to draw conclusions regarding its range of applicability.

A. EQUIPMENT AND APPARATUS

The main objections to the stretched tube technique employed in [30] to obtain the nozzle throat flowfield pressure distributions are that the tube introduces disturbances of unknown magnitude into the flowfield and for off-axis positions the velocity vector is not necessarily parallel to the tube. Rather than using this method, the one which has been utilized in this study is the splitter-plate technique whereby half-section cylindrical models were constructed and mounted on a plate whose surface corresponds to a symmetry plane for the axisymmetric geometry. Pressure taps were placed on the splitter plate in the transonic region of interest from which the desired transverse and streamwise pressure distributions were obtained.

The splitter plate also introduces disturbances into the flowfield in the form of the boundary layers which grow both on the plate and in the corners where the half-models meet the plate. These boundary layers, of course, are not present for the full axisymmetric configuration. However, for the high Reynolds number, favorable pressure gradient, nozzle flows under consideration, the boundary layers in the throat region are extremely thin. In fact, sample calculations using the code developed in [88] show that for the models and typical operating conditions used here, the boundary layer displacement thickness in the throat region is less than 0.05 mm which is less than 0.2% of the throat diameter in the worst case. It is therefore felt that the measurements obtained with the half-section models correspond closely to the "true" measurements for the full axisymmetric geometries. To further test this hypothesis both a full-section and the corresponding half-section models were constructed for a conventional axisymmetric nozzle configuration. Comparison of the wall pressure measurements from the two models then allows conclusions to be drawn regarding the effects of the splitter boundary layers. The results of these experiments will be reported in a later section.

Figure IV.1 is a photograph of the full section axisymmetric nozzle which was designed and constructed showing the wall pressure taps which were spiraled around the circumference of the nozzle through the throat region. Also visible in this photograph are the last few static holes which were carefully drilled normal to the wall contour; all burrs and irregularities were removed at the wall in the vicinity of the pressure taps. Unless specifically stated otherwise, the static holes all have the same diameter

of 0.51 mm and the model material is aluminum. Figure IV.2 shows the corresponding half-section axisymmetric model. The half-nozzle in the right background is mounted on the splitter plate in the foreground where the flow direction is from left to right. The entrance plate, which forms the left half of the splitter plate, fits inside an existing axisymmetric converging nozzle whose elliptic entrance section matches the curved boundaries of the entrance plate. The blocking flange in the left background is attached and sealed to the bottom of the splitter plate so that no flow is allowed to leak through the test section under the plate. In addition to the 8 wall taps on the half-nozzle which were used to obtain the wall pressure distribution for comparison with that of the full nozzle, 71 static pressure taps were located on the splitter plate so that the flowfield pressure distributions could be measured for this axisymmetric nozzle. These taps have been arranged in 12 staggered rows thereby providing throat region pressure measurements in a square grid, 3.81 mm on a side. It should also be mentioned that when the experiments were performed, the screw heads seen on the surface of the entrance plate were filled in with epoxy and sanded so that the entire surface of the splitter plate was extremely smooth and highly polished.

In order to obtain data for annular configurations, the centerbody shown in Fig. IV.3 is added. It should be noted that in terms of the theory presented in the last chapter, only the central portion of the centerbody, whose radius of curvature in the meridional plane is 50.8 mm, is of importance. The cylindrical sections upstream and downstream of this region merely provide a means for attaching the centerbody to the splitter plate. By displacing the centerbody relative to the outer nozzle, measurements for various

annular configurations could be made. As will be discussed in more detail in a later section, three such configurations were investigated. The splitter plate in this case is *not* the same one used for the conventional axisymmetric geometry of Fig. IV.2 since a slot is required for the centerbody wall taps and dowel pin and bolt holes are required to locate and hold the centerbody on the plate. The pressure taps on the splitter plate in this case have been arranged in 10 alternating rows of 5 taps each so that pressure measurements in a square, 3.18 mm grid are obtained. The measurements from these 50 splitter plate taps together with the 9 centerbody wall taps and the 8 nozzle wall taps allow the pressure field in the annular nozzle throat to be completely mapped.

Two views of the assembled apparatus of Fig. IV.3 are shown in Figs. IV.4 and IV.5. In Fig. IV.4, the view is in the downstream flow direction through the test section. In viewing this photograph, it should be remembered that the entrance plate is highly polished aluminum so that everything seen on its surface is a reflection from the half-nozzle mounted on the splitter plate. The pressure tap grid is detailed in Fig. IV.5, which looks upstream through the measurement region. The shorter row of taps seen below the plate is the set which passes through the slot in the splitter plate and is attached to the centerbody for measurement of its wall pressure distribution. In assembling the half-section models, Loctite anaerobic adhesive was used on all of the flat mating surfaces and silicone rubber sealant was also employed along all seams in noncritical regions. Together with the O-rings which were utilized between mating flanges, this sealing method prevented the occurrence of leaks in the half-model test sections.

A photograph of the partially assembled, annular, supersonic nozzle test section, as it is mounted on the brass converging inlet nozzle, is given in Fig. IV.6. The converging nozzle, in turn, is bolted to the faceplate of one of the test stands in the supersonic wind tunnel area of the Mechanical Engineering Laboratory. However, the supersonic jet cannot simply be exhausted to ambient conditions because of the very high noise levels associated with such a jet. Instead, the test section is connected to the facility silencing system. In this arrangement the supersonic jet exhausts into a viewing chamber which also contains a conically convergent jet-catcher/diffuser. A view of the annular nozzle test apparatus as seen through one of the side windows of the exit chamber is shown in Fig. IV.7. Downstream of this chamber the jet flow enters a double-walled silencing duct before passing through a final silencer and exiting to atmosphere outside of the laboratory. An overall view of the assembled test apparatus is given in Fig. IV.8 showing the first few feet of the double-walled silencing duct at the right. Dry, filtered, compressed air is supplied to the stagnation test chamber by a Gardner-Denver screw compressor through a 140 m^3 tank farm and a 152.4 mm supply line. The pressure in the stagnation chamber is regulated by means of a Fisher-Governor automatic controller and control valve. A schematic of the air flow circuit is presented in Fig. IV.9.

Pressures were measured with two CEC type 4-312 unbonded strain gage pressure transducers. A 0-700 kPa gage transducer was utilized in conjunction with a 48-port, motor-driven model J Scanivalve to record the test section static pressures. The stagnation chamber pressure was also continuously monitored by means of a 0-1000 kPa gage transducer. These pressure signals

were conditioned with two Daytronic model 870 conditioner-amplifier modules. The resulting output signals were recorded from a Daytronic model 890 digital meter and a Keithley model 179 digital voltmeter for the stagnation and static pressures, respectively. Additional equipment used in the course of the experiments is also described in the next section.

B. PROCEDURE

The first step in the experimental procedure involved calibration of the pressure transducers. This was accomplished by using vacuum and pressure sources in conjunction with two pressure measurement standards: a Wallace and Tiernan precision mercury manometer for the 0-200 kPa absolute pressure range and a Wallace and Tiernan bourdon tube absolute pressure gage for the 200-500 kPa range. Of the two devices the precision manometer is the more accurate, but it is limited to the lower pressure range by the allowable height of the mercury column. The calibrations were completed by obtaining linear, least-squares regressions between the digital readings of the output devices and the readings from the precision manometer and the absolute gage. For both transducers the calibration data was found to be extremely linear.

After the hardware for a given model configuration had been assembled, the experimental procedure for each test consisted first of recording the atmospheric pressure from a Setra Systems electronic barometer. The stagnation supply pressure was then set with the Fisher-Governor automatic controller and the static and stagnation chamber pressures read from the digital output devices as the Scanivalve was stepped from port to port with its solenoid controller. Since the half-section models all had more than 48 static taps, which is the number of available Scanivalve ports, approximately

half of the taps were connected to the Scanivalve for a given run and the rest were blocked off. In later tests these connections were reversed. The supply pressure in all of the experiments was approximately 400 kPa. It was not possible to vary this pressure level over a wide range since it had to be high enough to ensure that the measurement region was free from the shock waves which occur due to the exit boundary conditions but low enough so that sufficient time was available to record the data in these blowdown tests. For these reasons the Reynolds number based on sonic conditions and the throat height, Re_{2d}, also was not varied over a wide range.

To check the repeatability of the experiments, five runs were made for each geometrical arrangement. For each tap the data was reduced by calculating the mean and standard deviation of the static-to-stagnation pressure ratio readings, p/p_0, for the five tests. The resulting mean values were used in all of the data presented in the next section. In all cases the experiments were found to be highly repeatable. The standard deviation for a given measurement was generally less than 10^{-3} in units of p/p_0 where this variable spans almost the entire range from unity to zero through the transonic throat region. This corresponds to a Mach number standard deviation of 1.6×10^{-3} at sonic conditions.

Before presenting the experimental results it is appropriate to discuss the accuracy of the equipment used to obtain the pressure measurements. By utilizing micrometers and other precision measurement gages, the critical dimensions of the air flow models, including the static hole locations, were checked and found to be within $\pm$ 0.05 mm of the design specifications. Since the throat diameters of the models range from approximately 32 to 50 mm and

AD-A084 787 ILLINOIS UNIV AT URBANA-CHAMPAIGN DEPT OF MECHANICAL ... ETC(U)
A THEORETICAL AND EXPERIMENTAL INVESTIGATION OF TRANSONIC FLOW ...ETC(U)
JAN 80 J C DUTTON, A L ADDY DAAG29-79-C-0184
UNCLASSIFIED UILU-ENG-80-4001 ARO-13737.1-EX NL

2 OF 2
AD A084787

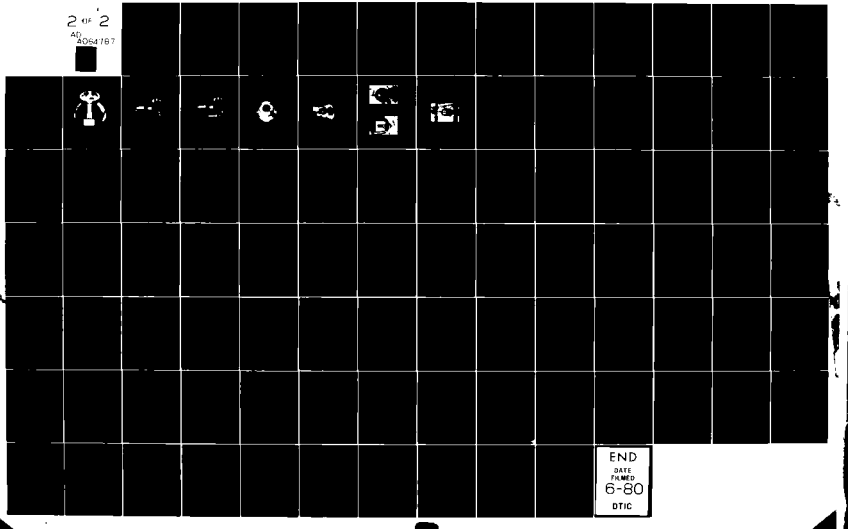

END
DATE FILMED
6-80
DTIC

since the static holes are 0.51 mm in diameter, the inaccuracies incurred in the precision machinework may be considered negligible. For the pressure measurements, the least accurate device used in the calibration procedure and the determination of atmospheric pressure was the 0-1000 kPa bourdon tube absolute pressure gage. The accuracy of this device is listed as $\pm$ 0.7 kPa. Considering the additional effects of calibration nonlinearity, amplifier drift, measurement fluctuations, etc., it is felt that the combined accuracy of the pressure measurement equipment is within $\pm$ 1.5 kPa.

However, since the data is generally presented in terms of the Mach number rather than the pressure ratio, it is natural to inquire how the inaccuracies in the individual measurements of the static and stagnation pressures affect the determination of the Mach number. This question can be answered by utilizing functional uncertainty analysis which is a technique whereby the fractional uncertainty of a functional relationship is calculated from the uncertainties of the individual measurements involved in it. As such it excludes the random errors of particular measurements and is concerned only with the accuracy of the measuring devices, or systematic error. The fractional uncertainty of a function F which depends on i variables, $F = F\left(x_i\right)$, is given by the expression [89],

$$\frac{U(F)}{F} = \left[\sum_i \left(\frac{\partial ln F}{\partial ln x_i} \frac{U\left(x_i\right)}{x_i}\right)^2\right]^{1/2} , \qquad \text{(IV-1)}$$

where U is used to denote the uncertainty. For the case at hand, the isentropic relation,

$$\frac{p_o}{p} = \left[1 + \frac{\gamma-1}{2} M^2\right]^{\gamma/(\gamma-1)} , \qquad \text{(IV-2)}$$

is employed to convert the pressure ratio to the corresponding Mach number. Using logarithmic differentiation, it is easily shown that,

$$\frac{\partial(\ln M)}{\partial(\ln p_0)} = -\frac{\partial(\ln M)}{\partial(\ln p)} = \frac{1 + \frac{\gamma-1}{2} M^2}{\gamma M^2} \quad . \tag{IV-3}$$

Therefore, the fractional uncertainty for the Mach number may be determined from,

$$\frac{U(M)}{M} = \left[\frac{1 + \frac{\gamma-1}{2} M^2}{\gamma M^2}\right]\left[\left[\frac{U(p_0)}{p_0}\right]^2 + \left[\frac{U(p)}{p}\right]^2\right]^{1/2} \tag{IV-4}$$

Using 1.5 kPa as the uncertainty of both the static and stagnation pressure measurements and 400 kPa as the value of the stagnation pressure for these experiments, the corresponding fractional uncertainty of the Mach number can be calculated through the transonic region. For M = 0.6 a value of 1.3% is obtained, while for M = 1.4 the fractional uncertainty in the Mach number is 0.63%. Similarly, the fractional uncertainty for the static-to-stagnation pressure ratio, p/p_0, is found to be 0.61% at M = 0.6 and 1.25% at M = 1.4. Thus the inaccuracies in the determination of both the Mach number and pressure ratio attributable to the measuring devices are expected to be on the order of one percent for the flowfields investigated here.

C. COMPARISON OF EXPERIMENTAL AND THEORETICAL RESULTS

Experimental measurements for a conventional axisymmetric configuration and three annular ones were obtained. A half-section drawing of the particular annular arrangement for which the centers of curvature of both the inner and outer wall contours lie along the Z = 0 plane is presented in Fig. IV.10. All dimensions are in millimeters. The air flow enters the test section from

the stagnation chamber at the left where it is first accelerated through the converging nozzle with its elliptical entrance section. At the exit of the converging nozzle the flow cross-sectional area has been reduced to a 50.8 mm radius. Further acceleration then occurs in the annular supersonic nozzle. Along the outer nozzle wall, a constant area cylindrical region is followed by 37.5° conically convergent section which is tangent to a circular arc contour. In the meridional plane, the radius of curvature of this arc is 25.4 mm, and the radial distance to the minimum point on the outer wall contour is also 25.4 mm. Along the centerbody, the flow is first accelerated from the stagnation point through a 25.4 mm radius arc to a cylindrical region with a 6.4 mm radius. This section is followed by a circular arc contour whose radius of curvature is 50.8 mm and a second, downstream cylindrical region with a 6.4 mm radius. The radial distance to the maximum point on the centerbody contour is 9.5 mm. For the axisymmetric, Laval nozzle case, the dimensions for the outer nozzle are identical, and the centerbody is simply removed. The other two annular configurations are obtained by displacing the centerbody relative to the outer nozzle both upstream and downstream by 12.7 mm. For these two configurations the main flow x-direction is inclined with respect to the Z-axis of symmetry.

To facilitate comparisons between the various configurations, the coordinate system used in the presentation of the data is the R-Z cylindrical system shown in Fig. IV.10. In this case the radial R-axis passes through the minimum point on the outer wall contour and the non-dimensionalizing length is chosen as the radial distance to this minimum point. This distance is also the same as the radius of curvature of the outer wall, 25.4 mm (or 1 inch).

In Fig. IV.11 the wall measurements from the full- and half-section models for the conventional axisymmetric configuration are compared. The pressure measurements were converted to Mach numbers using the isentropic relation, Eq. (IV-2), and for this case, the wall radius of curvature is equal to the throat half-height, $R_c = 1.0$. As can be seen in the figure, the wall Mach number measurements for the two models are essentially identical, with the root-mean-square difference between the data sets calculated to be $(\Delta M)_{rms} = 0.89 \times 10^{-2}$. For the first two and last four pressure taps in the streamwise direction, the Mach numbers measured with the half-section model are slightly higher, while at the remaining two axial stations, $Z = -0.3$ and $Z = -0.15$, the Mach number data for the full axisymmetric model is higher. These small, somewhat random differences between the measurements could, in part, be due to slight differences in the pressure tap locations for the two models since precise location of the taps on the curved walls was difficult both to achieve and to check. In any event, the very near coincidence of the two data sets lends credence to the argument that the measurements from the half-models should closely approximate those for the corresponding full axisymmetric geometries. Due to its thinness, the boundary layer on the splitter plate apparently has little effect on these measurements.

Also shown in Fig. IV.11 are the inviscid, wall Mach number results obtained from one-dimensional, isentropic, flow with area change analysis and also from the series solution developed in Chapter III. As in all of the comparisons to be made in this section, the third order, $\eta = 2$ expansion results are utilized as recommended in section III.D. From somewhat upstream

of the throat location, Z = 0, on downstream, it is seen that the one-dimensional analysis is seriously in error while the series solution results agree fairly well with the measurements. However, at the two most upstream wall tap locations, Z = - 0.6 and Z = - 0.45, the one-dimensional results agree more closely with the data th n do the results of the expansion solution. This lack of agreement between the series solution and the wall data at these upstream stations can be attributed to two approximations made in the theoretical analysis. First, since the transonic approximations embodied in Eqs. (III-10) and (III-11) have been utilized, it is expected that the solution will be valid only for nearly sonic conditions, i.e., $M \cong 1$. Therefore, for the relatively low Mach numbers measured at the two upstream taps, $M \cong 0.5$, it is not surprising that the series solution results do not agree well with the data. On the supersonic side, however, it is seen that the expansion solution agrees with the wall measurements for Mach numbers well above 1.5. Probably more important is the assumption that the coefficients in the Maclaurin series expansion for the wall contours have the same order of magnitude estimates as those for circular arcs. From the axial location Z = - 0.6 downstream to the exit, the outer wall contour of the experimental model is, in fact, a circular arc with $R_c = 1.0$. However, upstream from this station, the wall contour of the model consists of a 37.5° conically convergent section. Hence, it would not be expected that wall measurements taken near the tangency point between the conical inlet and the circular arc contour would agree well with the theory. The transition in the contour from a conical to a circular section is not allowed for in the analysis since no provision is made for the discontinuity in the second derivative which occurs at the tangency point.

Figure IV.12 presents a comparison between the contours of constant Mach number obtained from the expansion solution and those determined from the splitter plate measurements of the half-section model for the axisymmetric, Laval nozzle under consideration, R_c = 1.0. The data points were found by first converting the stagnation supply pressure measurement and the individual static tap pressure readings to the corresponding local Mach numbers using Eq. (IV-2). Since the constant Mach number contours for the configurations studied here are primarily radial in nature, the data points were determined by finding the axial Z-location at which the given Mach number was attained along each of the pressure tap rows that is a constant radial distance from the axis of symmetry. In addition to the outer wall, there are seven such rows: R = 0, 0.15, 0.3, 0.45, 0.6, 0.75, and 0.9. Hermite spline interpolation was utilized in obtaining the loci of the points at which the Mach number values of interest occur from the measurements of the individual taps along each row.

As can be seen in the figure, the correspondence between the series solution results and the experimental measurements is generally quite good except for the M = 0.6 contour and near the wall for the M = 0.8 iso-Mach curve. The disagreement in these regions can again be attributed to the fact that upstream of the Z = - 0.6 location the wall contour of the experimental model is conically convergent rather than being the circular arc contour of the downstream region as used in the implementation of the expansion solution. The experimental M = 0.6 contour is a nearly uniform, radial one which explains the agreement between the one-dimensional analysis and the wall measurements of Fig. IV.11 in the upstream region. In view of the

transonic approximations that have been made, the series solution developed in the preceding chapter would be expected to accurately predict the throat flowfields only for regions near the sonic line. Thus, the agreement between this analysis and the experimental data for Mach numbers up to 1.4 through such a wide region of the throat is somewhat surprising, particularly for the small wall radius of curvature of this model.

In Fig. IV.13 the expansion solution results are compared to the splitter plate flowfield measurements for an annular nozzle whose inner wall radius of curvature is twice that of the outer wall. This is the configuration drawn in Fig. IV.10 for which the centers of curvature of both wall contours and, therefore, the throat all lie along the Z = 0 plane so that the one-dimensional flow direction is parallel to the axis of symmetry, $\beta = 0$. Since the maximum radius of the centerbody is 0.375 units in these R-Z coordinates, the throat half-height is reduced to d = 0.625 resulting in dimensionless radii of curvature of $R_{ci} = 3.2$ and $R_{co} = 1.6$ for the inner and outer walls, respectively. The dimensionless distance to the inner throat wall location is $y_i = 0.6$. The data points have been obtained in a manner similar to that described for the conventional axisymmetric geometry of Fig. IV.12 except that for this and the other two annular configurations investigated, there are five rows of pressure taps at a constant radial coordinate in addition to the inner and outer walls: R = 7/16, 9/16, 11/16, 13/16, and 15/16. It is seen that the theoretical results correspond very closely to the measurements except, perhaps, near the tangency point between the conically convergent section and the circular arc contour along the outer wall, Z = - 0.6. Otherwise, the agreement is very good through the entire throat region from M = 0.6 to M = 1.4.

Figure IV.14 presents the comparison between the theoretical and experimental results for the annular configuration in which the centerbody has been translated downstream relative to the outer wall contour by a distance of 12.7 mm or 0.5 units in the R-Z coordinate system of the figure. For this geometry the main flow direction is inclined at an angle of approximately 5.45° (0.095 radians) away from the axis of symmetry. Also, the throat half-height is larger than for the preceding case in which the centers of curvature of both walls were on the Z = 0 plane so that the radii of curvature and distance to the inner throat wall location in the local x-y coordinates are all reduced: R_{ci} = 3.01, R_{co} = 1.50, and y_i = 0.51. Since this is the first example for which the location of the minimum area cross section is not obvious, it has been plotted as the dashed line in the figure. Also shown by the dotted line is the cross section of minimum distance between the two contours which joins their centers of curvature. As previously mentioned, the minimum area throat cross section for inclined nozzles is nearer the axis of symmetry than is the cross section of minimum distance, and, as can be seen in the figure, the two are not necessarily parallel. Even for the relatively small inclination angle of this configuration, there is a significant distance separating the two cross sections because of the relative proximity of the throat to the axis of symmetry. In comparing the analytical and experimental results in this figure, it is noted that the correspondence is quite close except in the upstream regions near the two walls where the circular arc contours of the experimental models end. Along the centerbody, the circular inner contour meets the upstream cylindrical section at Z = - 0.2, while the circular arc outer contour is tangent to the conical inlet at Z = - 0.6.

Elsewhere in the flowfield, the agreement between the theoretical and experimental iso-Mach curves from M = 0.6 to M = 1.4 is quite good.

The final experimental geometry investigated is shown in Fig. IV.15. In this case the centerbody was displaced upstream relative to the outer nozzle wall by 12.7 mm or 0.5 units in the R-Z coordinate system. The one-dimensional flow direction is inclined toward the axis of symmetry at an angle of 5.45°, and the cross sections of minimum area and minimum distance between the contours are identical to those of the preceding configuration as reflected through the Z = 0 plane. The radii of curvature and the distance to the inner nozzle wall also have the same values as the last example: R_{ci} = 3.01, R_{co} = 1.50, and y_i = 0.51. For this case the theoretical and measured Mach number contours are compared only for Mach numbers up to M = 1.2. For higher Mach numbers, the measurements were disturbed by the presence of a detached, oblique shock wave emanating from the inner wall near Z = 0.2 where the supersonic flow along the centerbody is turned parallel to the downstream cylindrical section. The series solution results again agree quite well with the experimental data except in the upstream region along the outer wall near the Z = - 0.6 tangency point.

Cross-plots comparing the experimental wall Mach numbers with those determined from the expansion solution and from isentropic, one-dimensional analysis could also be presented for the three annular configurations as was done for the conventional, axisymmetric nozzle, Fig. IV.11. However, as can be seen by studying Figs. IV.13-IV.15, the resulting figures and conclusions would all be similar to those for the Laval nozzle. Near the throat and downstream of it, the series solution agrees well with the measurements of

the Mach number along the walls, while the one-dimensional results are in error. However, in the upstream regions where the circular arc wall contours of the models make transitions to either conical or cylindrical sections, the agreement between the expansion solution and the data is understandably not as good.

Without exception, it is noted that in regions of the flowfields unaffected by the wall contour transitions, the shapes of the experimental and theoretical Mach number contours are similar but the measurements lie slightly downstream of the analytical results. This observation applies not only to the comparisons made in this section, Figs. IV.12-IV.15, but also to the comparisons made with existing data sets in Chapter III, Figs. III.10 and III.11.

One cause of this behavior results from the fact that the analysis is an inviscid one while the effect of wall friction causes a shift in the actual sonic line downstream from the corresponding inviscid one. This can be shown by means of the following argument. For a perfect gas with constant specific heats, one of the differential equations governing generalized one-dimensional flow with friction and area change may be written as [90],

$$\left(1-M^2\right) \frac{du}{u} = \frac{dF}{pA} - \frac{dA}{A} , \qquad \text{(IV-5)}$$

where u is the one-dimensional velocity, dF is the elemental wall shear force opposing the flow, p is the static pressure, and A is the flow cross-sectional area. At the sonic line the left hand side of this equation vanishes, resulting in,

$$dA = \frac{dF}{p} . \qquad \text{(IV-6)}$$

Since the wall shear force and the static pressure are inherently positive, dA must also be a positive quantity. It is therefore concluded that the effect of friction is to shift the sonic line downstream into the diverging part of the supersonic nozzle for which dA/dx > 0.

A second reason that the experimentally determined iso-Mach curves are generally slightly downstream from the theoretical predictions is related to measurement errors introduced by the static holes. Since the pressure calibrations were performed in a no-flow test in which the transducers were directly connected to a pressure source, the accuracy estimate made in the previous section considered only the errors resulting from the transducers, signal conditioning equipment, calibration procedure and equipment, etc. However, with flow across the holes an additional error is present since it is well known [91-94] that the pressure measured by a static hole is not necessarily identical to the static pressure in the flowfield at that point.

The pressure tap configuration used in this study is shown in Fig. IV.16. It is very similar to the one used by Shaw [92] in his study of pressure tap errors with the inside diameter of the tap twice that of the hole. Also, in the present experiments the hole depth to diameter ratio, ℓ/d_h, was nominally equal to two. Using dimensional analysis and the results of extensive experiments for incompressible turbulent flow, Shaw correlated the static pressure errors as a function of the hole depth-to-diameter ratio and the Reynolds number based on the hole diameter and friction velocity,

$$\frac{\Delta p}{\tau_0} = f\left(Re^+, \ell/d_h\right) \qquad \text{(IV-7)}$$

where

$$Re^{+} = \frac{d_h}{\nu}\left(\frac{\tau_w}{\rho}\right)^{1/2}; \qquad (IV-8)$$

τ_w is the wall shear stress and ν is the kinematic viscosity of the fluid. Shaw found that for deep holes, $\ell/d_h \geq 1.5$, the pressure error is positive and is independent of the hole depth, ℓ. The dimensionless error, $\Delta p/q_0$, increases from zero at $Re^{+} = 0$ until it reaches an asymptotic value of 2.75 at $Re^{+} = 800$, above which the error is constant.

Using a somewhat different pressure tap configuration, Livesey, et al. [93] performed a similar set of experiments and analysis of static hole errors. The results were correlated in the same form as those of Shaw, but for deep holes it was found that the positive error does not reach an asymptotic limit but instead increases monotonically and nearly linearly for all hole Reynolds numbers. Below $Re^{+} = 1000$ the error predicted by the correlation of Livesey, et al. is lower than that found by Shaw. At $Re^{+} = 1000$ the correlations intersect so that above this point the monotonically increasing error predicted by Livesey, et al. exceeds the limiting value of Shaw.

It is important to note that the positive static pressure errors found by both of these investigators are consistent with the trends exhibited in Figs. III.10, III.11, and IV.12-IV.15. For these cases the Mach number measured at a given point is lower than the corresponding predicted value so that the static pressure is higher. Therefore, taking into account the predicted static hole errors puts the data and theory in closer agreement. By using the boundary layer analysis developed in [88] to predict the wall shear stress, it is found that the hole Reynolds numbers for the experiments

of this investigation ranged from $Re^+ = 870$ at M = 0.6 to $Re^+ = 1120$ at M = 1.4. For these values, the errors predicted by Shaw and Livesey, et al. agree quite closely so that Shaw's limit of $\Delta p/\tau_0 = 2.75$ was used. For M = 0.6 this corresponds to a static pressure error of approximately + 0.2% while for M = 1.0 and M = 1.4 the errors are calculated as + 0.5% and + 0.9%, respectively. The percent root-mean-square difference between the theoretical and measured values of the static pressure for the data presented in Figs. IV.12-IV.15 is somewhat higher than these predictions for the static pressure error. For the axisymmetric, Laval nozzle of Fig. IV.12 the percentage difference is found to be $(\Delta p/p)_{rms} = 3.5\%$, while for the annular configurations of Figs. IV.13, IV.14, and IV.15 the differences are 2.5%, 2.6%, and 3.3%, respectively. It should be remembered, however, that the investigations of both Shaw and Livesey, et al. considered only incompressible flow. Rayle [91], as reported by Chue [94], found that for transonic speeds the static pressure error is two to three times that for incompressible flow for the 0.51 mm diameter static holes used in this investigation. Thus, the static hole errors may be as large as 2-3% for these experiments.

It is felt that the major reasons for the downstream shift of the experimental constant Mach number curves from the corresponding analytical ones are the two just discussed: wall friction, which is not accounted for in the theoretical model, and errors in the static pressure measurements. Other effects such as heat transfer, condensation, particulates suspended in the flow, etc. are thought to be negligible. It should be emphasized that the discrepancies are small and, for the most part, the agreement between the measurements and the theory is quite good through a surprisingly wide region of the throat flowfields.

Figure IV.1 Photograph of full-section, conventional axisymmetric nozzle

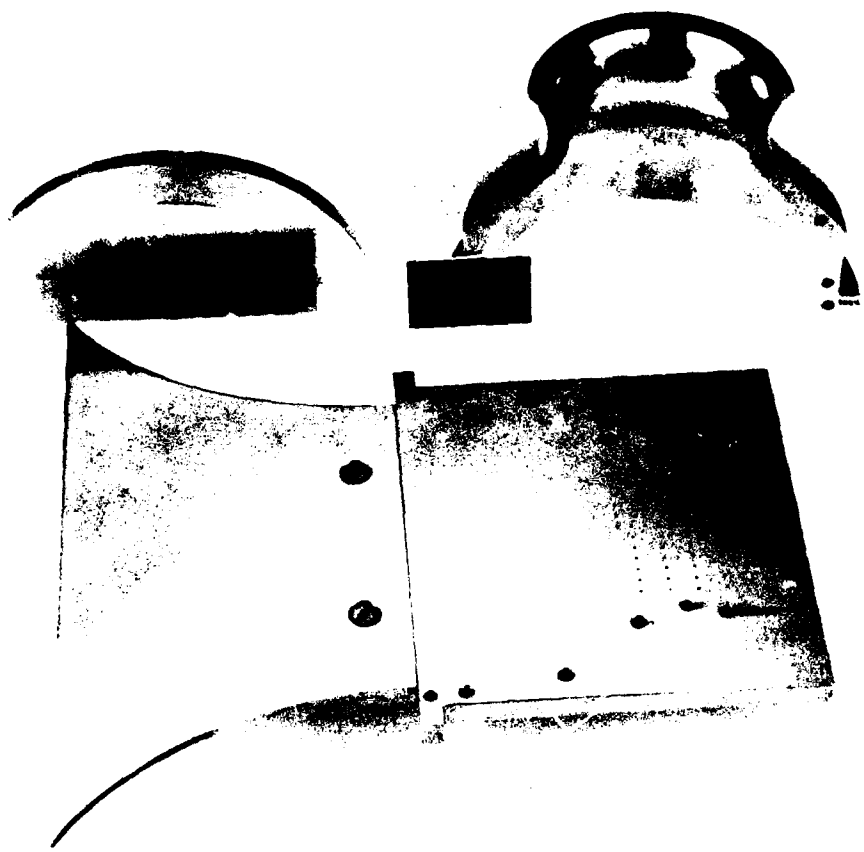

Figure IV.2 Photograph of disassembled, half-section, conventional axisymmetric nozzle

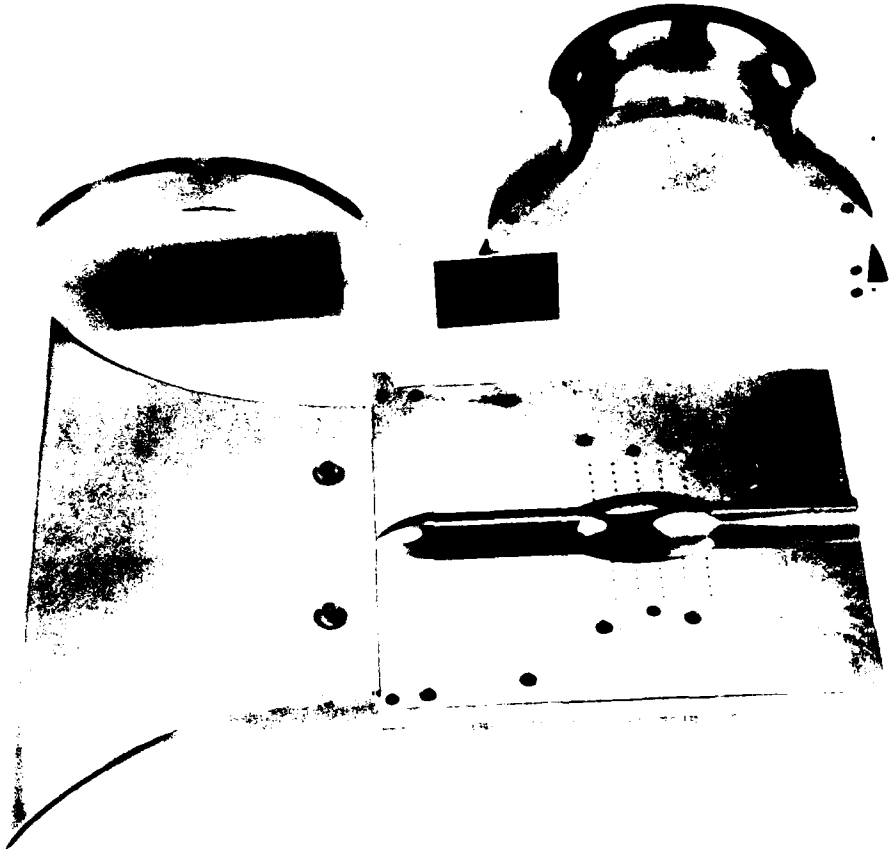

Figure IV.3 Photograph of disassembled, half-section, annular nozzle

Figure IV.4 View downstream through test section of assembled, half-section, annular nozzle

Figure IV.5 View upstream through measurement region of assembled, half-section, annular nozzle

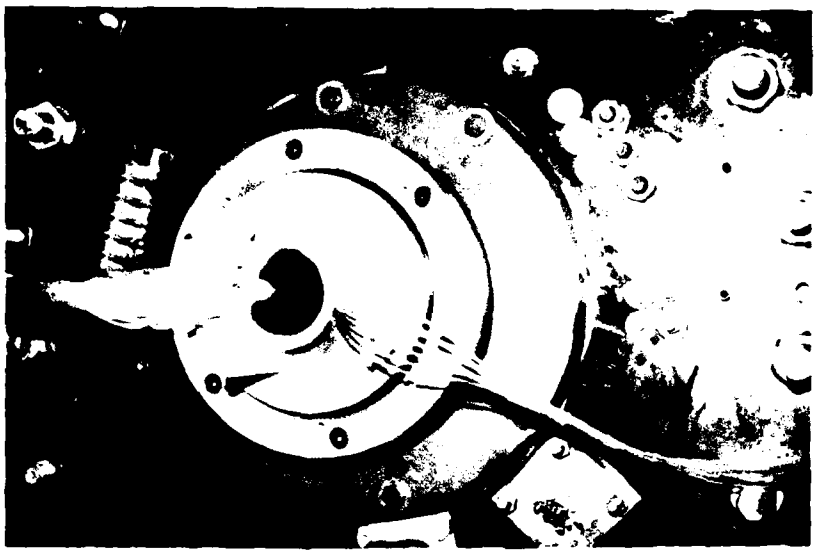

Figure IV.6 Partially assembled, annular nozzle test apparatus

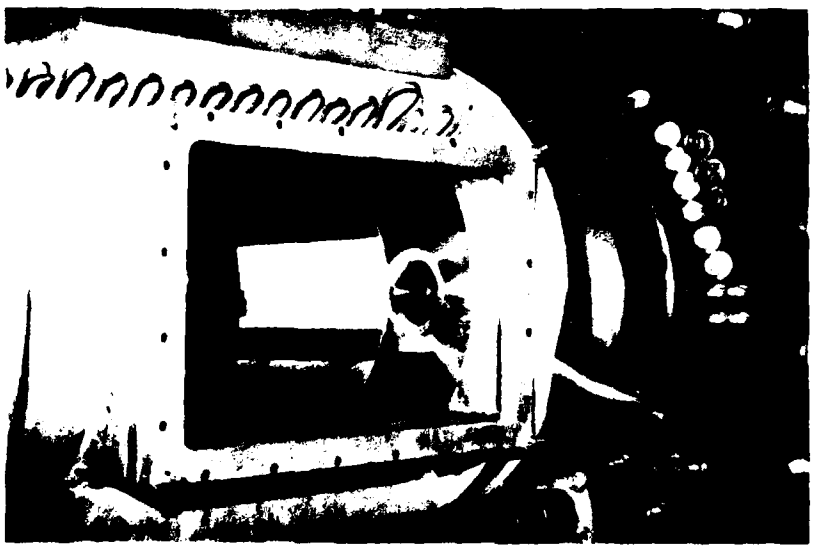

Figure IV.7 View of annular nozzle through side window of viewing chamber

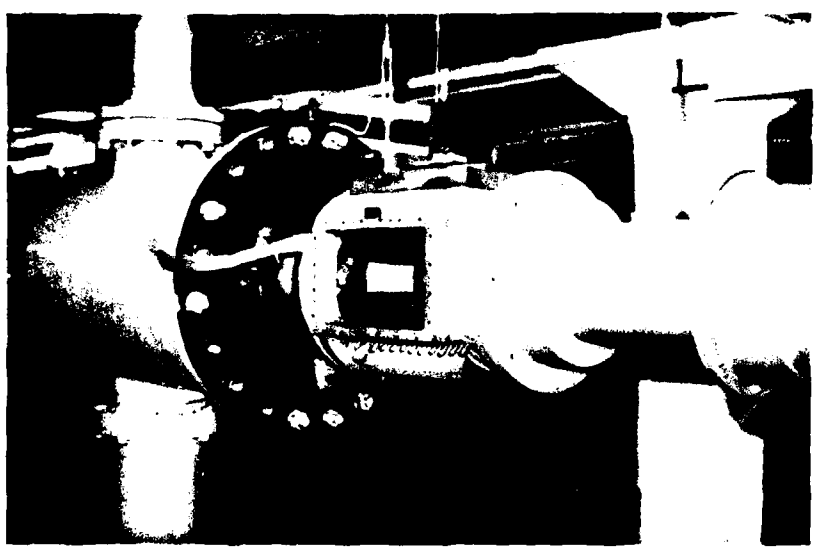

Figure IV.8 Overall view of fully assembled, annular nozzle test apparatus

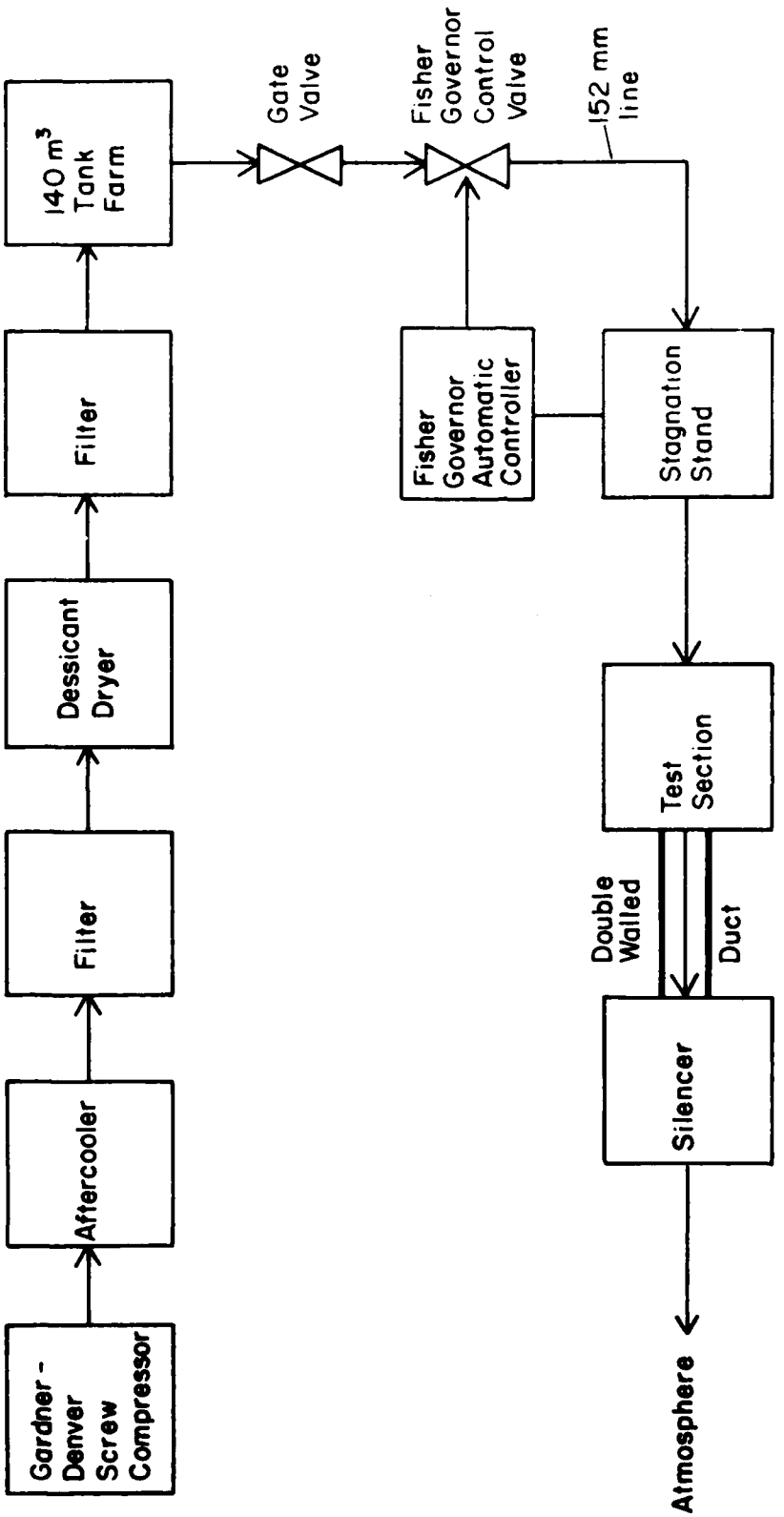

Figure IV.9 Schematic diagram of air flow circuit

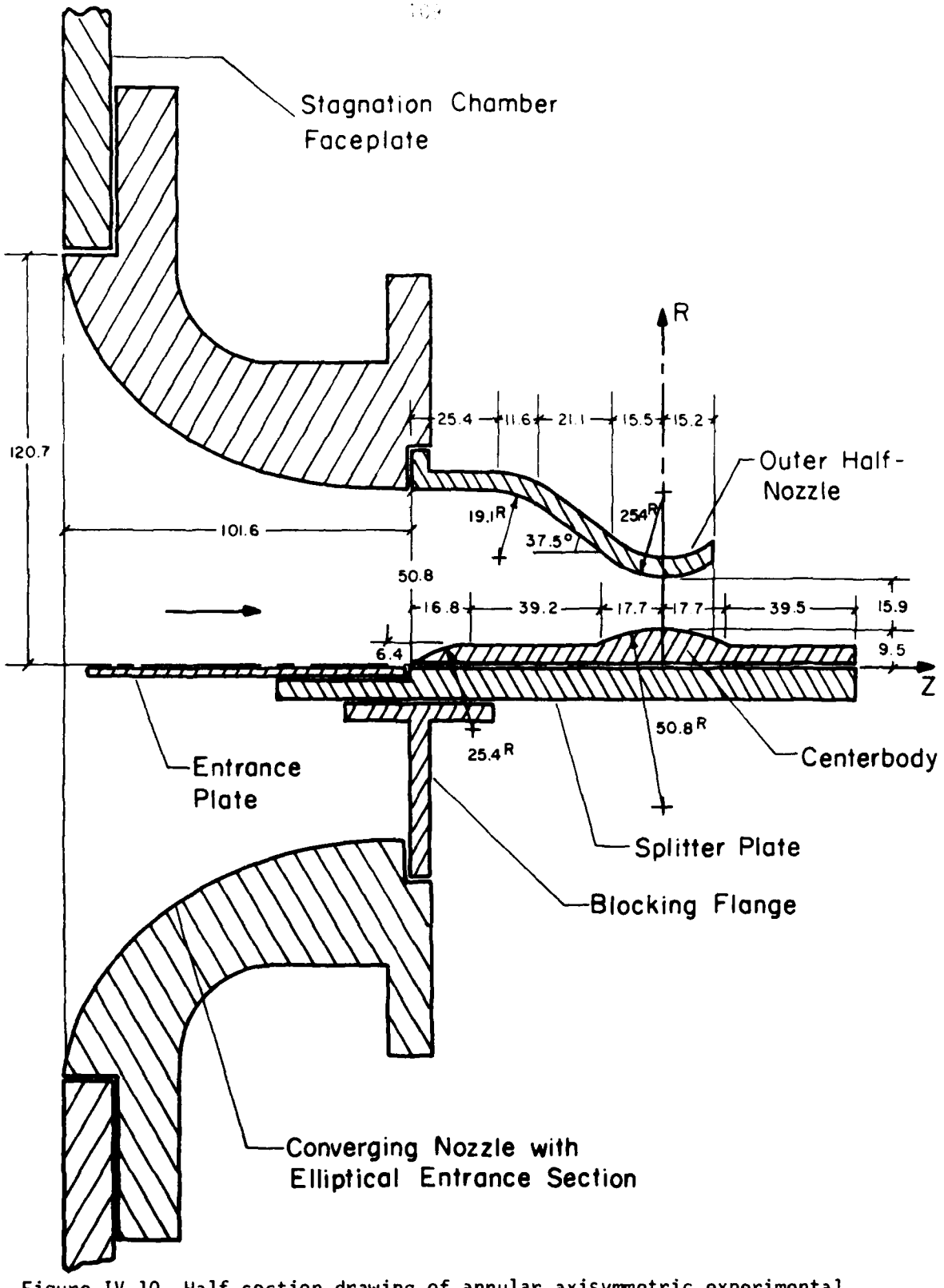

Figure IV.10 Half-section drawing of annular axisymmetric experimental configuration; all dimensions are in millimeters

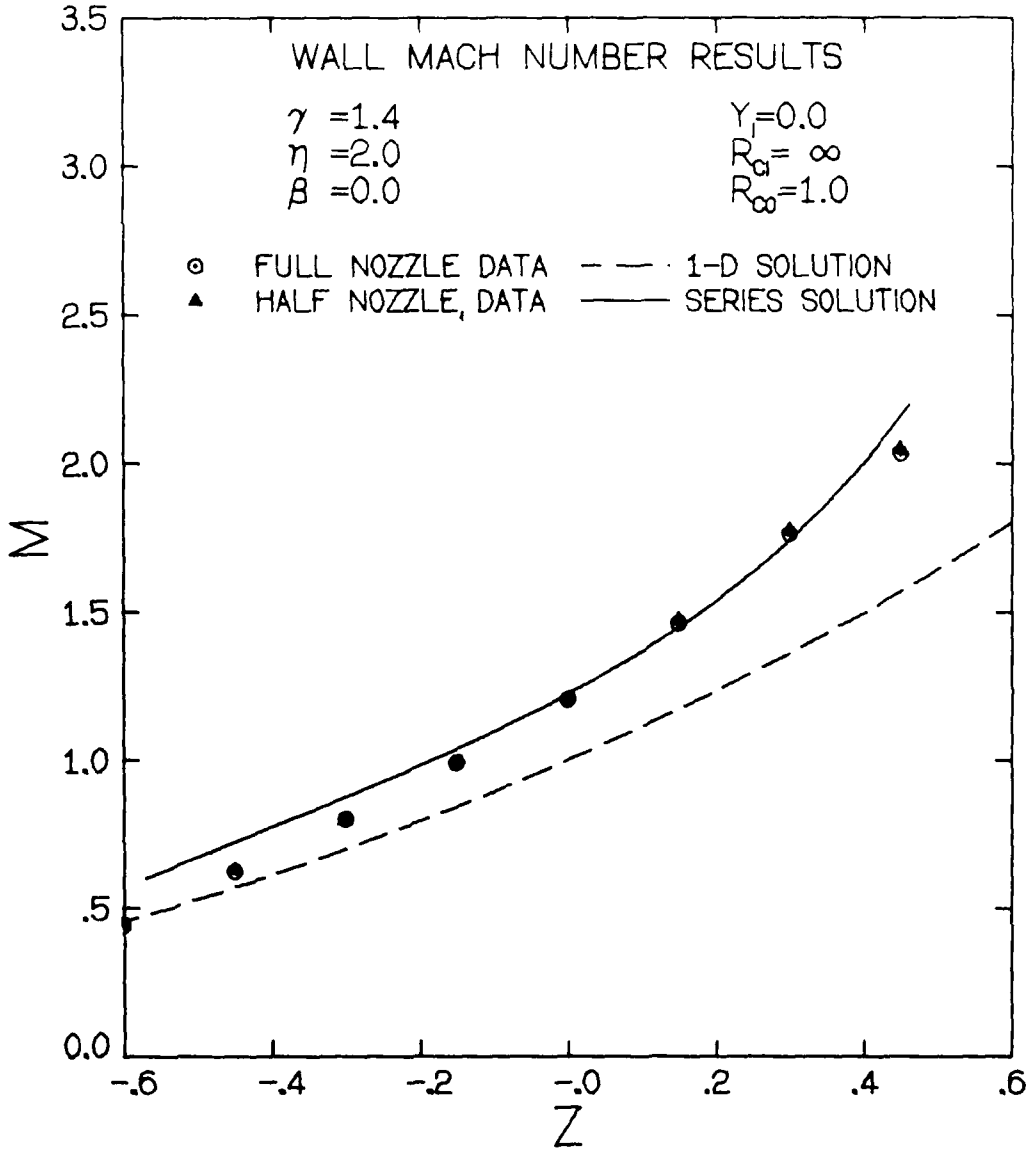

Figure IV.11 Comparison of full- and half-section wall Mach number measurements with one-dimensional solution and series expansion solution for conventional axisymmetric nozzle; $Re_{2d} = 2.68 \times 10^6$ for full nozzle and $Re_{2d} = 3.09 \times 10^6$ for half nozzle experiments

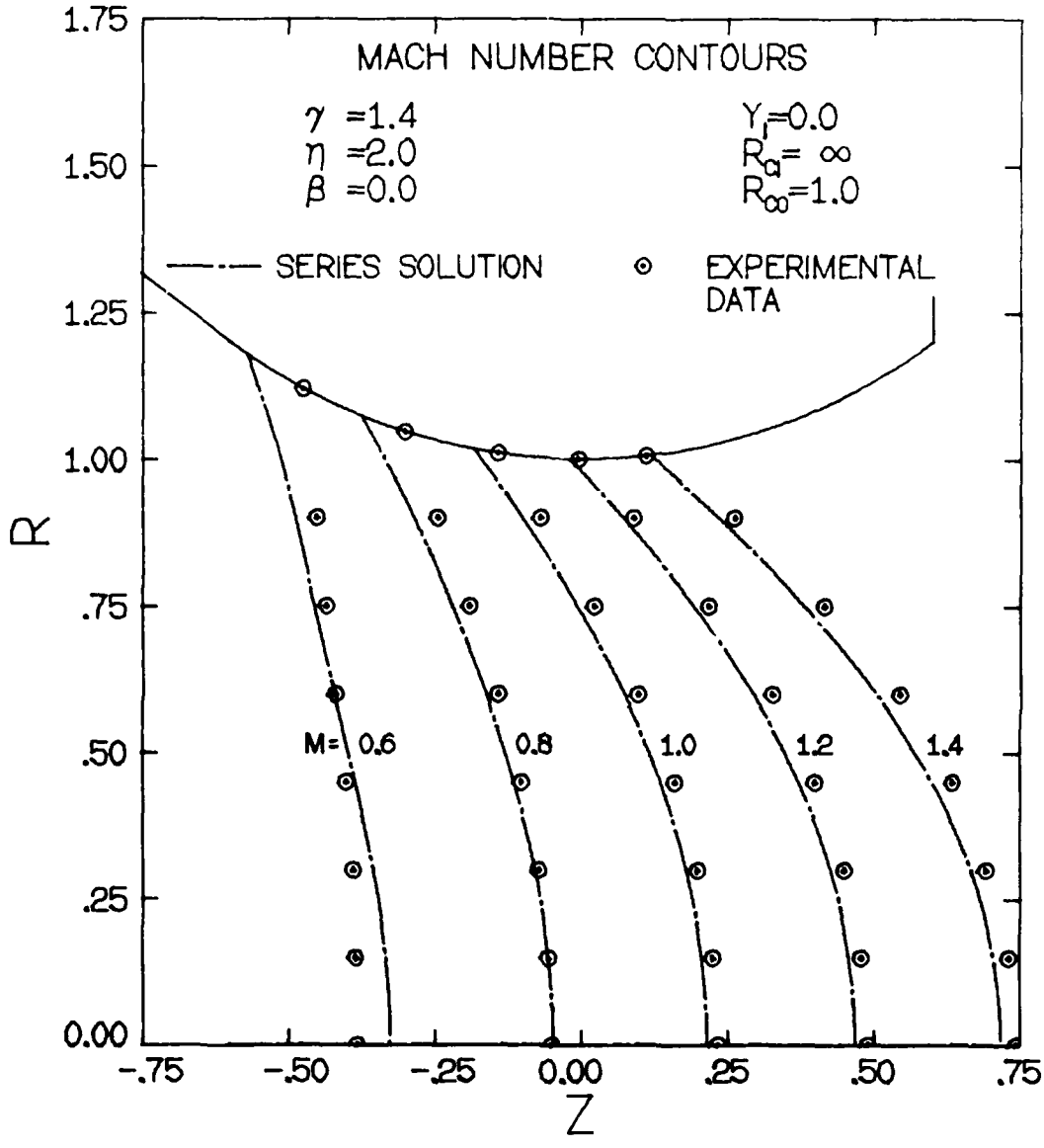

Figure IV.12 Comparison of constant Mach number contours from series expansion solution with experimental data for conventional axisymmetric nozzle; $Re_{2d} = 3.04 \times 10^6$ for experiments

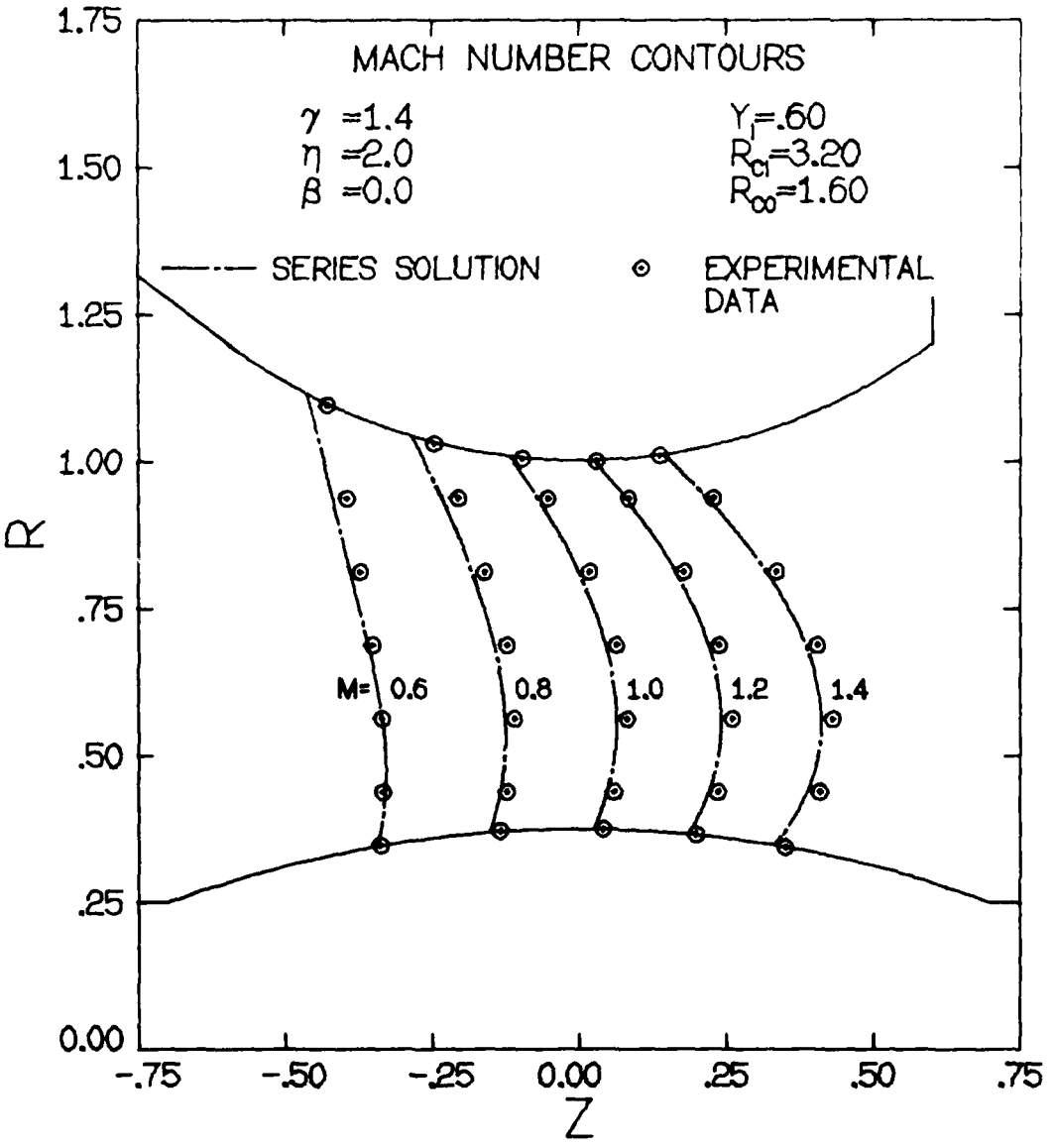

Figure IV.13 Comparison of constant Mach number contours from series expansion solution with experimental data for annular nozzle with centerbody center of curvature along Z = 0 plane; $Re_{2d} = 1.96 \times 10^6$ for experiments

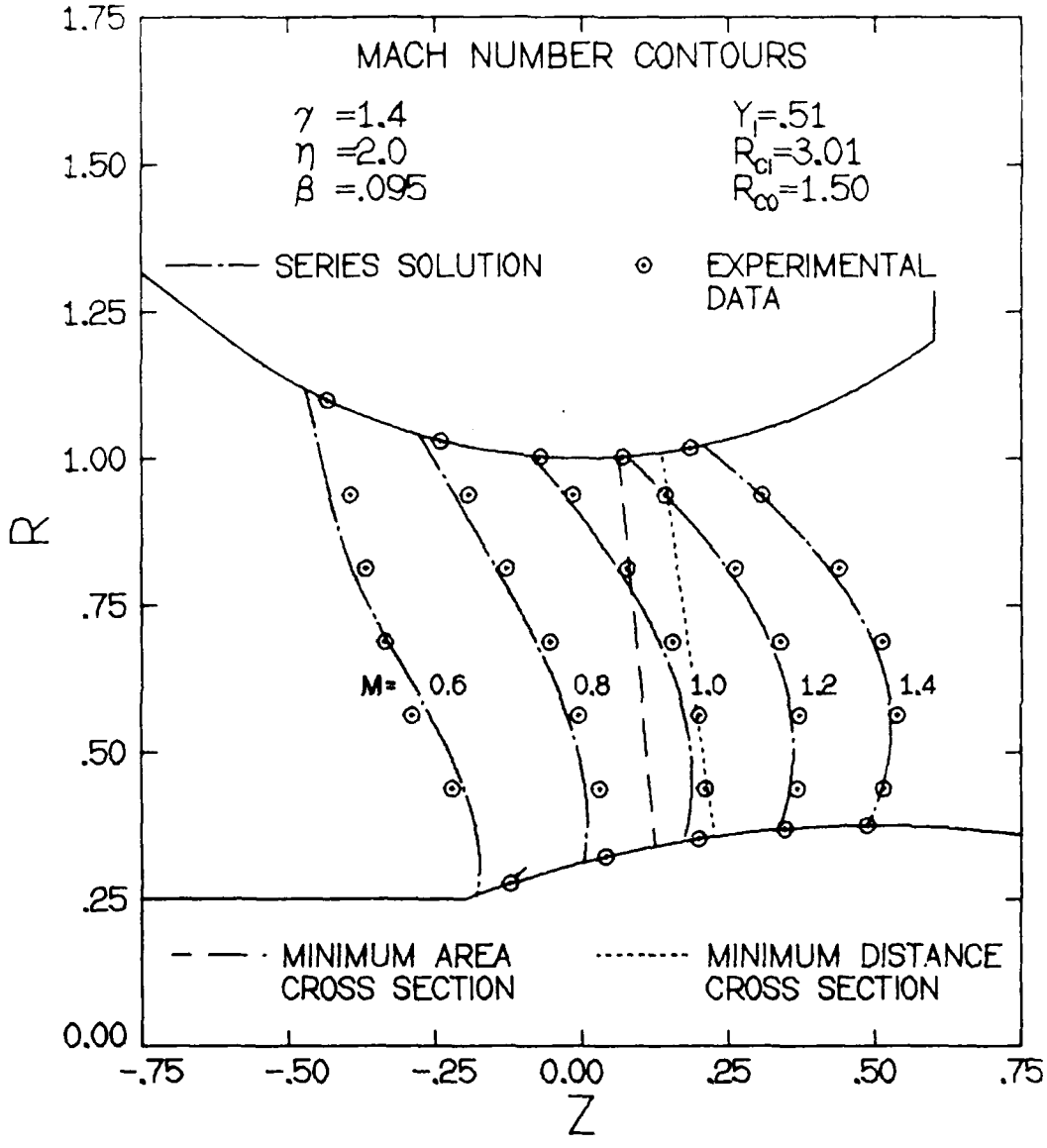

Figure IV.14 Comparison of constant Mach number contours from series expansion solution with experimental data for annular nozzle with centerbody center of curvature along Z = 0.5 plane; $Re_{2d} = 2.08 \times 10^6$ for experiments [Flagged data point obtained by extrapolation]

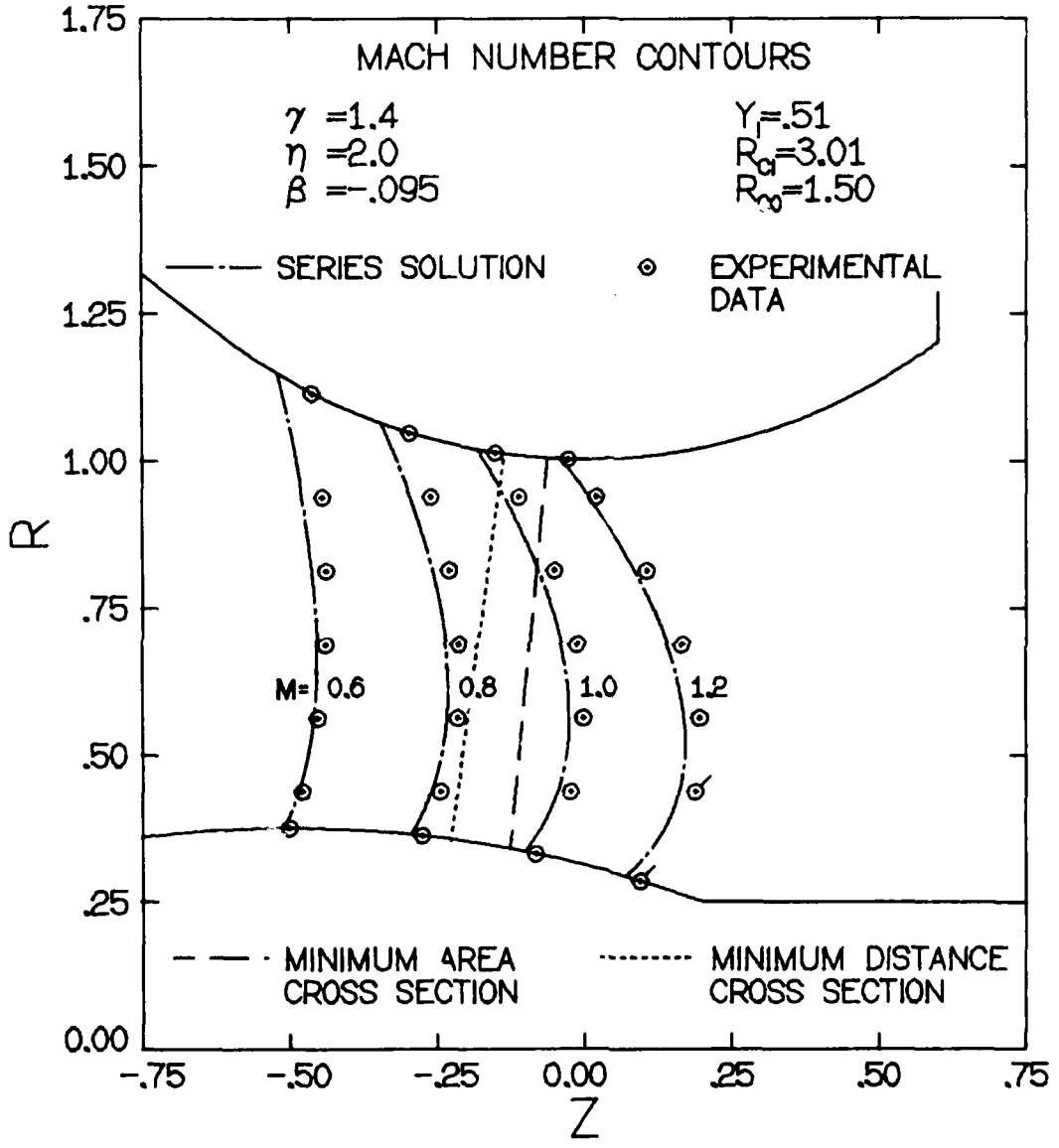

Figure IV.15 Comparison of constant Mach number contours from series expansion solution with experimental data for annular nozzle with centerbody center of curvature along Z = - 0.5 plane; Re_{2d} = 2.08 x 10^6 for experiments [Flagged data points obtained by extrapolation]

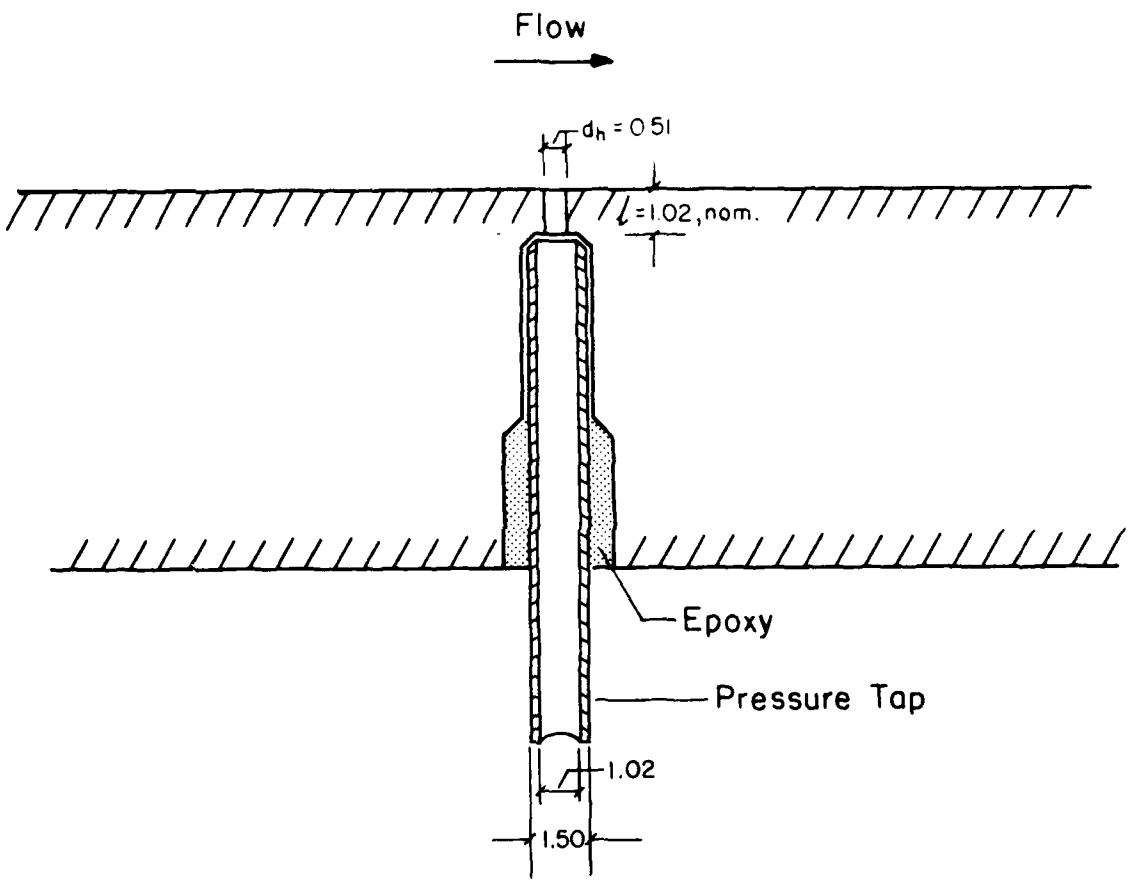

Figure IV.16 Half-section drawing of static hole-pressure tap arrangement; all dimensions are in millimeters

V. CONCLUSIONS AND RECOMMENDATIONS

As a result of the integrated theoretical and experimental investigation of nozzle throat flowfields which has been reported herein, the following conclusions may be drawn:

(1) The approximate series expansion solution which has been developed provides a direct means of analyzing the transonic flow in the throat region of a wide variety of two-dimensional nozzle configurations including axisymmetric, annular, and planar nozzles. For annular nozzles, the throat may be inclined with respect to the axis of symmetry, and for both planar and annular geometries the two bounding walls may have unequal radii of curvature at the throat.

(2) Based on the series of parametric studies which was performed, it is suggested that third order solutions be employed together with $\eta = 2$, where η is the parameter in the expansion variable definition, Eq. (III-22).

(3) From the parametric studies and from comparisons between the series solution results and experimental data, it is concluded that the expansion solution accurately describes the transonic flowfield through a significant region of the throat for nozzles whose wall radius of curvature is of the order of the throat half-height or larger. In addition, for an axisymmetric nozzle with the small dimensionless wall radius of curvature of $R_c = 0.625$, it was found that the series solution is accurate from the sonic line up to a Mach number of approximately 1.4.

(4) An accurate, slightly supersonic starting line for initiating the hyperbolic computations for the supersonic portion of the flowfield is the constant Mach number contour emanating from one of the throat wall locations.

This initial value line is recommended because the wall boundary conditions are exactly satisfied only at the throat. It may be more convenient, however, to use other starting lines for compatibility with the scheme used to analyze the supersonic flowfield.

(5) The numerical implementation of the expansion solution is extremely fast and reliable since it simply consists of the straightforward evaluation of a series of constants and functions. Typical problems require less than two seconds of central processor (CPU) time on the University of Illinois CDC Cyber 175 digital computer. This feature makes feasible parametric studies and iterative calculations as might be necessitated in the nozzle design situation.

(6) For applications in which a very high degree of accuracy is required, it may be advantageous to employ the approximate series solution as the initial condition for one of the time-dependent numerical techniques. This scheme may speed the convergence of the time-dependent methods to the steady state asymptotic limit.

(7) Based on the comparison of the wall pressure measurements from the full- and half-section models of the conventional, axisymmetric nozzle, it is concluded that the splitter plate technique is valid for obtaining flowfield pressure distributions for these high Reynolds number, accelerated flows. The boundary layer on the splitter plate is extremely thin so that it has little effect on the flowfield pressure measurements.

(8) For the axisymmetric, Laval nozzle and the three annular configurations investigated here, the agreement between the theoretical and experimental results for the constant Mach number contours is quite good through a

significant region of the throat. Only near the points where the circular arc contours of the experimental models make transitions to either the conical inlet or cylindrical approach sections is there a noticeable discrepancy between the analysis and the measurements.

(9) The small downstream shift of the experimental iso-Mach curves from the corresponding theoretical ones can be attributed to wall friction, which is neglected in the theory, and to pressure measurement errors related to the static pressure taps.

The understanding of the topic of internal transonic flowfields is by no means complete. To further enhance the state of knowledge in this area, the following studies are recommended:

(1) Through the use of alternate expansion techniques it may be possible to obtain solutions which are valid for nozzles whose throat wall radius of curvature is small compared to the throat half-height. Alternate expansions should also be investigated for the case of highly inclined, annular nozzles, particularly for the radial flow case which has practical applications.

(2) The possibility of extending the series solution technique to unconventional, three-dimensional, supersonic nozzles should also be investigated. It is felt, however, that the most likely candidates for analyzing the flowfields in this class of nozzles are numerical methods.

(3) In order to investigate the effect of the Reynolds number on these flows, experimentation over a wider range of pressures is needed. Additional experiments are also required for nozzles having a small throat wall radius of curvature and for highly inclined annular nozzles.

(4) For further flowfield information, such as detailed measurements of the velocity components, a laser doppler velocimeter system may be employed.

The theoretical solution and experimental static pressure measurements of the present investigation provide a basis for setting up and checking out such a system.

(5) An area which seemingly has received very little attention is that of converging-diverging nozzles operating in the unchoked, Taylor regime for which the operating pressure ratio is important. An important application of this problem is jet engine inlets for subsonic aircraft.

(6) In a related area, it appears that additional work is needed to better understand static pressure tap errors which are incurred in compressible flow measurements.

REFERENCES

1. Dosanjh, D. S., Yu, J. C., and Abdelhamid, A. N., "Reduction of Noise from Supersonic Jet Flows," AIAA Journal, Vol. 9, Dec. 1971, pp. 2346-2453.

2. Mikkelsen, C. D., Sandberg, M. R., and Addy, A. L., "Theoretical and Experimental Analysis of the Constant-Area, Supersonic-Supersonic Ejector," Department of Mechanical and Industrial Engineering, University of Illinois at Urbana-Champaign, Report No. UILU-ENG-76-4003, Oct. 1976.

3. Dutton, J. C. and Addy, A. L., "One-Dimensional Analyses of Supersonic-Supersonic, Ejector-Diffuser Systems for Chemical Laser Applications," Department of Mechanical and Industrial Engineering, University of Illinois at Urbana-Champaign, Report No. UILU-ENG-78-4015, Sept. 1978.

4. Spiegel, J. M., Hofstetter, R. V., and Kuehn, D. M., "Applications of Auxiliary Air Injectors to Supersonic Wind Tunnels," NACA RM A53I01, 1953.

5. Hunczak, H. R. and Rousso, M. D., "Starting and Operating Limits of Two Supersonic Wind Tunnels Utilizing Auxiliary Air Injection," NACA TN 3262, 1954.

6. Hasel, L. E. and Sinclair, A. R., "A Preliminary Investigation of Methods for Improving the Pressure-Recovery Characteristics of Variable-Geometry Supersonic-Subsonic Diffuser Systems," NACA RM L57H02, 1957.

7. Stokes, G. M., "Description of a 2-Foot Hypersonic Facility at the Langley Research Center," NASA TN D-939, 1961.

8. Chow, W. L. and Addy, A. L., "Interaction between Primary and Secondary Streams of Supersonic Ejector Systems and their Performance Characteristics," AIAA Journal, Vol. 2, April 1964, pp. 686-695.

9. Chow, W. L. and Yeh, P. S., "Characteristics of Supersonic Ejector Systems with Nonconstant Area Shroud," AIAA Journal, Vol. 3, March 1965, pp. 525-527.

10. Guile, R. N., Zumpano, F. R., and Eckerle, W. A., "Chemical Laser Advanced Diffuser/Ejector (CLADE) Far Advanced Technical Concepts," U.S. Army Contract DAAH 01-76-C-1032, Monthly Technical Progress Reports Nos. 1-9, July 1976-March 1977.

11. Navier, C. L. M. H., Memoires de l'Academie, Vol. 9, 1830, p. 311.

12. Saint Venant, B. de and Wantzel, G., J. de l'École Polytechnique, Vol. 27, 1839, p. 85.

13. Hall, I. M. and Sutton, E. P., "Transonic Flow in Ducts and Nozzles; a Survey," Symposium Transsonicum, Springer Verlag, Berlin, 1964, pp. 325-344.

14. Flack, R. D. and Thompson, H. D., "An Experimental and Analytical Investigation of Internal Transonic Flow," U.S. Army Missile Command Technical Report No. RD-73-20, Oct. 1973.

15. Brown, E. F. and Hamilton, G. L., "Survey of Methods for Exhaust-Nozzle Flow Analysis," J. Aircraft, Vol. 13, Jan. 1976, pp. 4-11.

16. Meyer, T., "Ueber zweidimensionale Bewegungsvorgänge in einem Gas, das mit Ueberschallgeschwindigkeit strömt, V. D. I. Forschungsheft, Vol. 62, 1908, pp. 31-67.

17. Lighthill, M. J., "The Hodograph Transformation in Trans-sonic Flow; I," Proc. Roy. Soc., London, Ser. A, Vol. 191, Nov. 1947, pp. 323-341.

18. Ferguson, D. F. and Lighthill, M. J., "The Hodograph Transformation in Trans-sonic Flow; IV," Proc. Roy, Soc., London, Ser. A, Vol. 192, Dec. 1947, pp. 135-142.

19. Frankl, F., "On the Problems of Chaplygin for Mixed Sub and Supersonic Flows," NACA TM 1155, 1947.

20. Cherry, T. M., "A Transformation of the Hodograph Equation," Phil. Trans. Roy. Soc., London, Ser. A, Vol. 904, 1953, pp. 583-626.

21. Cherry, T. M., "Some Nozzle Flows Found by the Hodograph Method," J. Australian Math. Soc., Vol. 1, Aug. 1959, pp. 80-94.

22. Cherry, T. M., "Nozzle Flows Found by the Hodograph Method, II, "J. Australian Math. Soc., Vol. 1, Aug. 1960, pp. 357-367.

23. Lord, W. T., "A Theoretical Study of Annular Supersonic Nozzles," Aeronautical Research Council, Reports and Memoranda No. 3227, Oct. 1959.

24. Hopkins, D. F. and Hill, D. E., "Effect of Small Radius of Curvature on Transonic Flow in Axisymmetric Nozzles," AIAA Journal, Vol. 4, Aug. 1966, pp. 1337-1343.

25. Hopkins, D. F. and Hill, D. E., "Transonic Flow in Unconventional Nozzles," AIAA Journal, Vol. 6, May 1968, pp. 838-842.

26. Morden, D. B. and Farquhar, B. W., "Comment on 'Transonic Flow in Unconventional Nozzles'," AIAA Journal, Vol. 7, Aug. 1969, pp. 1661-1662.

27. Norton, D. J., "Subsonic, Transonic, and Supersonic Nozzle Flow by the Inverse Technique," J. of Spacecraft and Rockets, Vol. 9, June 1972, pp. 457-459.

28. Van Tuyl, A. H., "Calculation of Nozzle Flows Using Padé Fractions," AIAA Journal, Vol. 11, April 1973, pp. 537-541.

29. Klopfer, G. H. and Holt, M., "Steady Transonic Flow Through Plane and Axisymmetric Nozzles," Symposium Transsonicum II, Springer Verlag, Berlin, 1976, pp. 376-383.

30. Cuffel, R. F., Back, L. H., and Massier, P. F., "Transonic Flowfield in a Supersonic Nozzle with Small Throat Radius of Curvature," AIAA Journal, Vol. 7, July 1969, pp. 1364-1366.

31. Ishii, R., "A New Method of Nozzle Design," AIAA Journal, Vol. 16, July 1978, pp. 756-759.

32. Taylor, G. I., "The Flow of Air at High Speeds Past Curved Surfaces," Aeronautical Research Council, Reports and Memoranda No. 1381, 1930.

33. Sauer, R., "Genera' Characteristics of the Flow through Nozzles at Near Critical Speeds," NACA TM 1147, 1947.

34. Oswatitsch, K. and Rothstein, W., "Flow Pattern in a Converging-Diverging Nozzle," NACA TM 1215, 1949.

35. Hall, I. M., "Transonic Flow in Two-Dimensional and Axially-Symmetric Nozzles," Quart. Journ. Mech. and Applied Math., Vol. XV, Pt. 4, 1962, pp. 487-508.

36. Moore, A. W. and Hall, I. M., "Transonic Flow in the Throat Region of an Annular Nozzle with an Arbitrary Smooth Profile," Aeronautical Research Council, Reports and Memoranda No. 3480, Jan. 1965.

37. Thompson, H. D. and Flack, R. D., "Transonic Flow Computation in Annular and Unsymmetric Two-Dimensional Nozzles," U.S. Army Missile Command Technical Report No. RD-73-21, Dec. 1973.

38. Moore, A. W., "The Transonic Flow in the Throat Region of a Two-Dimensional Nozzle with Walls of Arbitrary Smooth Profile," Aeronautical Research Council, Reports and Memoranda No. 3481, Jan. 1965.

39. Szaniawski, A., "Equations of Plane Symmetric Transonic Viscous and Heat Conducting Flow," Archiwum Mechaniki Stosowanej, Vol. 16, 1964, pp. 1117-1129.

40. Kopystynski, J. and Szaniawski, A., "Structure of Flow in a Nozzle Throat," Archiwum Mechaniki Stosowanej, Vol. 17, 1965, pp. 453-466.

41. Szaniawski, A., "Transonic Approximations to the Flow through a Nozzle," Archiwum Mechaniki Stosowanej, Vol. 17, 1965, pp. 79-85.

42. Szaniawski, A., "Flow in the Throat of a Laval Nozzle," Symposium Transsonicum II, Springer Verlag, Berlin, 1976, pp. 208-215.

43. Sichel, M., "The Effect of Longitudinal Viscosity on the Flow at a Nozzle Throat," Journal of Fluid Mechanics, Vol. 25, Aug. 1966, pp. 769-786.

44. Sichel, M., "Theory of Viscous Transonic Flow: A Survey," NATO AGARD Conference Proceedings No. 35, Transonic Aerodynamics, Paper 10, Sept. 1968.

45. Kliegel, J. R. and Quan, V., "Convergent-Divergent Nozzle Flows," AIAA Journal, Vol. 6, Sept. 1968, pp. 1728-1734.

46. Kliegel, J. R. and Levine, J. N., "Transonic Flow in Small Throat Radius of Curvature Nozzles," AIAA Journal, Vol. 7, July 1969, pp. 1375-1378.

47. Levine, J. N. and Coats, D. E., "Transonic Flow in a Converging-Diverging Nozzle," NASA CR111104, Sept. 1970.

48. Taulbee, D. B. and Boraas, S., "Transonic Nozzle Flow with Nonuniform Total Energy," AIAA Journal, Vol. 9, Oct. 1971, pp. 2102-2104.

49. Boraas, S., "Transonic Nozzle Flow with a Parabolic Temperature Distribution," AIAA Journal, Vol. 10, Dec. 1972, pp. 1720-1722.

50. Boraas, S., "Transonic Nozzle Flow with Nonuniform Gas Properties," AIAA Journal, Vol. 11, Feb. 1973, pp. 210-215.

51. Ishii, R., "Reply by Author to S. Boraas," AIAA Journal, Vol. 15, Sept. 1977, pp. 1375-1376.

52. Smithey, W. J. H. and Naber, M. E., "Sonic Line for a Coaxial Axisymmetric Nozzle," AIAA Journal, Vol. 11, April 1973, pp. 569-570.

53. Flack, R. D. and Thompson, H. D., "Comparison of Pressure and LDV Velocity Measurements with Predictions in Transonic Flow," AIAA Journal Vol. 13, Jan. 1975, pp. 53-59.

54. Ishii, R., "Transonic Nozzle Flows of Gases with a Rate Process," AIAA Journal, Vol. 15, March 1977, pp. 299-300.

55. Boraas, S., "Comment on 'Transonic Nozzle Flows of Gases with a Rate Process'," AIAA Journal, Vol. 15, Sept. 1977, p. 1375.

56. Ishii, R., "Transonic Nozzle Flows of Real Gases with Nonuniform Gas Properties," Phys. Fluids, Vol. 21, April 1978, pp. 540-548.

57. Saunders, L. M., "Numerical Solution of the Flow Field in the Throat Region of a Nozzle," Tech. Note BSVD-P-66-TN-001, Brown Engineering Co., Inc., Huntsville, Alabama, 1966.

58. Back, L. H., Massier, P. F., and Gier, H. L., "Comparison of Measured and Predicted Flows through Conical Supersonic Nozzles, with Emphasis on the Transonic Region," AIAA Journal, Vol. 3, Sept. 1965, pp. 1606-1614.

59. Migdal, D., Klein, K., and Moretti, G., "Time-Dependent Calculations for Transonic Nozzle Flow," AIAA Journal, Vol. 7, Feb. 1969, pp. 372-374.

60. Wehofer, S. and Moger, W. C., "Transonic Flow in Conical Convergent and Convergent-Divergent Nozzles with Nonuniform Inlet Conditions," AIAA Paper 70-635, 1970.

61. Brunell, R. D., "Numerical Solutions for Compressible Flow in Planar Converging-Diverging Ducts," Ph.D. dissertation, University of Notre Dame, 1970.

62. Laval, P., "Time-Dependent Calculation Method for Transonic Nozzle Flows," Proceedings of the Second International Conference on Numerical Methods in Fluid Dynamics, 1970. Published in: Lecture Notes in Physics, Vol. 8, Springer Verlag, New York, 1971, pp. 187-192.

63. Masure, B., Solignac, J. L., and Laval, P., "Mass Flow Rate Measurement by Means of a Sonic Throat," ONERA T.P. no. 956, 1971.

64. Serra, R. A., "Determination of Internal Gas Flows by a Transient Numerical Technique," AIAA Journal, Vol. 10, May 1972, pp. 603-611.

65. Cline, M. C., "Computation of Steady Nozzle Flow by a Time-Dependent Method," AIAA Journal, Vol. 12, April 1974, pp. 419-420.

66. Cline, M. C., "The Computation of Steady Nozzle Flow by a Time-Dependent Method," NASA TM X-71918, April 1974.

67. Cline, M. C., "Computation of Two-Dimensional, Viscous Nozzle Flow," AIAA Journal, Vol. 14, March 1976, pp. 295-296.

68. Cline, M. C., "VNAP: A Computer Program for Computation of Two-Dimensional, Time-Dependent, Compressible, Viscous, Internal Flow," Los Alamos Scientific Laboratory Report LA-7326, Nov. 1978.

69. Dorodnitsyn, A. A., "A Contribution to the Solution of Mixed Problems of Transonic Aerodynamics," Advances in Aeronautical Sciences, Vol. 2, Sept. 1958, pp. 832-844.

70. Holt, M., "The Design of Plane and Axisymmetric Nozzles by the Method of Integral Relations," Symposium Transsonicum, Springer Verlag, Berlin, 1964, pp. 310-324.

71. Liddle, S. G. and Archer, R. D., "Transonic Flow in Nozzles Using the Method of Integral Relations," J. of Spacecraft and Rockets, Vol. 8, July 1971, pp. 722-728.

72. Liddle, S. G., "Integral Relations Method Computations of Annular and Asymmetric Plane Nozzle Flowfields," J. of Spacecraft and Rockets, Vol. 11, March 1974, pp. 146-151.

73. Katsanis, T., "A Computer Program for Calculating Velocities and Streamlines for Two-Dimensional, Incompressible Flow in Axial Blade Rows," NASA TN D-3762, Jan. 1967.

74. Emmons, H. W., "The Numerical Solution of Compressible Fluid Flow Problems," NACA TN 932, March 1944.

75. Emmons, H. W., "The Theoretical Flow of a Frictionless, Adiabatic, Perfect Gas Inside of a Two-Dimensional Hyperbolic Nozzle," NACA TN 1003, Feb. 1945.

76. Prozan, R. J. and Kooker, D. E., "The Error Minimization Technique with Application to a Transonic Nozzle Solution," Journal of Fluid Mechanics, Vol. 43, 1970, pp. 269-277.

77. Brown, E. F., Brecht, T. J. F., and Walsh, K. E., "A Relaxation Solution of Transonic Nozzle Flows Including Rotational Flow Effects," J. Aircraft, Vol. 14, Oct. 1977, pp. 944-951.

78. Fanning, A. E. and Mueller, T. J., "Direct Method for Calculating the Transonic Region of Propulsive Nozzles," AIAA Paper 78-206, Jan. 1978.

79. Jacobs, W., "Geswindigkeitsverteilungen in zweidimensionalen gekrümmten Lavaldüsen," Jahrbuch wiss. Gesellschaft Luftfahrt, 1954, pp. 57-62.

80. Thompson, H. D., Stevenson, W. H., Flack, R. D., and Zammitt, R. E., "Laser Doppler Velocimeter Measurements in High Speed Flows," U.S. Army Missile Command Technical Report No. RD-CR-75-2, Dec. 1974.

81. Stanton, T. E., "The Variation of Velocity in the Neighbourhood of the Throat of a Constriction in a Wind Channel." Aeronautical Research Council, Reports and Memoranda No. 1388, May 1930.

82. Massier, P. F., Back, L. H., Noel, M. B., and Saheli, F., "Viscous Effects on the Flow Coefficient for a Supersonic Nozzle," AIAA Journal, Vol. 8, March 1970, pp. 605-607.

83. Back, L. H. and Cuffel, R. F., "Flow Coefficients for Supersonic Nozzles with Comparatively Small Radius of Curvature Throats," J. of Spacecraft and Rockets, Vol. 8, Feb. 1971, pp. 196-198.

84. Back, L. H., Cuffel, R. F., and Massier, P. F., "Influence of Contraction Section Shape and Inlet Flow Direction on Supersonic Nozzle Flow and Performance," J. of Spacecraft and Rockets, Vol. 9, June 1972, pp. 420-427.

85. Bresnahan, D. L. and Johns, A. L., "Cold Flow Investigation of a Low Angle Turbojet Plug Nozzle with Fixed Throat and Translating Shroud at Mach Numbers from 0 to 2.0," NASA TM X-3114, Aug. 1968.

86. Zucrow, M. J. and Hoffman, J. D., Gas Dynamics, 1st Ed., Vol. 1, Wiley, New York, 1976, pp. 538-545.

87. Dutton, J. C., unpublished results, Department of Mechanical and Industrial Engineering, University of Illinois at Urbana-Champaign, 1978.

88. Dutton, J. C. and Addy, A. L., "Theory, Computer Program, and Illustrative Examples for the Two-Dimensional Boundary Layer Flow of Ideal Gases," U.S. Army Missile Research and Development Command Technical Report T-CR-78-10, March 1978.

89. Holman, J. P., Experimental Methods for Engineers, 2nd Ed., McGraw-Hill Book Co., New York, 1971, pp. 37-44.

90. Shapiro, A. H., The Dynamics and Thermodynamics of Compressible Fluid Flow, Vol. 1, The Ronald Press Co., New York, 1953, pp. 229-232.

91. Rayle, R. E., Jr., "An Investigation of the Influence of Orifice Geometry on Static Pressure Measurements," M.S. thesis, M. I. T., 1949.

92. Shaw, R., "The Influence of Hole Dimensions on Static Pressure Measurements," Journal of Fluid Mechanics, Vol. 7, April 1960, pp. 550-564.

93. Livesey, J. L., Jackson, J. D., and Southern, C. J., "The Static Hole Error Problem," Aircraft Engineering, Vol. 34, Feb. 1962, pp. 43-47.

94. Chue, S. H., "Pressure Probes for Fluid Measurement," Prog. Aerospace Sci., Vol. 16, 1975, pp. 147-223.

APPENDIX A. INVESTIGATION OF EQUATIONS FOR CIRCULAR ARC CONTOURS

Assuming that the bounding walls of the annular nozzle are circular arcs, their equations in the x-y coordinate system may be written as

$$(x-a_i)^2 + (y-b_i)^2 = R_{ci}^2 \tag{A-1}$$

and $$(x-a_o)^2 + (y-b_o)^2 = R_{co}^2 , \tag{A-2}$$

where (a_i, b_i) and (a_o, b_o) are the coordinates of the centers and R_{ci} and R_{co} are the radii, Fig. A.1. In the Maclaurin series expansions of these contour equations,

$$y = g(x) = y_i + g'(0)x + g''(0)\frac{x^2}{2!} + g'''(0)\frac{x^3}{3!} + \ldots \tag{A-3}$$

$$y = h(x) = y_o + h'(0)x + h''(0)\frac{x^2}{2!} + h'''(0)\frac{x^3}{3!} + \ldots , \tag{A-4}$$

the coefficients can be calculated as

$$g'(0) = \frac{a_i}{\left(R_{ci}^2 - a_i^2\right)^{1/2}} \qquad g''(0) = \frac{-R_{ci}^2}{\left(R_{ci}^2 - a_i^2\right)^{3/2}}$$

$$g'''(0) = \frac{3R_{ci}^2 a_i}{\left(R_{ci}^2 - a_i^2\right)^{5/2}} \qquad g^{iv}(0) = \frac{-3R_{ci}^2\left(R_{ci}^2 + 4a_i^2\right)}{\left(R_{ci}^2 - a_i^2\right)^{7/2}} \tag{A-5}$$

$$\vdots \qquad\qquad \vdots$$

and

$$h'(0) = \frac{-a_o}{\left(R_{co}^2 - a_o^2\right)^{1/2}} \qquad h''(0) = \frac{R_{co}^2}{\left(R_{co}^2 - a_o^2\right)^{3/2}}$$

$$h'''(0) = \frac{-3R_{co}^2 a_o}{\left(R_{co}^2 - a_o^2\right)^{5/2}} \qquad h^{iv}(0) = \frac{3R_{co}^2\left(R_{co}^2 + 4a_o^2\right)}{\left(R_{co}^2 - a_o^2\right)^{7/2}} \tag{A-6}$$

$$\vdots \qquad\qquad \vdots$$

From the definition of the expansion parameter, Eq. (III-20), it is known that the radii of curvature, R_{ci} and R_{co}, are $\mathcal{O}(\varepsilon^{-1})$. However, as can be seen from Eqs. (A-5) and (A-6), estimates for the x coordinates of the centers, a_i and a_o, must also be obtained in order to complete the order of magnitude analysis of the Maclaurin series coefficients.

To do this, the cross-sectional flow area in the nozzle throat in x-y coordinates is first written as

$$A(x) = 2\pi \int_{g(x)}^{h(x)} \frac{R}{d}\, dy = 2\pi \int_{g(x)}^{h(x)} (x \sin\beta + y \cos\beta)\, dy \ , \qquad \text{(A-7)}$$

where the transformations in Eqs. (III-3) and (III-4) have been used. Performing the integration and using the expansions in Eqs. (A-3) and (A-4), the first few terms in the expression for the area are

$$\begin{aligned} \frac{A(x)}{2\pi} = {} & \frac{\cos\beta}{2}\left(y_o^2 - y_i^2\right) + \left[\sin\beta(y_o - y_i) + \cos\beta(y_o h'(0) - y_i g'(0))\right] x \\ & + \left[\sin\beta(h'(0) - g'(0)) + \frac{\cos\beta}{2}\left(y_o h''(0) - y_i g''(0) + h'(0)^2 - g'(0)^2\right)\right] x^2 \\ & + \ldots \end{aligned} \qquad \text{(A-8)}$$

Since by definition the area is minimum at the throat plane, x = 0, dA/dx must vanish there. This leads to the relation

$$\tan\beta = y_i g'(0) - y_o h'(0) \ , \qquad \cos\beta \neq 0^{\dagger} \qquad \text{(A-9)}$$

since $y_o - y_i = 1$. Defining an average, symmetric throat slope, j'(0), and an average y location in the nozzle throat, $\bar{y}$, by

$$2\bar{y} j'(0) \equiv y_i g'(0) - y_o h'(0) \ , \qquad \text{(A-10)}$$

---

†The radial flow case, $\beta = \pi/2$, was previously ruled out, Eq. (III-28).

Eq. (A-9) yields the following relation for j'(0),

$$j'(0) = \frac{1}{2} \frac{\tan\bar{\alpha}}{y} . \tag{A-11}$$

In view of the previous restriction placed on $\tan\bar{\alpha}/y$, Eq. (III-30), the throat slope quantities, j'(0), g'(0), and h'(0), may be estimated as $(\epsilon^{3/2})$. Combining this information with the expressions for g'(0) and h'(0) from Eqs. (A-5) and (A-6) and the fact that the radii R_{ci} and R_{co} are $\mathcal{O}(\epsilon^{-1})$ results in the conclusion that the x coordinates of the centers of curvature, a_i and a_o, are $\mathcal{O}(\epsilon^{1/2})$ under the present assumptions. The order of magnitude estimates for the Maclaurin series coefficients for circular arc boundaries can then be completed as,

$$\begin{aligned} &g'(0),\ h'(0) = \mathcal{O}(\epsilon^{3/2}) && g''(0),\ h''(0) = \mathcal{O}(\epsilon) \\ &g'''(0),\ h'''(0) = \mathcal{O}(\epsilon^{7/2}) && g^{iv}(0),\ h^{iv}(0) = \mathcal{O}(\epsilon^{3}) \\ &\quad\vdots && \quad\vdots \end{aligned} \tag{A-12}$$

Although the details of the boundary condition evaluations have been presented here only for circular contours, the results are also valid for other contours whose Maclaurin series coefficients have similar orders of magnitude. Thus, the solutions developed in Chapter III are expected to apply to other conic section contours such as parabolic, hyperbolic, and elliptic arcs. It should also be noted that the boundary conditions at straight walls are identically satisfied since the wall slope is exactly matched and all higher derivatives vanish for this case.

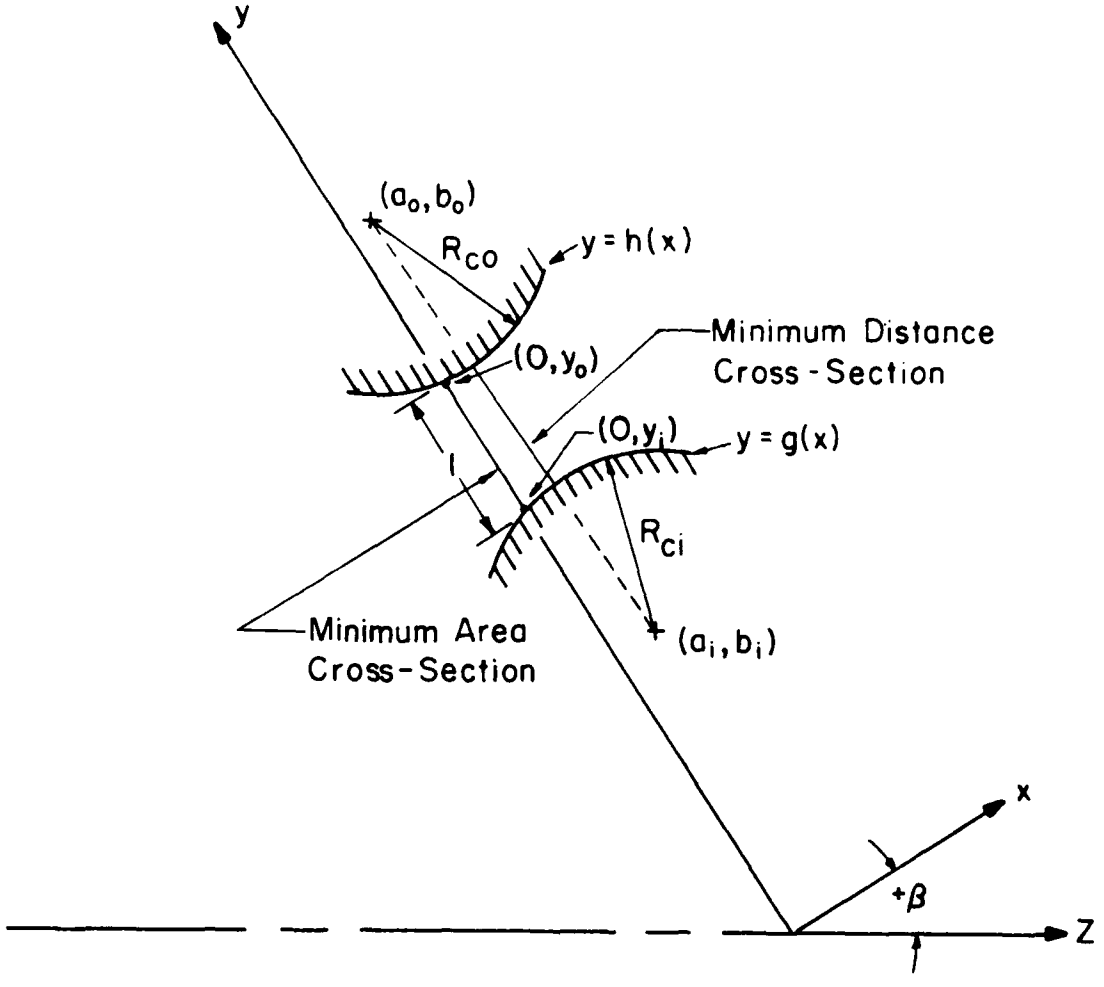

Figure A.1 Configuration and nomenclature for investigation of circular arc contour equations

APPENDIX B. SOLUTION SUMMARY

Referring to Fig. III.1, the only quantities which need to be specified in order to initiate the solution are: γ, the ratio of specific heats; ϵ, the parameter in the expansion variable, Eq. (III-22); N, the number of terms of the series to be included; and the equations for the inner and outer wall contours, G(R,Z)=0 and H(R,Z)=0. With the geometrical configuration given, the following quantities may be determined: the minimum area cross-section, i.e., the throat wall points (Z_i, R_i) and (Z_o, R_o); d, the throat half-height; Z*, the Z-location of the x-y origin; and β, the angle of inclination of the x-axis with respect to the symmetry axis. Utilizing the coordinate transformations listed in Eqs. (III-3) and (III-4), the parameters y_i, y_o, g'(0), h'(0), g"(0), and h"(0) in the x-y coordinate system can be evaluated; y = g(x) and y = h(x) are the transformed equations of the boundaries.

In order to carry out the initialization of the solution as well as its further evaluation, a library of FORTRAN routines has been developed and used. The throat plane is located numerically using a pivoting scheme whereby the location of the inner or outer wall point is alternately fixed and a sweep is made across the opposite contour until the minimum area section for the given fixed point is found. This process is continued until the fractional change in area between iterations is less than a prespecified convergence value, e.g., 10^{-10}. This method has been thoroughly checked by substituting results obtained with it into the Lagrange multiplier formulation of the problem of minimizing the flow cross-sectional area in an

annular nozzle with circular arc walls. Since the resulting equations have been found to be satisfied to a high degree of numerical accuracy, e.g., residuals on the order of 10^{-5} or smaller, it is concluded that this method can be used to locate accurately and reliably the throat plane. The contour derivatives g'(0), h'(0), g"(0), and h"(0) are also evaluated numerically using second order accurate, centered differences and a nodal spacing of $\Delta x = 10^{-3}$. The truncation error is therefore on the order of 10^{-6} which is sufficiently accurate for the present purposes.

Once the quantities mentioned above have been found, all of the flow-field properties of interest can be determined by the straightforward evaluation of a series of constants and functions. Given the point (Z,R) at which the information is desired, transformation Eqs. (III-3) and (III-4) are first employed to find the corresponding (x,y) coordinates and the following parameters are then evaluated,

$$\varepsilon = \frac{h''(0)-g''(0)}{2+\eta[h''(0)-g''(0)]} \tag{B-1}$$

$$z = \left(\frac{\gamma+1}{2}\,\varepsilon\right)^{-1/2} x \tag{B-2}$$

$$g_1 = \left(\frac{\gamma+1}{2}\right)^{-1/2} \varepsilon^{-3/2} g'(0) \tag{B-3}$$

$$h_1 = \left(\frac{\gamma+1}{2}\right)^{-1/2} \varepsilon^{-3/2} h'(0) \tag{B-4}$$

$$g_2 = \frac{2g''(0)}{h''(0)-g''(0)} \tag{B-5}$$

$$h_2 = \frac{2h''(0)}{h''(0)-g''(0)} \tag{B-6}$$

The transonic perturbation velocity components (u_1,v_1), (u_2,v_2), and (u_3,v_3) are then found as follows.

First Order Solution

The u_1 and v_1 velocity components from the first order solution are given by,

$$u_1(z,y) = A_1(y) + B_0 + B_1 z \tag{B-7}$$

$$v_1(z,y) = A_0'(y) + A_1'(y)z \ , \tag{B-8}$$

where the constants are determined in the following order,

$$B_2 = \frac{-\left(h_2 y_i - g_2 y_o\right) y_o y_i}{y_o^2 - y_i^2} \tag{B-9}$$

$$B_1 = \frac{\left(h_2 y_o - B_2\right)^{1/2}}{y_o} \tag{B-10}$$

$$B_4 = \frac{1}{4} B_1^3 y_o^3 + B_1 B_2 y_o \ln y_o - \frac{1}{2} B_1 B_2 y_o - B_1 \tag{B-11}$$

$$B_5 = \frac{1}{4} B_1^3 y_i^3 + B_1 B_2 y_i \ln y_i - \frac{1}{2} B_1 B_2 y_i - B_1 \tag{B-12}$$

$$B_3 = \frac{-\left[h_1 y_i - g_1 y_o - B_4 y_i - B_5 y_o\right] y_o y_i}{y_o^2 - y_i^2} \tag{B-13}$$

$$B_0 = \frac{h_1 y_o - B_4 y_o - B_3}{B_1 y_o^2} \tag{B-14}$$

$$B_6 = B_0 B_1 - \frac{1}{2} B_1 B_2 \ , \tag{B-15}$$

and the functions of y are determined as,

$$A_1'(y) = B_1^2 y + \frac{B_2}{y} \tag{B-16}$$

$$A_1(y) = \frac{1}{2} B_1^2 y^2 + B_2 \ln y \tag{B-17}$$

$$A_o'(y) = \frac{1}{4} B_1^3 y^3 + B_1 B_2 y \ln y - \frac{1}{2} B_1 B_2 y - B_1 + B_0 B_1 y + \frac{B_3}{y} . \qquad \text{(B-18)}$$

The discharge coefficient constant C_{D1} is found as,

$$C_{D4} = \frac{1}{4} B_0 B_1^2 - \frac{1}{16} B_1^2 B_2 \qquad \text{(B-19)}$$

$$C_{D5} = \frac{1}{2} B_0^2 + \frac{1}{4} B_2^2 - \frac{1}{2} B_0 B_2 \qquad \text{(B-20)}$$

$$C_{D6} = B_0 B_2 - \frac{1}{2} B_2^2 \qquad \text{(B-21)}$$

$$C_{D1} = \frac{1}{24} B_1^4 \left(y_o^6 - y_i^6\right) + C_{D4}\left(y_o^4 - y_i^4\right) + C_{D5}\left(y_o^2 - y_i^2\right) + \frac{1}{2} B_2^2 \left[y_o^2 \left(\ln y_o\right)^2 - y_i^2 \left(\ln y_i\right)^2\right]$$
$$+ \frac{1}{4} B_1^2 B_2 \left(y_o^4 \ln y_o - y_i^4 \ln y_i\right) + C_{D6}\left(y_o^2 \ln y_o - y_i^2 \ln y_i\right) . \qquad \text{(B-22)}$$

Second Order Solution

The u_2 and v_2 velocity components from the second order solution are given by

$$u_2(z,y) = [C_1(y) + D_0] + [2C_2(y) + D_1]z + D_2 z^2 \qquad \text{(B-23)}$$

$$v_2(z,y) = C_0'(y) + C_1'(y)z + C_2'(y)z^2 , \qquad \text{(B-24)}$$

where the constants are determined in the order,

$$D_3 = \frac{1}{2} B_1^2 y_o^2 + B_2 \ln y_o + B_0 \qquad \text{(B-25)}$$

$$D_4 = h_1 D_3 \qquad \text{(B-26)}$$

$$D_5 = h_2 n + h_2 D_3 + h_1 B_1 \qquad \text{(B-27)}$$

$$D_6 = h_2 B_1 \qquad \text{(B-28)}$$

$$D_7 = \frac{1}{2} B_1^2 y_i^2 + B_2 \ln y_i + B_0 \qquad \text{(B-29)}$$

$$D_8 = g_1 D_7 \qquad \text{(B-30)}$$

$$D_9 = g_2 n + g_1 B_1 + g_2 D_7 \tag{B-31}$$

$$D_{10} = g_2 B_1 \tag{B-32}$$

$$D_{11} = \frac{\left(D_{10} y_o - D_6 y_i\right) y_o y_i}{y_o^2 - y_i^2} \tag{B-33}$$

$$D_2 = \frac{D_6 y_o - \left(\frac{2\gamma-1}{2}\right) B_1^3 y_o^2 - D_{11}}{3 B_1 y_o^2} \tag{B-34}$$

$$D_{12} = \left(\frac{2\gamma-1}{2}\right) B_1^3 + 3 B_1 D_2 \tag{B-35}$$

$$D_{13} = 4 B_1 D_{12} + 2 B_1^2 D_2 + (2\gamma+1) B_1^4 \tag{B-36}$$

$$D_{14} = 8 B_1 D_{11} + 4 B_2 D_2 + (4\gamma-2) B_1^2 B_2 \tag{B-37}$$

$$D_{15} = 4 B_1^2 B_2 + 4 B_0 D_2 + (4\gamma-2) B_0 B_1^2 \tag{B-38}$$

$$D_{17} = \frac{1}{4} D_{13} y_o^3 + \left(\frac{1}{2} D_{15} - \frac{1}{4} D_{14}\right) y_o + \frac{1}{2} D_{14} y_o \ln y_o + 2 B_2^2 \frac{\ln y_o}{y_o} - \beta_1 B_1 \tag{B-39}$$

$$D_{18} = \frac{1}{4} D_{13} y_i^3 + \left(\frac{1}{2} D_{15} - \frac{1}{4} D_{14}\right) y_i + \frac{1}{2} D_{14} y_i \ln y_i + 2 B_2^2 \frac{\ln y_i}{y_i} - \beta_1 B_1 \tag{B-40}$$

$$D_{16} = \frac{\left(D_9 y_o - D_5 y_i - D_{18} y_o + D_{17} y_i\right) y_i y_o}{y_o^2 - y_i^2} \tag{B-41}$$

$$D_1 = \frac{D_5 y_o - D_{17} y_o - D_{16}}{2 B_1 y_o^2} \tag{B-42}$$

$$D_{19} = \frac{1}{2} D_{15} - \frac{1}{4} D_{14} + 2B_1 D_1 \tag{B-43}$$

$$D_{20} = \frac{1}{2} D_{19} - \frac{1}{8} D_{14} \tag{B-44}$$

$$D_{21} = B_1^2 D_{12} + \frac{1}{8} B_1 D_{13} + \left(\frac{2\gamma+1}{4}\right) B_1^5 \tag{B-45}$$

$$D_{22} = 2B_0 D_{12} + B_1^2 D_1 + (2\gamma-1) B_0 B_1^3 + 2B_1 D_{20} + 2B_1^2 B_6 + \frac{1}{2} B_1^3 B_2 \tag{B-46}$$

$$D_{23} = -\frac{9}{2} \beta_1 B_1^2 \tag{B-47}$$

$$D_{24} = -2\beta_1 B_2 - \beta_1 B_0 \tag{B-48}$$

$$D_{25} = 4B_2 D_{11} + (2\gamma+1) B_1 B_2^2 \tag{B-49}$$

$$D_{26} = 2B_2 D_{12} + 2B_1^2 D_{11} + \frac{1}{2} B_1 D_{14} + (2\gamma+1) B_1^3 B_2 \tag{B-50}$$

$$D_{27} = 4B_0 D_{11} + 2B_2 D_1 + (4\gamma-2) B_0 B_1 B_2 + 2B_1 D_{16} + 2B_1 B_2^2 \tag{B-51}$$

$$D_{28} = 2B_0 D_1 + (2\gamma-1) B_0^2 B_1 + 2B_1^2 B_3 + 2B_2 B_6 \tag{B-52}$$

$$\begin{aligned} D_{30} = {} & \frac{1}{6} D_{21} y_o^5 + \left(\frac{1}{4} D_{22} - \frac{1}{16} D_{26}\right) y_o^3 + \frac{1}{3} D_{23} y_o^2 + \left(\frac{1}{4} D_{25} - \frac{1}{4} D_{27} + \frac{1}{2} D_{28}\right) y_o \\ & + \frac{1}{2} D_{25} y_o \left(\ln y_o\right)^2 + \frac{1}{4} D_{26} y_o^3 \ln y_o + \left(\frac{1}{2} D_{27} - \frac{1}{2} D_{25}\right) y_o \ln y_o - \beta_1 B_2 \ln y_o \\ & + 2B_2 B_3 \frac{\ln y_o}{y_o} + \left(D_{24} + \beta_1 B_2\right) \end{aligned} \tag{B-53}$$

$$\begin{aligned} D_{31} = {} & \frac{1}{6} D_{21} y_i^5 + \left(\frac{1}{4} D_{22} - \frac{1}{16} D_{26}\right) y_i^3 + \frac{1}{3} D_{23} y_i^2 + \left(\frac{1}{4} D_{25} - \frac{1}{4} D_{27} + \frac{1}{2} D_{28}\right) y_i \\ & + \frac{1}{2} D_{25} y_i \left(\ln y_i\right)^2 + \frac{1}{4} D_{26} y_i^3 \ln y_i + \left(\frac{1}{2} D_{27} - \frac{1}{2} D_{25}\right) y_i \ln y_i - \beta_1 B_2 \ln y_i \\ & + 2B_2 B_3 \frac{\ln y_i}{y_i} + \left(D_{24} + \beta_1 B_2\right) \end{aligned} \tag{B-54}$$

$$D_{29} = \frac{\left(D_8 y_o - D_4 y_i - D_{31} y_o + D_{30} y_i\right) y_i y_o}{y_o^2 - y_i^2} \tag{B-55}$$

$$D_0 = \frac{D_4 y_o - D_{30} y_o - D_{29}}{B_1 y_o^2} \tag{B-56}$$

$$D_{32} = \frac{1}{4} D_{22} - \frac{1}{16} D_{26} \tag{B-57}$$

$$D_{33} = \frac{1}{4} D_{25} - \frac{1}{4} D_{27} + \frac{1}{2} D_{28} + B_1 D_0 \tag{B-58}$$

$$D_{34} = \frac{1}{2} D_{27} - \frac{1}{2} D_{25} \tag{B-59}$$

$$D_{35} = D_{24} + \beta_1 B_2 \ . \tag{B-60}$$

The functions of y are given by,

$$C_2'(y) = D_{12} y + \frac{D_{11}}{y} \tag{B-61}$$

$$C_2(y) = \frac{1}{2} D_{12} y^2 + D_{11} \ln y \tag{B-62}$$

$$C_1'(y) = \frac{1}{4} D_{13} y^3 + D_{19} y + \frac{D_{16}}{y} + \frac{1}{2} D_{14} y \ln y + 2B_2^2 \frac{\ln y}{y} - \beta_1 B_1 \tag{B-63}$$

$$C_1(y) = \frac{1}{16} D_{13} y^4 + D_{20} y^2 - \beta_1 B_1 y + B_2^2 (\ln y)^2 + \frac{1}{4} D_{14} y^2 \ln y + D_{16} \ln y \tag{B-64}$$

$$C_0'(y) = \frac{1}{6} D_{21} y^5 + D_{32} y^3 + \frac{1}{3} D_{23} y^2 + D_{33} y + \frac{D_{29}}{y} + \frac{1}{2} D_{25} y (\ln y)^2 + \frac{1}{4} D_{26} y^3 \ln y + D_{34} y \ln y - \beta_1 B_2 \ln y + 2B_2 B_3 \frac{\ln y}{y} + D_{35} \ . \tag{B-65}$$

The discharge coefficient constant C_{D2} is found from,

$$C_{D10} = \frac{1}{24} B_1^3 B_6 - \frac{1}{144} B_1^4 B_2 \tag{B-66}$$

$$C_{D11} = \frac{1}{16} B_1^3 B_3 + \frac{1}{8} B_6^2 - \frac{1}{16} B_1 B_2 B_6 + \frac{1}{64} B_1^2 B_2^2 \tag{B-67}$$

$$C_{D12} = \frac{1}{9} \beta_1 B_1 B_2 - \frac{1}{3} \beta_1 B_6 \tag{B-68}$$

$$C_{D13} = \frac{1}{2} B_3 B_6 + \frac{1}{4} \beta_1^2 - \frac{1}{4} B_1 B_2 B_3 \tag{B-69}$$

$$C_{D14} = \frac{1}{4} B_1 B_2 B_6 - \frac{1}{16} B_1^2 B_2^2 \tag{B-70}$$

$$\begin{aligned} C_{D7} = {} & \frac{1}{256} B_1^6 \left(y_o^8 - y_i^8\right) + C_{D10}\left(y_o^6 - y_i^6\right) - \frac{1}{20} \beta_1 B_1^3 \left(y_o^5 - y_i^5\right) + C_{D11}\left(y_o^4 - y_i^4\right) \\ & + C_{D12}\left(y_o^3 - y_i^3\right) + C_{D13}\left(y_o^2 - y_i^2\right) - \beta_1 B_3 \left(y_o - y_i\right) + \frac{1}{8} B_1^2 B_2^2 \left[y_o^4 \left(\ln y_o\right)^2 \right. \\ & \left. - y_i^4 \left(\ln y_i\right)^2\right] + \frac{1}{24} B_1^4 B_2 \left(y_o^6 \ln y_o - y_i^6 \ln y_i\right) + C_{D14}\left(y_o^4 \ln y_o - y_i^4 \ln y_i\right) \\ & - \frac{1}{3} \beta_1 B_1 B_2 \left(y_o^3 \ln y_o - y_i^3 \ln y_i\right) + \frac{1}{2} B_1 B_2 B_3 \left(y_o^2 \ln y_o - y_i^2 \ln y_i\right) \\ & + \frac{1}{2} B_3^2 \ln\left(y_o / y_i\right) \end{aligned} \tag{B-71}$$

$$C_{D15} = \frac{1}{6} B_1^2 D_{20} + \frac{1}{48} B_0 D_{13} - \frac{1}{144} B_1^2 D_{14} - \frac{1}{288} B_2 D_{13} \tag{B-72}$$

$$\begin{aligned} C_{D16} = {} & \frac{1}{4} B_1^2 D_0 + \frac{1}{2} B_0 D_{20} + \frac{1}{32} B_1^2 B_2^2 + \frac{1}{64} B_2 D_{14} - \frac{1}{16} B_1^2 D_{16} \\ & - \frac{1}{8} B_2 D_{20} - \frac{1}{32} B_0 D_{14} \end{aligned} \tag{B-73}$$

$$C_{D17} = \frac{2}{9} \beta_1 B_1 B_2 - \frac{2}{3} \beta_1 B_0 B_1 \tag{B-74}$$

$$C_{D18} = B_0 D_0 - \frac{3}{4} B_2^3 + \frac{1}{2} B_2 D_{16} + \frac{1}{2} B_0 B_2^2 - \frac{1}{2} B_2 D_0 - \frac{1}{2} B_0 D_{16} \tag{B-75}$$

$$C_{D19} = \frac{1}{4} B_1^2 B_2^2 + \frac{1}{8} B_2 D_{14} \tag{B-76}$$

$$C_{D20} = B_2 D_{16} + B_0 B_2^2 - \frac{3}{2} B_2^3 \tag{B-77}$$

$$C_{D21} = \frac{1}{24} B_1^2 D_{14} + \frac{1}{48} B_2 D_{13} \tag{B-78}$$

$$C_{D22} = \frac{1}{4} B_1^2 D_{16} + \frac{1}{2} B_2 D_{20} + \frac{1}{8} B_0 D_{14} - \frac{1}{8} B_1^2 B_2^2 - \frac{1}{16} B_2 D_{14} \qquad \text{(B-79)}$$

$$C_{D23} = \frac{3}{2} B_2^3 - B_2 D_{16} - B_0 B_2^2 + B_2 D_0 + B_0 D_{16} \qquad \text{(B-80)}$$

$$\begin{aligned} C_{D8} = {} & \frac{1}{128} B_1^2 D_{13} \left(y_o^8 - y_i^8\right) + C_{D15} \left(y_o^6 - y_i^6\right) - \frac{1}{5} B_1 B_1^3 \left(y_o^5 - y_i^5\right) + C_{D16} \left(y_o^4 - y_i^4\right) \\ & + C_{D17} \left(y_o^3 - y_i^3\right) + C_{D18} \left(y_o^2 - y_i^2\right) + B_2^3 \left[y_o^2 \left(\ln y_o\right)^3 - y_i^2 \left(\ln y_i\right)^3\right] \\ & + C_{D19} \left[y_o^4 \left(\ln y_o\right)^2 - y_i^4 \left(\ln y_i\right)^2\right] + C_{D20} \left[y_o^2 \left(\ln y_o\right)^2 - y_i^2 \left(\ln y_i\right)^2\right] \\ & + C_{D21} \left(y_o^6 \ln y_o - y_i^6 \ln y_i\right) + C_{D22} \left(y_o^4 \ln y_o - y_i^4 \ln y_i\right) \\ & - \frac{2}{3} B_1 B_1 B_2 \left(y_o^3 \ln y_o - y_i^3 \ln y_i\right) + C_{D23} \left(y_o^2 \ln y_o - y_i^2 \ln y_i\right) \end{aligned} \qquad \text{(B-81)}$$

$$C_{D24} = \frac{1}{8} B_0 B_1^4 - \frac{1}{48} B_1^4 B_2 \qquad \text{(B-82)}$$

$$C_{D25} = \frac{3}{8} B_0^2 B_1^2 + \frac{3}{64} B_1^2 B_2^2 - \frac{3}{16} B_0 B_1^2 B_2 \qquad \text{(B-83)}$$

$$C_{D26} = \frac{1}{2} B_0^3 - \frac{3}{4} B_0^2 B_2 + \frac{3}{4} B_0 B_2^2 - \frac{3}{8} B_2^3 \qquad \text{(B-84)}$$

$$C_{D27} = \frac{3}{2} B_0 B_2^2 - \frac{3}{4} B_2^3 \qquad \text{(B-85)}$$

$$C_{D28} = \frac{3}{4} B_0 B_1^2 B_2 - \frac{3}{16} B_1^2 B_2^2 \qquad \text{(B-86)}$$

$$C_{D29} = \frac{3}{4} B_2^3 - \frac{3}{2} B_0 B_2^2 + \frac{3}{2} B_0^2 B_2 \qquad \text{(B-87)}$$

$$\begin{aligned} C_{D9} = {} & \left(\frac{2\gamma - 3}{3}\right) \left[\frac{1}{64} B_1^6 \left(y_o^8 - y_i^8\right) + C_{D24} \left(y_o^6 - y_i^6\right) + C_{D25} \left(y_o^4 - y_i^4\right) + C_{D26} \left(y_o^2 - y_i^2\right) \right. \\ & + \frac{1}{2} B_2^3 \left[y_o^2 \left(\ln y_o\right)^3 - y_i^2 \left(\ln y_i\right)^3\right] + \frac{3}{8} B_1^2 B_2^2 \left[y_o^4 \left(\ln y_o\right)^2 - y_i^4 \left(\ln y_i\right)^2\right] \\ & + C_{D27} \left[y_o^2 \left(\ln y_o\right)^2 - y_i^2 \left(\ln y_i\right)^2\right] + \frac{1}{8} B_1^4 B_2 \left(y_o^6 \ln y_o - y_i^6 \ln y_i\right) \\ & \left. + C_{D28} \left(y_o^4 \ln y_o - y_i^4 \ln y_i\right) + C_{D29} \left(y_o^2 \ln y_o - y_i^2 \ln y_i\right)\right] \end{aligned} \qquad \text{(B-88)}$$

$$C_{D2} = C_{D7} + C_{D8} + C_{D9} \quad . \tag{B-89}$$

Third Order Solution

The u_3 and v_3 velocity components from the third order solution are given by,

$$u_3(z,y) = \left[E_1(y)+F_0\right] + \left[2E_2(y)+F_1\right]z + \left[3E_3(y)+F_2\right]z^2 + F_3 z^3 \tag{B-90}$$

$$v_3(z,y) = E_0'(y) + E_1'(y)z + E_2'(y)z^2 + E_3'(y)z^3 \quad , \tag{B-91}$$

where the constants are determined in the following order,

$$F_4 = h_1\left[\frac{1}{16} D_{13} y_o^4 + D_{20} y_o^2 - \beta_1 B_1 y_o + B_2^2 \left(\ln y_o\right)^2 + \frac{1}{4} D_{14} y_o^2 \ln y_o + D_{16} \ln y_o + D_o\right] \tag{B-92}$$

$$\begin{aligned} F_5 = {} & h_2 \eta^2 + h_2 \eta\left[\frac{1}{2} B_1^2 y_o^2 + B_2 \ln y_o + B_0\right] + h_2\left[\frac{1}{16} D_{13} y_o^4 + D_{20} y_o^2 \right. \\ & \left. - \beta_1 B_1 y_o + B_2^2 \left(\ln y_o\right)^2 + \frac{1}{4} D_{14} y_o^2 \ln y_o + D_{16} \ln y_o + D_o\right] \\ & + h_1\left[D_{12} y_o^2 + 2D_{11} \ln y_o + D_1\right] - \left(\frac{\gamma+1}{2}\right) h_1\left[\frac{3}{4} B_1^3 y_o^2 \right. \\ & \left. + B_6 + B_1 B_2 \ln y_o + B_1 B_2 - \frac{B_3}{y_o^2}\right] \end{aligned} \tag{B-93}$$

$$\begin{aligned} F_6 = {} & h_2 \eta B_1 + h_1 D_2 + h_2\left[D_{12} y_o^2 + 2D_{11} \ln y_o + D_1\right] - \left(\frac{\gamma+1}{2}\right) h_1\left[B_1^2 - \frac{B_2}{y_o^2}\right] \\ & - \left(\frac{\gamma+1}{4}\right) h_2\left[\frac{3}{4} B_1^3 y_o^2 + B_6 + B_1 B_2 \ln y_o + B_1 B_2 - \frac{B_3}{y_o^2}\right] \end{aligned} \tag{B-94}$$

$$F_7 = h_2 D_2 - \left(\frac{\gamma+1}{4}\right) h_2\left[B_1^2 - \frac{B_2}{y_o^2}\right] \tag{B-95}$$

$$F_8 = g_1\left[\frac{1}{16} D_{13} y_i^4 + D_{20} y_i^2 - \cdots B_1 y_i + B_2^2 (\cdots y_i)^2 + \frac{1}{4} D_{14} y_i^2 \cdots y_i + D_{16} \cdots y_i + D_0\right] \quad \text{(B-96)}$$

$$F_9 = g_2 \cdots^2 + g_2 n\left[\frac{1}{2} B_1^2 y_i^2 + B_2 \cdots y_i + B_0\right] + g_1\left[D_{12} y_i^2 + 2D_{11} \cdots y_i + D_1\right]$$
$$+ g_2\left[\frac{1}{16} D_{13} y_i^4 + D_{20} y_i^2 - \cdots B_1 y_i + B_2^2 (\cdots y_i)^2 + \frac{1}{4} D_{14} y_i^2 \cdots y_i + D_{16} \cdots y_i + D_0\right] - \left(\frac{\gamma+1}{2}\right) g_1\left[\frac{3}{4} B_1^3 y_i^2 + B_6 + B_1 B_2 \cdots y_i + B_1 B_2 - \frac{B_3}{y_i^2}\right] \quad \text{(B-97)}$$

$$F_{10} = g_2 n B_1 + g_1 D_2 + g_2\left[D_{12} y_i^2 + 2D_{11} \cdots y_i + D_1\right] - \left(\frac{\gamma+1}{2}\right) g_1\left[B_1^2 - \frac{B_2}{y_i^2}\right]$$
$$- \left(\frac{\gamma+1}{4}\right) g_2\left[\frac{3}{4} B_1^3 y_i^2 + B_6 + B_1 B_2 \cdots y_i + B_1 B_2 - \frac{B_3}{y_i^2}\right] \quad \text{(B-98)}$$

$$F_{11} = g_2 D_2 - \left(\frac{\gamma+1}{4}\right) g_2\left[B_1^2 - \frac{B_2}{y_i^2}\right] \quad \text{(B-99)}$$

$$F_{12} = 2(\gamma-1) B_1 D_{12} + 2(\gamma-1) B_1^2 D_2 + (\gamma-1) B_1^4 + 4D_2^2 + 4B_1^2 D_2 \quad \text{(B-100)}$$

$$F_{13} = \frac{\left(F_{11} y_o - F_7 y_i\right) y_i y_o}{y_o^2 - y_i^2} \quad \text{(B-101)}$$

$$F_3 = \frac{F_7 y_o - \frac{1}{2} F_{12} y_o^2 - F_{13}}{4B_1 y_o^2} \quad \text{(B-102)}$$

$$F_{14} = \frac{1}{2} F_{12} + 4B_1 F_3 \quad \text{(B-103)}$$

$$F_{15} = 3B_1^2F_3 + (\gamma+2)B_1^3D_2 + 9B_1F_{14} + 6D_2D_{12} + 3(\gamma+2)B_1^2D_{12} + (2\gamma)B_1^5 + (\gamma-1)B_1D_{13} \quad \text{(B-104)}$$

$$F_{16} = \left(\frac{\gamma+1}{2}\right)\beta_1B_1^2 - \beta_1D_2 \quad \text{(B-105)}$$

$$F_{17} = \left(\frac{5\gamma-1}{2}\right)B_1B_2^2 + 6B_2D_{11} \quad \text{(B-106)}$$

$$F_{18} = \left(\frac{\gamma+1}{2}\right)\beta_1B_2 \quad \text{(B-107)}$$

$$F_{19} = 6B_2F_3 + 2(\gamma+2)B_1B_2D_2 + 18B_1F_{13} + 12D_2D_{11} + 2(2\gamma+1)B_1^2D_{11} + 2(\gamma-1)B_2D_{12} + (\gamma-1)B_1D_{14} + 3(\gamma-1)B_1^3B_2 \quad \text{(B-108)}$$

$$F_{20} = \left(\frac{3\gamma+5}{2}\right)B_1^3B_2 + 6B_1^2D_{11} + 6B_2D_{12} + 2(\gamma-1)B_0D_{12} + 2(\gamma-1)B_1D_{19} + \left(\frac{\gamma-1}{2}\right)B_1D_{14} + 2(\gamma-1)B_6D_2 + (\gamma-1)B_1^2B_6 + (\gamma-1)B_1B_2D_2 + (2\gamma+1)B_1^2D_1 + 2(\gamma-1)B_0B_1^3 + 6B_0F_3 + 6D_1D_2 + 6B_0B_1D_2 \quad \text{(B-109)}$$

$$F_{22} = \frac{1}{4}F_{15}y_o^3 + F_{16} + F_{17}\frac{\ln y_o}{y_o} - \frac{F_{18}}{y_o^2} + F_{19}\left[\frac{1}{2}y_o\ln y_o - \frac{1}{4}y_o\right] + \frac{1}{2}F_{20}y_o \quad \text{(B-110)}$$

$$F_{23} = \frac{1}{4}F_{15}y_i^3 + F_{16} + F_{17}\frac{\ln y_i}{y_i} - \frac{F_{18}}{y_i^2} + F_{19}\left[\frac{1}{2}y_i\ln y_i - \frac{1}{4}y_i\right] + \frac{1}{2}F_{20}y_i \quad \text{(B-111)}$$

$$F_{21} = \frac{\left(F_{10}y_o - F_6y_i - F_{23}y_o + F_{22}y_i\right)y_iy_o}{y_o^2 - y_i^2} \quad \text{(B-112)}$$

$$F_2 = \frac{F_6 y_o - F_{21} - F_{22} y_o}{3B_1 y_o^2} \tag{B-113}$$

$$F_{24} = \frac{1}{2} F_{20} - \frac{1}{4} F_{19} + 3B_1 F_2 \tag{B-114}$$

$$F_{25} = \frac{1}{2} F_{24} - \frac{1}{8} F_{19} \tag{B-115}$$

$$F_{26} = 3B_1^2 F_{14} + \frac{1}{2} B_1 F_{15} + 2D_{12}^2 + \frac{1}{4} D_2 D_{13} + \left(\frac{5\gamma+4}{8}\right) B_1^2 D_{13} + (\gamma+2) B_1^3 D_{12} + \frac{1}{2} B_1^4 D_2 + \left(\frac{2\gamma+1}{2}\right) B_1^6 + (\gamma-1) B_1 D_{21} \tag{B-116}$$

$$F_{27} = 2B_1^2 F_2 + (\gamma+1) B_1^3 D_1 + 2B_0 B_1^2 D_2 + 6B_0 F_{14} + 8B_1 F_{25} + 4D_1 D_{12} + 4B_0 B_1 D_{12} + 4D_2 D_{20} + (2\gamma) B_1^2 D_{20} + (2\gamma) B_1^3 B_6 + \left(\frac{3\gamma+7}{4}\right) B_1^4 B_2 + (\gamma+3) B_1^2 D_{19} + B_2 D_{13} + (2\gamma) B_0 B_1^4 + 2(\gamma+1) B_6 D_{12} + B_1^3 D_{11} + \frac{1}{4} (\gamma-1) B_1^2 D_{14} + (\gamma-1) B_0 D_{13} + 4(\gamma-1) B_1 D_{32} + \frac{1}{4} (\gamma-1) B_1 D_{26} + (\gamma-1) B_1 B_2 D_{12} \tag{B-117}$$

$$F_{28} = 8B_1 F_{16} - 4\beta_1 B_1 D_2 - \left(\frac{19\gamma+43}{8}\right) \beta_1 B_1^3 - 5\beta_1 D_{12} + (\gamma-1) B_1 D_{23} \tag{B-118}$$

$$F_{29} = 8B_1 F_{18} - 2(\gamma+2) \beta_1 B_1 B_2 - 4\beta_1 D_{11} + (\gamma-1) \beta_1 B_0 B_1 + (\gamma-1) B_1 D_{35} - \beta_1 D_1 + \frac{1}{2} (\gamma+1) \beta_1 B_6 \tag{B-119}$$

$$F_{30} = (3\gamma-1) B_1 B_2 B_3 + 4B_2 D_{16} + (2\gamma) B_0 B_2^2 + 4B_3 D_{11} \tag{B-120}$$

$$F_{31} = \left(\frac{\gamma+1}{2}\right) \beta_1 B_3 \tag{B-121}$$

$$F_{32} = 12B_2 F_{13} + 4B_1 F_{17} + 8D_{11}^2 + 6B_2^2 D_2 + (5\gamma-3) B_1^2 B_2^2 + 4(\gamma+1) B_1 B_2 D_{11} + (\gamma-1) B_2 D_{14} + (\gamma-1) B_1 D_{25} \tag{B-122}$$

$$F_{33} = 6B_1^2F_{13} + 6B_2F_{14} + 2B_1F_{19} + 8D_{11}D_{12} + D_2D_{14} + \left(\frac{2\gamma+3}{2}\right)B_1^2D_{14}$$
$$+ 2(\gamma+1)B_1^3D_{11} + 2(\gamma+3)B_1B_2D_{12} + 2B_1^2B_2D_2 + (4\gamma)B_1^4B_2$$
$$+ (\gamma-1)B_2D_{13} + (\gamma-1)B_1D_{26} \qquad \text{(B-123)}$$

$$F_{34} = 4B_2F_2 + 2(\gamma+1)B_1B_2D_1 + 4B_0B_2D_2 + 12B_0F_{13} + 8B_1F_{21} + 8D_1D_{11}$$
$$+ 8B_0B_1D_{11} + 4D_2D_{16} + (2\gamma)B_1^2D_{16} + 2(\gamma+6)B_1^2B_2^2 + \left(\frac{\gamma+3}{2}\right)B_2D_{14}$$
$$+ 2(\gamma+1)B_1B_2D_{11} + 2(\gamma-1)B_2D_{19} + (\gamma-1)B_0D_{14} + (\gamma-1)B_1D_{25} \qquad \text{(B-124)}$$
$$+ 2(\gamma-1)B_1D_{34} + 4(\gamma-1)B_6D_{11} + 4(\gamma-1)B_0B_1^2B_2 + 2(\gamma-1)B_1B_2B_6$$

$$F_{35} = \frac{1}{2}(\gamma+1)B_1B_1B_2 - 2B_1D_{11} \qquad \text{(B-125)}$$

$$F_{36} = 2(\gamma+4)B_2^3 \qquad \text{(B-126)}$$

$$F_{37} = (\gamma+1)B_1^3B_3 + (\gamma+1)B_1B_2B_6 + 4B_1^2D_{16} + 4B_2D_{19} + (\gamma)B_1^2B_2^2 + (\gamma+3)B_0B_1^2B_2$$
$$+ 4B_3D_{12} + 4B_6D_{11} + 2(\gamma-1)B_0D_{19} + \frac{1}{2}(\gamma-1)B_0D_{14} + 2(\gamma-1)B_1D_{33}$$
$$+ (\gamma-1)B_1D_{34} + 2(\gamma-1)B_6D_1 + 2(\gamma-1)B_0B_1B_6 + (\gamma-1)B_1B_2D_1 \qquad \text{(B-127)}$$
$$+ (2\gamma)B_1^2D_0 + (\gamma-1)B_0^2B_1^2 + 4B_0F_2 + 2D_1^2 + 4D_0D_2 + 4B_0B_1D_1 + 2B_0^2D_2$$

$$F_{39} = \frac{1}{6}F_{26}y_o^5 + \frac{1}{4}F_{27}y_o^3 + \frac{1}{3}F_{28}y_o^2 + F_{29} + F_{30}\frac{\ln y_o}{y_o} - \frac{F_{31}}{y_o^2}$$
$$+ F_{32}\left[\frac{1}{2}y_o\left(\ln y_o\right)^2 - \frac{1}{2}y_o\ln y_o + \frac{1}{4}y_o\right] + F_{33}\left[\frac{1}{4}y_o^3\ln y_o - \frac{1}{16}y_o^3\right]$$
$$+ F_{34}\left[\frac{1}{2}y_o\ln y_o - \frac{1}{4}y_o\right] + F_{35}\left[\ln y_o - 1\right] + \frac{1}{2}F_{36}\frac{\left(\ln y_o\right)^2}{y_o}$$
$$+ \frac{1}{2}F_{37}y_o \qquad \text{(B-128)}$$

$$F_{40} = \frac{1}{6} F_{26} y_i^5 + \frac{1}{4} F_{27} y_i^3 + \frac{1}{3} F_{28} y_i^2 + F_{29} + F_{30} \frac{\ln y_i}{y_i} - \frac{F_{31}}{y_i^2}$$

$$+ F_{32}\left[\frac{1}{2} y_i (\ln y_i)^2 - \frac{1}{2} y_i \ln y_i + \frac{1}{4} y_i\right] + F_{33}\left[\frac{1}{4} y_i^3 \ln y_i - \frac{1}{16} y_i^3\right]$$

$$+ F_{34}\left[\frac{1}{2} y_i \ln y_i - \frac{1}{4} y_i\right] + F_{35}\left[\ln y_i - 1\right] + \frac{1}{2} F_{36} \frac{(\ln y_i)^2}{y_i}$$

$$+ \frac{1}{2} F_{37} y_i \qquad \text{(B-129)}$$

$$F_{38} = \frac{\left(F_9 y_0 - F_5 y_i - F_{40} y_o + F_{39} y_i\right) y_i y_o}{y_o^2 - y_i^2} \qquad \text{(B-130)}$$

$$F_1 = \frac{F_5 y_o - F_{39} y_o - F_{38}}{2B_1 y_o^2} \qquad \text{(B-131)}$$

$$F_{41} = \frac{1}{4} F_{27} - \frac{1}{16} F_{33} \qquad \text{(B-132)}$$

$$F_{42} = \frac{1}{4} F_{32} - \frac{1}{4} F_{34} + \frac{1}{2} F_{37} + 2B_1 F_1 \qquad \text{(B-133)}$$

$$F_{43} = \frac{1}{2} F_{34} - \frac{1}{2} F_{32} \qquad \text{(B-134)}$$

$$F_{44} = F_{29} - F_{35} \qquad \text{(B-135)}$$

$$F_{45} = \frac{1}{4} F_{41} - \frac{1}{64} F_{33} \qquad \text{(B-136)}$$

$$F_{46} = \frac{1}{2} F_{42} + \frac{1}{8} F_{32} - \frac{1}{4} F_{43} \qquad \text{(B-137)}$$

$$F_{47} = F_{44} - F_{35} \qquad \text{(B-138)}$$

$$F_{48} = \frac{1}{2} F_{43} - \frac{1}{4} F_{32} \qquad \text{(B-139)}$$

$$F_{49} = \frac{1}{8} B_1^2 F_{15} + \frac{1}{18} B_1 F_{26} + \frac{1}{8} D_{12} D_{13} + \frac{1}{4} B_1^4 D_{12} + \left(\frac{\gamma+2}{16}\right) B_1^3 D_{13}$$
$$+ \left(\frac{5\gamma+3}{32}\right) B_1^7 + \left(\frac{3\gamma-1}{6}\right) B_1^2 D_{21} \qquad \text{(B-140)}$$

$$F_{50} = 2B_1^2 F_{25} + \frac{1}{4} B_0 F_{15} + 2B_1 F_{45} + 2D_{12} D_{20} + \frac{1}{8} D_1 D_{13} + \frac{1}{8} B_0 B_1 D_{13}$$
$$+ B_0 B_1^2 D_{12} + \frac{1}{4} B_1^4 D_1 + (\gamma) B_1^3 D_{20} + \left(\frac{\gamma+1}{2}\right) B_1^4 B_6 + (2\gamma) B_1^2 D_{32}$$
$$+ \frac{1}{3} B_2 D_{21} + \left(\frac{\gamma+1}{8}\right) B_1^5 B_2 + \left(\frac{\gamma}{2}\right) B_0 B_1^5 + \frac{1}{2} B_1^3 D_{19} + \left(\frac{\gamma+3}{8}\right) B_6 D_{13}$$
$$+ \left(\frac{\gamma-1}{8}\right) B_1^2 D_{26} + (\gamma-1) B_0 D_{21} + \left(\frac{\gamma-1}{16}\right) B_1 B_2 D_{13} \qquad \text{(B-141)}$$

$$F_{51} = 2B_1^2 F_{16} + \frac{2}{9} B_1 F_{28} - 2\beta_1 B_1 D_{12} - \left(\frac{2\gamma+3}{2}\right) \beta_1 B_1^4 + \left(\frac{3\gamma+1}{6}\right) B_1^2 D_{23}$$
$$- \frac{9}{16} \beta_1 D_{13} \qquad \text{(B-142)}$$

$$F_{52} = B_1^2 F_1 + B_0 B_1^2 D_1 + (\gamma) B_1^3 D_0 + 4B_0 F_{25} + 2B_1 F_{46} + 2D_0 D_{12} + B_0^2 D_{12}$$
$$+ 2D_1 D_{20} + 2B_0 B_1 D_{20} + \left(\frac{\gamma+3}{4}\right) B_1^4 B_3 + \left(\frac{\gamma-1}{2}\right) B_1 B_6^2 + (\gamma+1) B_1^2 D_{33}$$
$$+ 2B_2 D_{32} + B_1^2 B_2 B_6 + (\gamma+1) B_0 B_1^2 B_6 + \left(\frac{\gamma}{2}\right) B_0 B_1^3 B_2 + \frac{1}{2} B_1^3 D_{16}$$
$$+ 2B_6 D_{19} + \frac{1}{2} B_3 D_{13} + \left(\frac{\gamma-1}{2}\right) B_1^2 D_{34} + 4(\gamma-1) B_0 D_{32} + \left(\frac{\gamma-1}{4}\right) B_0 D_{26}$$
$$+ 2(\gamma-1) B_6 D_{20} + (\gamma-1) B_1 B_2 D_{20} + \left(\frac{\gamma-1}{2}\right) B_0^2 B_1^3 \qquad \text{(B-143)}$$

$$F_{53} = 2B_1^2 F_{18} + 4B_0 F_{16} + 2B_1 F_{47} - 2\beta_1 B_1 D_1 + (\gamma-5) \beta_1 B_0 B_1^2 - (3\gamma-1) \beta_1 B_1 B_6$$
$$+ \left(\frac{\gamma+3}{2}\right) B_1^2 D_{35} + \frac{2}{3} B_2 D_{23} - \left(\frac{3\gamma-1}{2}\right) \beta_1 B_1^2 B_2 - 2\beta_1 D_{19} + (\gamma-1) B_0 D_{23}$$
$$- \beta_1 D_{20} \qquad \text{(B-144)}$$

$$F_{54} = 4B_0 F_{18} + 2B_1 F_{31} - (\gamma+1) \beta_1 B_1 B_3 + 2B_2 D_{35} - (\gamma+1) \beta_1 B_0 B_2 - 2\beta_1 D_{16}$$
$$+ (\gamma-1) B_0 D_{35} - \beta_1 D_0 + (\gamma-1) \beta_1 B_0^2 \qquad \text{(B-145)}$$

$$F_{55} = \left(\frac{\gamma-1}{2}\right)B_1B_3^2 + 2B_2D_{29} + (2\gamma)B_0B_2B_3 + 2B_3D_{16} \quad \text{(B-146)}$$

$$F_{56} = 2B_2F_{17} + \frac{1}{3}B_1F_{36} + 6B_2^2D_{11} + (3\gamma-1)B_1B_2^3 + (\gamma-1)B_2D_{25} \quad \text{(B-147)}$$

$$F_{57} = B_1^2F_{17} + B_2F_{19} + \frac{1}{2}B_1F_{32} + 3B_2^2D_{12} + D_{11}D_{14} + 2B_1^2B_2D_{11}$$
$$+ (3\gamma)B_1^3B_2^2 + \left(\frac{\gamma+2}{2}\right)B_1B_2D_{14} + \left(\frac{\gamma+1}{2}\right)B_1^2D_{25} + (\gamma-1)B_2D_{26} \quad \text{(B-148)}$$

$$F_{58} = 4B_2F_{21} + 2B_0F_{17} + B_1F_{30} + 4D_{11}D_{16} + 3B_2^2D_1 + (2\gamma)B_0B_1B_2^2$$
$$+ 4B_0B_2D_{11} + (2\gamma)B_1B_2D_{16} + (\gamma)B_2D_{25} + \frac{3(\gamma+3)}{2}B_1B_2^3 + 2(\gamma-1)B_2D_{34}$$
$$+ (\gamma-1)B_0D_{25} + 3(\gamma-1)B_2^2B_6 \quad \text{(B-149)}$$

$$F_{59} = -\beta_1B_2^2 \quad \text{(B-150)}$$

$$F_{60} = \frac{1}{2}B_1^2F_{19} + \frac{1}{4}B_2F_{15} + \frac{1}{8}B_1F_{33} + \frac{1}{2}D_{12}D_{14} + \frac{1}{4}D_{11}D_{13} + B_1^2B_2D_{12}$$
$$+ \frac{1}{2}B_1^4D_{11} + \left(\frac{\gamma+1}{4}\right)B_1^3D_{14} + \left(\frac{\gamma+4}{8}\right)B_1B_2D_{13} + \left(\frac{2\gamma+1}{2}\right)B_1^5B_2$$
$$+ \left(\frac{\gamma}{2}\right)B_1^2D_{26} + (\gamma-1)B_2D_{21} \quad \text{(B-151)}$$

$$F_{61} = 2B_1^2F_{21} + 4B_2F_{25} + B_0F_{19} + 2B_1F_{48} + 2D_{12}D_{16} + 4D_{11}D_{20} + \frac{1}{2}D_1D_{14}$$
$$+ \frac{1}{2}B_0B_1D_{14} + 2B_0B_1^2D_{11} + 2B_0B_2D_{12} + B_1^2B_2D_1 + (\gamma)B_1^3D_{16}$$
$$+ (2\gamma)B_1B_2D_{20} + (2\gamma)B_1^2B_2B_6 + (\gamma+1)B_1^2D_{34} + \left(\frac{\gamma+1}{4}\right)B_2D_{26}$$
$$+ \left(\frac{\gamma+4}{2}\right)B_1^3B_2^2 + (2\gamma)B_0B_1^3B_2 + \left(\frac{\gamma+1}{2}\right)B_6D_{14} + 2B_1B_2D_{19} + \left(\frac{\gamma-1}{2}\right)B_1^2D_{25}$$
$$+ 4(\gamma-1)B_2D_{32} + (\gamma-1)B_0D_{26} + \left(\frac{\gamma-1}{4}\right)B_1B_2D_{14} \quad \text{(B-152)}$$

$$F_{62} = 4B_2F_{16} + 2B_1F_{35} - 4\beta_1B_1D_{11} - \left(\frac{5\gamma+11}{2}\right)\beta_1B_1^2B_2 - \frac{5}{4}\beta_1D_{14}$$
$$+ (\gamma-1)B_2D_{23} \quad \text{(B-153)}$$

$$F_{63} = 2B_2F_1 + 2B_0B_2D_1 + (2\gamma)B_1B_2D_0 + 4B_0F_{21} + 2B_1F_{38} + 4D_0D_{11}$$
$$+ 2B_0^2D_{11} + 2D_1D_{16} + 2B_0B_1D_{16} + (\gamma+5)B_1^2B_2B_3 + (\gamma+1)B_2D_{34}$$
$$+ 6B_2^2B_6 + (\gamma+1)B_0B_1B_2^2 + (\gamma+1)B_1B_2D_{16} + B_3D_{14} + 2(\gamma-1)B_2D_{33}$$
$$+ (\gamma-1)B_0D_{25} + 2(\gamma-1)B_0D_{34} + 2(\gamma-1)B_6D_{16} + (\gamma-1)B_0^2B_1B_2$$
$$+ 2(\gamma-1)B_0B_2B_6 \qquad \text{(B-154)}$$

$$F_{64} = 4B_2F_{18} - (\gamma+7)B_1B_2^2 + (\gamma-1)B_2D_{35} + (\gamma-1)B_1B_0B_2 - B_1D_{16} \qquad \text{(B-155)}$$

$$F_{65} = 2(\gamma+4)B_2^2B_3 \qquad \text{(B-156)}$$

$$F_{66} = (\gamma-1)B_1B_3B_6 + \left(\frac{\gamma+5}{2}\right)B_1^2B_1 + 2B_1^2D_{29} + 2B_2D_{33} + (\gamma)B_1^2B_2B_3$$
$$+ 2B_0B_1^2B_3 + 2B_0B_2B_6 + 2B_6D_{16} + 2B_3D_{19} + 2(\gamma-1)B_0D_{33}$$
$$+ (\gamma-1)B_0D_{34} + 2(\gamma-1)B_6D_0 + (\gamma-1)B_0^2B_6 + (\gamma-1)B_1B_2D_0$$
$$+ \left(\frac{\gamma-1}{2}\right)B_0^2B_1B_2 + 2B_0F_1 + 2D_0D_1 + B_0^2D_1 + 2B_0B_1D_0 \qquad \text{(B-157)}$$

$$F_{68} = \frac{1}{6}F_{50} - \frac{1}{36}F_{60} \qquad \text{(B-158)}$$

$$F_{69} = \frac{1}{4}F_{52} + \frac{1}{32}F_{57} - \frac{1}{16}F_{61} \qquad \text{(B-159)}$$

$$F_{70} = \frac{1}{3}F_{53} - \frac{1}{9}F_{62} \qquad \text{(B-160)}$$

$$F_{71} = \frac{1}{4}F_{58} - \frac{3}{8}F_{56} - \frac{1}{4}F_{63} + \frac{1}{2}F_{66} \qquad \text{(B-161)}$$

$$F_{72} = \frac{1}{2}F_{58} - \frac{3}{4}F_{56} \qquad \text{(B-162)}$$

$$F_{73} = \frac{1}{4}F_{61} - \frac{1}{8}F_{57} \qquad \text{(B-163)}$$

$$F_{74} = \frac{3}{4} F_{56} - \frac{1}{2} F_{58} + \frac{1}{2} F_{63} \tag{B-164}$$

$$F_{75} = F_{64} - 2F_{59} \tag{B-165}$$

$$F_{76} = F_{54} + 2F_{59} - F_{64} \tag{B-166}$$

$$\begin{aligned} F_{77} = {} & \frac{1}{8} F_{49} y_o^7 + F_{68} y_o^5 + \frac{1}{5} F_{51} y_o^4 + F_{69} y_o^3 + F_{70} y_o^2 + F_{71} y_o \\ & + \frac{1}{2} F_{56} y_o \left(\ln y_o\right)^3 + \frac{1}{4} F_{57} y_o^3 \left(\ln y_o\right)^2 + F_{72} y_o \left(\ln y_o\right)^2 + F_{59} \left(\ln y_o\right)^2 \\ & + \frac{1}{2} F_{65} \frac{\left(\ln y_o\right)^2}{y_o} + \frac{1}{6} F_{60} y_o^5 \ln y_o + F_{73} y_o^3 \ln y_o + \frac{1}{3} F_{62} y_o^2 \ln y_o \\ & + F_{74} y_o \ln y_o + F_{75} \ln y_o + F_{55} \frac{\ln y_o}{y_o} + F_{76} \end{aligned} \tag{B-167}$$

$$\begin{aligned} F_{78} = {} & \frac{1}{8} F_{49} y_i^7 + F_{68} y_i^5 + \frac{1}{5} F_{51} y_i^4 + F_{69} y_i^3 + F_{70} y_i^2 + F_{71} y_i \\ & + \frac{1}{2} F_{56} y_i \left(\ln y_i\right)^3 + \frac{1}{4} F_{57} y_i^3 \left(\ln y_i\right)^2 + F_{72} y_i \left(\ln y_i\right)^2 + F_{59} \left(\ln y_i\right)^2 \\ & + \frac{1}{2} F_{65} \frac{\left(\ln y_i\right)^2}{y_i} + \frac{1}{6} F_{60} y_i^5 \ln y_i + F_{73} y_i^3 \ln y_i + \frac{1}{3} F_{62} y_i^2 \ln y_i \\ & + F_{74} y_i \ln y_i + F_{75} \ln y_i + F_{55} \frac{\ln y_i}{y_i} + F_{76} \end{aligned} \tag{B-168}$$

$$F_{67} = \frac{\left(F_8 y_o - F_4 y_i - F_{78} y_o + F_{77} y_i\right) y_i y_o}{y_o^2 - y_i^2} \tag{B-169}$$

$$F_0 = \frac{F_4 y_o - F_{77} y_o - F_{67}}{B_1 y_o^2} \tag{B-170}$$

$$F_{79} = F_{71} + B_1 F_0 \ . \tag{B-171}$$

The functions of y are given by,

$$E_3'(y) = F_{14}y + \frac{F_{13}}{y} \tag{B-172}$$

$$E_3(y) = \frac{1}{2}F_{14}y^2 + F_{13}\ln y \tag{B-173}$$

$$E_2'(y) = \frac{1}{4}F_{15}y^3 + F_{24}y + \frac{F_{21}}{y} - \frac{F_{18}}{y^2} + \frac{1}{2}F_{19}y\ln y + F_{17}\frac{\ln y}{y} + F_{16} \tag{B-174}$$

$$E_2(y) = \frac{1}{16}F_{15}y^4 + F_{25}y^2 + F_{16}y + \frac{F_{18}}{y} + \frac{1}{2}F_{17}(\ln y)^2 + \frac{1}{4}F_{19}y^2\ln y + F_{21}\ln y \tag{B-175}$$

$$E_1'(y) = \frac{1}{6}F_{26}y^5 + F_{41}y^3 + \frac{1}{3}F_{28}y^2 + F_{42}y + \frac{F_{38}}{y} - \frac{F_{31}}{y^2} + \frac{1}{2}F_{32}y(\ln y)^2 + \frac{1}{2}F_{36}\frac{(\ln y)^2}{y} + \frac{1}{4}F_{33}y^3\ln y + F_{43}y\ln y + F_{35}\ln y + F_{30}\frac{\ln y}{y} + F_{44} \tag{B-176}$$

$$E_1(y) = \frac{1}{36}F_{26}y^6 + F_{45}y^4 + \frac{1}{9}F_{28}y^3 + F_{46}y^2 + F_{47}y + \frac{F_{31}}{y} + \frac{1}{6}F_{36}(\ln y)^3 + \frac{1}{4}F_{32}y^2(\ln y)^2 + \frac{1}{2}F_{30}(\ln y)^2 + \frac{1}{16}F_{33}y^4\ln y + F_{48}y^2\ln y + F_{35}y\ln y + F_{38}\ln y \tag{B-177}$$

$$E_0'(y) = \frac{1}{8}F_{49}y^7 + F_{68}y^5 + \frac{1}{5}F_{51}y^4 + F_{69}y^3 + F_{70}y^2 + F_{79}y + \frac{F_{67}}{y} + \frac{1}{2}F_{56}y(\ln y)^3 + \frac{1}{4}F_{57}y^3(\ln y)^2 + F_{72}y(\ln y)^2 + F_{59}(\ln y)^2 + \frac{1}{2}F_{65}\frac{(\ln y)^2}{y} + \frac{1}{6}F_{60}y^5\ln y + F_{73}y^3\ln y + \frac{1}{3}F_{62}y^2\ln y + F_{74}y\ln y + F_{75}\ln y + F_{55}\frac{\ln y}{y} + F_{76}\ . \tag{B-178}$$

The third order discharge coefficient constant C_{D3} is determined from,

$$C_{D36} = \frac{1}{4} B_1^3 D_{32} + \frac{1}{6} B_6 D_{21} \quad \text{(B-179)}$$

$$C_{D37} = \frac{1}{12} B_1^3 D_{23} - \frac{1}{6} \beta_1 D_{21} \quad \text{(B-180)}$$

$$C_{D38} = \frac{1}{4} B_1^3 D_{33} + B_6 D_{32} + \frac{1}{6} B_3 D_{21} \quad \text{(B-181)}$$

$$C_{D39} = \frac{1}{4} B_1^3 D_{35} + \frac{1}{3} B_6 D_{23} - \beta_1 D_{32} \quad \text{(B-182)}$$

$$C_{D40} = \frac{1}{4} B_1^3 D_{29} + B_6 D_{33} + B_3 D_{32} - \frac{1}{3} \beta_1 D_{23} \quad \text{(B-183)}$$

$$C_{D41} = B_6 D_{35} + \frac{1}{3} B_3 D_{23} - \beta_1 D_{33} \quad \text{(B-184)}$$

$$C_{D42} = B_6 D_{29} + B_3 D_{33} - \beta_1 D_{35} \quad \text{(B-185)}$$

$$C_{D43} = B_3 D_{35} - \beta_1 D_{29} \quad \text{(B-186)}$$

$$C_{D44} = \frac{1}{8} B_1^3 D_{25} + \frac{1}{4} B_1 B_2 D_{26} \quad \text{(B-187)}$$

$$C_{D45} = \frac{1}{2} B_6 D_{25} + B_1 B_2 D_{34} \quad \text{(B-188)}$$

$$C_{D46} = - \beta_1 B_1 B_2^2 - \frac{1}{2} \beta_1 D_{25} \quad \text{(B-189)}$$

$$C_{D47} = 2 B_1 B_2^2 B_3 + \frac{1}{2} B_3 D_{25} \quad \text{(B-190)}$$

$$C_{D48} = \frac{1}{16} B_1^3 D_{26} + \frac{1}{6} B_1 B_2 D_{21} \quad \text{(B-191)}$$

$$C_{D49} = \frac{1}{4} B_1^3 D_{34} + \frac{1}{4} B_6 D_{26} + B_1 B_2 D_{32} \quad \text{(B-192)}$$

$$C_{D50} = \frac{1}{3} B_1 B_2 D_{23} - \frac{1}{4} \beta_1 B_1^3 B_2 - \frac{1}{4} \beta_1 D_{26} \quad \text{(B-193)}$$

$$C_{D51} = \frac{1}{2} B_1^3 B_2 B_3 + B_6 D_{34} + B_1 B_2 D_{33} + \frac{1}{4} B_3 D_{26} \quad \text{(B-194)}$$

$$C_{D52} = -\beta_1 B_2 B_6 + B_1 B_2 D_{35} - \beta_1 D_{34} \tag{B-195}$$

$$C_{D53} = 2B_2 B_3 B_6 + B_1 B_2 D_{29} + B_3 D_{34} + \beta_1^2 B_2 \tag{B-196}$$

$$C_{D54} = \frac{1}{8} C_{D36} - \frac{1}{64} C_{D48} \tag{B-197}$$

$$C_{D55} = \frac{1}{6} C_{D38} + \frac{1}{108} C_{D44} - \frac{1}{36} C_{D49} \tag{B-198}$$

$$C_{D56} = \frac{1}{5} C_{D39} - \frac{1}{25} C_{D50} \tag{B-199}$$

$$C_{D57} = \frac{1}{4} C_{D40} - \frac{3}{256} B_1 B_2 D_{25} + \frac{1}{32} C_{D45} - \frac{1}{16} C_{D51} \tag{B-200}$$

$$C_{D58} = \frac{1}{3} C_{D41} + \frac{2}{27} C_{D46} - \frac{1}{9} C_{D52} \tag{B-201}$$

$$C_{D59} = \frac{1}{2} C_{D42} + \frac{1}{4} C_{D47} - \frac{1}{4} C_{D53} \tag{B-202}$$

$$C_{D60} = C_{D43} + 3\beta_1 B_2 B_3 \tag{B-203}$$

$$C_{D61} = \frac{1}{4} C_{D45} - \frac{3}{32} B_1 B_2 D_{25} \tag{B-204}$$

$$C_{D62} = \frac{1}{6} C_{D49} - \frac{1}{18} C_{D44} \tag{B-205}$$

$$C_{D63} = \frac{3}{64} B_1 B_2 D_{25} - \frac{1}{8} C_{D45} + \frac{1}{4} C_{D51} \tag{B-206}$$

$$C_{D64} = \frac{1}{3} C_{D52} - \frac{2}{9} C_{D46} \tag{B-207}$$

$$C_{D65} = \frac{1}{2} C_{D53} - \frac{1}{2} C_{D47} \tag{B-208}$$

$$\begin{aligned} C_{D30} = {} & \frac{1}{240} B_1^3 D_{21} \left(y_o^{10} - y_i^{10}\right) + C_{D54}\left(y_o^8 - y_i^8\right) + \frac{1}{7} C_{D37}\left(y_o^7 - y_i^7\right) + C_{D55}\left(y_o^6 - y_i^6\right) \\ & + C_{D56}\left(y_o^5 - y_i^5\right) + C_{D57}\left(y_o^4 - y_i^4\right) + C_{D58}\left(y_o^3 - y_i^3\right) + C_{D59}\left(y_o^2 - y_i^2\right) \\ & + C_{D60}\left(y_o - y_i\right) + \frac{1}{8} B_1 B_2 D_{25}\left[y_o^4 \left(\ln y_o\right)^3 - y_i^4 \left(\ln y_i\right)^3\right] \end{aligned}$$

$$+ \frac{1}{6} C_{D44}\left[y_o^6 \left(\ln y_o\right)^2 - y_i^6 \left(\ln y_i\right)^2\right] + C_{D61}\left[y_o^4 \left(\ln y_o\right)^2 - y_i^4 \left(\ln y_i\right)^2\right]$$

$$+ \frac{1}{3} C_{D46}\left[y_o^3 \left(\ln y_o\right)^2 - y_i^3 \left(\ln y_i\right)^2\right] + \frac{1}{2} C_{D47}\left[y_o^2 \left(\ln y_o\right)^2 - y_i^2 \left(\ln y_i\right)^2\right]$$

$$+ B_2 B_3^2\left[\left(\ln y_o\right)^2 - \left(\ln y_i\right)^2\right] + \frac{1}{8} C_{D48}\left[y_o^8 \ln y_o - y_i^8 \ln y_i\right] + C_{D62}\left[y_o^6 \ln y_o - y_i^6 \ln y_i\right]$$

$$+ \frac{1}{5} C_{D50}\left[y_o^5 \ln y_o - y_i^5 \ln y_i\right] + C_{D63}\left[y_o^4 \ln y_o - y_i^4 \ln y_i\right] + C_{D64}\left[y_o^3 \ln y_o - y_i^3 \ln y_i\right]$$

$$+ C_{D65}\left[y_o^2 \ln y_o - y_i^2 \ln y_i\right] - 3B_1 B_2 B_3\left[y_o \ln y_o - y_i \ln y_i\right] + B_3 D_{29} \ln(y_o/y_i) \quad \text{(B-209)}$$

$$C_{D66} = \frac{1}{4} B_1^5 B_6 + \frac{1}{16} B_0 B_1^6 \quad \text{(B-210)}$$

$$C_{D67} = \frac{1}{4} B_1^5 B_3 + \frac{1}{2} B_1^2 B_6^2 + \frac{1}{2} B_0 B_1^3 B_6 \quad \text{(B-211)}$$

$$C_{D68} = -\beta_1 B_1^2 B_6 - \frac{1}{2} \beta_1 B_0 B_1^3 \quad \text{(B-212)}$$

$$C_{D69} = B_1^2 B_3 B_6 + \frac{1}{2} \beta_1^2 B_1^2 + \frac{1}{2} B_0 B_1^3 B_3 + B_0 B_6^2 \quad \text{(B-213)}$$

$$C_{D70} = -\beta_1 B_1^2 B_3 - 2\beta_1 B_0 B_6 \quad \text{(B-214)}$$

$$C_{D71} = 2B_0 B_3 B_6 + \beta_1^2 B_0 + \frac{1}{2} B_1^2 B_3^2 \quad \text{(B-215)}$$

$$C_{D72} = 2B_1 B_2^2 B_6 + B_0 B_1^2 B_2^2 \quad \text{(B-216)}$$

$$C_{D73} = \frac{3}{2} B_1^3 B_2 B_6 + \frac{1}{2} B_0 B_1^4 B_2 \quad \text{(B-217)}$$

$$C_{D74} = \frac{3}{2} B_1^3 B_2 B_3 + B_2 B_6^2 + 2B_0 B_1 B_2 B_6 \quad \text{(B-218)}$$

$$C_{D75} = -2\beta_1 B_2 B_6 - 2\beta_1 B_0 B_1 B_2 \quad \text{(B-219)}$$

$$C_{D76} = 2B_2 B_3 B_6 + \beta_1^2 B_2 + 2B_0 B_1 B_2 B_3 \quad \text{(B-220)}$$

$$C_{D77} = \frac{1}{8} C_{D66} - \frac{5}{1024} B_1^6 B_2 \quad \text{(B-221)}$$

$$C_{D78} = \frac{1}{6} C_{D67} + \frac{1}{108} B_1^4 B_2^2 - \frac{1}{36} C_{D73} \tag{B-222}$$

$$C_{D79} = \frac{1}{5} C_{D68} + \frac{3}{50} \beta_1 B_1^3 B_2 \tag{B-223}$$

$$C_{D80} = \frac{1}{4} C_{D69} - \frac{3}{128} B_1^2 B_2^3 + \frac{1}{32} C_{D72} - \frac{1}{16} C_{D74} \tag{B-224}$$

$$C_{D81} = \frac{1}{3} C_{D70} - \frac{4}{27} \beta_1 B_1 B_2^2 - \frac{1}{9} C_{D75} \tag{B-225}$$

$$C_{D82} = \frac{1}{2} C_{D71} + \frac{1}{2} B_1 B_2^2 B_3 - \frac{1}{4} C_{D76} \tag{B-226}$$

$$C_{D83} = 2\beta_1 B_2 B_3 - 2\beta_1 B_0 B_3 \tag{B-227}$$

$$C_{D84} = \frac{1}{4} C_{D72} - \frac{3}{16} B_1^2 B_2^3 \tag{B-228}$$

$$C_{D85} = \frac{1}{6} C_{D73} - \frac{1}{18} B_1^4 B_2^2 \tag{B-229}$$

$$C_{D86} = \frac{3}{32} B_1^2 B_2^3 - \frac{1}{8} C_{D72} + \frac{1}{4} C_{D74} \tag{B-230}$$

$$C_{D87} = \frac{4}{9} \beta_1 B_1 B_2^2 + \frac{1}{3} C_{D75} \tag{B-231}$$

$$C_{D88} = \frac{1}{2} C_{D76} - B_1 B_2^2 B_3 \tag{B-232}$$

$$\begin{aligned} C_{D31} = \left(\frac{\gamma-1}{2}\right) \Bigg[& \frac{1}{320} B_1^8 \left(y_o^{10} - y_i^{10}\right) + C_{D77}\left(y_o^8 - y_i^8\right) - \frac{1}{28} \beta_1 B_1^5 \left(y_o^7 - y_i^7\right) \\ & + C_{D78}\left(y_o^6 - y_i^6\right) + C_{D79}\left(y_o^5 - y_i^5\right) + C_{D80}\left(y_o^4 - y_i^4\right) + C_{D81}\left(y_o^3 - y_i^3\right) \\ & + C_{D82}\left(y_o^2 - y_i^2\right) + C_{D83}\left(y_o - y_i\right) + \frac{1}{4} B_1^2 B_2^3 \left[y_o^4 \left(\ln y_o\right)^3 - y_i^4 \left(\ln y_i\right)^3\right] \\ & + \frac{1}{6} B_1^4 B_2^2 \left[y_o^6 \left(\ln y_o\right)^2 - y_i^6 \left(\ln y_i\right)^2\right] + C_{D84}\left[y_o^4 \left(\ln y_o\right)^2 - y_i^4 \left(\ln y_i\right)^2\right] \\ & - \frac{2}{3} \beta_1 B_1 B_2^2 \left[y_o^3 \left(\ln y_o\right)^2 - y_i^3 \left(\ln y_i\right)^2\right] + B_1 B_2^2 B_3 \left[y_o^2 \left(\ln y_o\right)^2 - y_i^2 \left(\ln y_i\right)^2\right] \\ & + \frac{1}{2} B_2 B_3^2 \left[\left(\ln y_o\right)^2 - \left(\ln y_i\right)^2\right] + \frac{5}{128} B_1^6 B_2 \left[y_o^8 \ln y_o - y_i^8 \ln y_i\right] \end{aligned}$$

$$+ C_{D85}\left[y_o^6 \ln y_o - y_i^6 \ln y_i\right] - \frac{3}{10} B_1 B_1^3 B_2 \left[y_o^5 \ln y_o - y_i^5 \ln y_i\right]$$

$$+ C_{D86}\left[y_o^4 \ln y_o - y_i^4 \ln y_i\right] + C_{D87}\left[y_o^3 \ln y_o - y_i^3 \ln y_i\right] + C_{D88}\left[y_o^2 \ln y_o - y_i^2 \ln y_i\right]$$

$$- 2B_1 B_2 B_3\left[y_o \ln y_o - y_i \ln y_i\right] + B_0 B_3^2 \ln(y_o/y_i)\Big] \qquad \text{(B-233)}$$

$$C_{D89} = \frac{1}{2} B_1^2 F_{45} + \frac{1}{36} B_0 F_{26} \qquad \text{(B-234)}$$

$$C_{D90} = \frac{1}{2} B_1^2 F_{46} + B_0 F_{45} \qquad \text{(B-235)}$$

$$C_{D91} = \frac{1}{2} B_1^2 F_{47} + \frac{1}{9} B_0 F_{28} \qquad \text{(B-236)}$$

$$C_{D92} = \frac{1}{2} B_1^2 F_0 + B_0 F_{46} \qquad \text{(B-237)}$$

$$C_{D93} = \frac{1}{2} B_1^2 F_{31} + B_0 F_{47} \qquad \text{(B-238)}$$

$$C_{D94} = \frac{1}{12} B_1^2 F_{36} + \frac{1}{4} B_2 F_{32} \qquad \text{(B-239)}$$

$$C_{D95} = \frac{1}{2} B_2 F_{30} + \frac{1}{6} B_0 F_{36} \qquad \text{(B-240)}$$

$$C_{D96} = \frac{1}{8} B_1^2 F_{32} + \frac{1}{16} B_2 F_{33} \qquad \text{(B-241)}$$

$$C_{D97} = \frac{1}{4} B_1^2 F_{30} + B_2 F_{48} + \frac{1}{4} B_0 F_{32} \qquad \text{(B-242)}$$

$$C_{D98} = B_2 F_{38} + \frac{1}{2} B_0 F_{30} \qquad \text{(B-243)}$$

$$C_{D99} = \frac{1}{32} B_1^2 F_{33} + \frac{1}{36} B_2 F_{26} \qquad \text{(B-244)}$$

$$C_{D100} = \frac{1}{2} B_1^2 F_{48} + B_2 F_{45} + \frac{1}{16} B_0 F_{33} \qquad \text{(B-245)}$$

$$C_{D101} = \frac{1}{2} B_1^2 F_{35} + \frac{1}{9} B_2 F_{28} \qquad \text{(B-246)}$$

$$C_{D102} = \frac{1}{2} B_1^2 F_{38} + B_2 F_{46} + B_0 F_{48} \qquad \text{(B-247)}$$

$$C_{D103} = B_2 F_{47} + B_0 F_{35} \tag{B-248}$$

$$C_{D104} = B_2 F_0 + B_0 F_{38} \tag{B-249}$$

$$C_{D105} = \frac{1}{8} C_{D89} - \frac{1}{64} C_{D99} \tag{B-250}$$

$$C_{D106} = \frac{1}{6} C_{D90} + \frac{1}{108} C_{D96} - \frac{1}{36} C_{D100} \tag{B-251}$$

$$C_{D107} = \frac{1}{5} C_{D91} - \frac{1}{25} C_{D101} \tag{B-252}$$

$$C_{D108} = \frac{1}{4} C_{D92} + \frac{1}{32} C_{D97} - \frac{1}{16} C_{D102} - \frac{3}{128} C_{D94} \tag{B-253}$$

$$C_{D109} = \frac{1}{3} C_{D93} + \frac{2}{27} B_2 F_{35} - \frac{1}{9} C_{D103} \tag{B-254}$$

$$C_{D110} = \frac{1}{2} B_0 F_0 + \frac{1}{8} B_2 F_{36} - \frac{3}{8} C_{D95} + \frac{1}{4} C_{D98} - \frac{1}{4} C_{D104} \tag{B-255}$$

$$C_{D111} = B_0 F_{31} - B_2 F_{31} \tag{B-256}$$

$$C_{D112} = \frac{1}{2} C_{D95} - \frac{1}{6} B_2 F_{36} \tag{B-257}$$

$$C_{D113} = \frac{1}{4} C_{D97} - \frac{3}{16} C_{D94} \tag{B-258}$$

$$C_{D114} = \frac{1}{4} B_2 F_{36} - \frac{3}{4} C_{D95} + \frac{1}{2} C_{D98} \tag{B-259}$$

$$C_{D115} = \frac{1}{6} C_{D100} - \frac{1}{18} C_{D96} \tag{B-260}$$

$$C_{D116} = \frac{1}{4} C_{D102} - \frac{1}{8} C_{D97} + \frac{3}{32} C_{D94} \tag{B-261}$$

$$C_{D117} = \frac{1}{3} C_{D103} - \frac{2}{9} B_2 F_{35} \tag{B-262}$$

$$C_{D118} = \frac{3}{4} C_{D95} - \frac{1}{4} B_2 F_{36} - \frac{1}{2} C_{D98} + \frac{1}{2} C_{D104} \tag{B-263}$$

$$C_{D32} = 2\Bigg[\frac{1}{720} B_1^2 F_{26}\left(y_o^{10}-y_i^{10}\right) + C_{D105}\left(y_o^8-y_i^8\right) + \frac{1}{126} B_1^2 F_{28}\left(y_o^7-y_i^7\right)$$
$$+ C_{D106}\left(y_o^6-y_i^6\right) + C_{D107}\left(y_o^5-y_i^5\right) + C_{D108}\left(y_o^4-y_i^4\right) + C_{D109}\left(y_o^3-y_i^3\right)$$
$$+ C_{D110}\left(y_o^2-y_i^2\right) + C_{D111}\left(y_o-y_i\right) + \frac{1}{12} B_2 F_{36}\left[y_o^2\left(\ln y_o\right)^4 - y_i^2\left(\ln y_i\right)^4\right]$$
$$+ \frac{1}{4} C_{D94}\left[y_o^4\left(\ln y_o\right)^3 - y_i^4\left(\ln y_i\right)^3\right] + C_{D112}\left[y_o^2\left(\ln y_o\right)^3 - y_i^2\left(\ln y_i\right)^3\right]$$
$$+ \frac{1}{6} C_{D96}\left[y_o^6\left(\ln y_o\right)^2 - y_i^6\left(\ln y_i\right)^2\right] + C_{D113}\left[y_o^4\left(\ln y_o\right)^2 - y_i^4\left(\ln y_i\right)^2\right]$$
$$+ \frac{1}{3} B_2 F_{35}\left[y_o^3\left(\ln y_o\right)^2 - y_i^3\left(\ln y_i\right)^2\right] + C_{D114}\left[y_o^2\left(\ln y_o\right)^2 - y_i^2\left(\ln y_i\right)^2\right]$$
$$+ \frac{1}{8} C_{D99}\left[y_o^8 \ln y_o - y_i^8 \ln y_i\right] + C_{D115}\left[y_o^6 \ln y_o - y_i^6 \ln y_i\right]$$
$$+ \frac{1}{5} C_{D101}\left[y_o^5 \ln y_o - y_i^5 \ln y_i\right] + C_{D116}\left[y_o^4 \ln y_o - y_i^4 \ln y_i\right]$$
$$+ C_{D117}\left[y_o^3 \ln y_o - y_i^3 \ln y_i\right] + C_{D118}\left[y_o^2 \ln y_o - y_i^2 \ln y_i\right]$$
$$+ B_2 F_{31}\left[y_o \ln y_o - y_i \ln y_i\right]\Bigg] \qquad \text{(B-264)}$$

$$C_{D119} = \frac{1}{8} D_0 D_{13} + D_{20}^2 \qquad \text{(B-265)}$$

$$C_{D120} = 2D_0 D_{20} + \beta_1^2 B_1^2 \qquad \text{(B-266)}$$

$$C_{D121} = \frac{1}{8} B_2^2 D_{13} + \frac{1}{16} D_{14}^2 \qquad \text{(B-267)}$$

$$C_{D122} = 2B_2^2 D_{20} + \frac{1}{2} D_{14} D_{16} \qquad \text{(B-268)}$$

$$C_{D123} = 2B_2^2 D_0 + D_{16}^2 \qquad \text{(B-269)}$$

$$C_{D124} = \frac{1}{8} D_{13} D_{16} + \frac{1}{2} D_{14} D_{20} \qquad \text{(B-270)}$$

$$C_{D125} = 2D_{16} D_{20} + \frac{1}{2} D_0 D_{14} \qquad \text{(B-271)}$$

$$C_{D126} = \frac{1}{64} D_{13}D_{20} - \frac{1}{2048} D_{13}D_{14} \tag{B-272}$$

$$C_{D127} = \frac{1}{6} C_{D119} + \frac{1}{108} C_{D121} - \frac{1}{36} C_{D124} \tag{B-273}$$

$$C_{D128} = \frac{1}{50} \beta_1 B_1 D_{14} - \frac{2}{5} \beta_1 B_1 D_{20} \tag{B-274}$$

$$C_{D129} = \frac{1}{4} C_{D120} - \frac{3}{256} B_2^2 D_{14} + \frac{1}{32} C_{D122} - \frac{1}{16} C_{D125} \tag{B-275}$$

$$C_{D130} = \frac{2}{9} \beta_1 B_1 D_{16} - \frac{2}{3} \beta_1 B_1 D_0 - \frac{4}{27} \beta_1 B_1 B_2^2 \tag{B-276}$$

$$C_{D131} = \frac{1}{2} D_0^2 + \frac{3}{4} B_2^4 - \frac{3}{4} B_2^2 D_{16} + \frac{1}{4} C_{D123} - \frac{1}{2} D_0 D_{16} \tag{B-277}$$

$$C_{D132} = B_2^2 D_{16} - B_2^4 \tag{B-278}$$

$$C_{D133} = \frac{1}{4} C_{D122} - \frac{3}{32} B_2^2 D_{14} \tag{B-279}$$

$$C_{D134} = \frac{3}{2} B_2^4 - \frac{3}{2} B_2^2 D_{16} + \frac{1}{2} C_{D123} \tag{B-280}$$

$$C_{D135} = \frac{1}{6} C_{D124} - \frac{1}{18} C_{D121} \tag{B-281}$$

$$C_{D136} = \frac{3}{64} B_2^2 D_{14} - \frac{1}{8} C_{D122} + \frac{1}{4} C_{D125} \tag{B-282}$$

$$C_{D137} = \frac{4}{9} \beta_1 B_1 B_2^2 - \frac{2}{3} \beta_1 B_1 D_{16} \tag{B-283}$$

$$C_{D138} = \frac{3}{2} B_2^2 D_{16} - \frac{3}{2} B_2^4 - \frac{1}{2} C_{D123} + D_0 D_{16} \tag{B-284}$$

$$\begin{aligned} C_{D33} = {} & \frac{1}{2560} D_{13}^2 \left(y_o^{10} - y_i^{10}\right) + C_{D126}\left(y_o^8 - y_i^8\right) - \frac{1}{56} \beta_1 B_1 D_{13}\left(y_o^7 - y_i^7\right) \\ & + C_{D127}\left(y_o^6 - y_i^6\right) + C_{D128}\left(y_o^5 - y_i^5\right) + C_{D129}\left(y_o^4 - y_i^4\right) + C_{D130}\left(y_o^3 - y_i^3\right) \\ & + C_{D131}\left(y_o^2 - y_i^2\right) + \frac{1}{2} B_2^4 \left[y_o^2 \left(\ln y_o\right)^4 - y_i^2 \left(\ln y_i\right)^4\right] \\ & + \frac{1}{8} B_2^2 D_{14} \left[y_o^4 \left(\ln y_o\right)^3 - y_i^4 \left(\ln y_i\right)^3\right] + C_{D132}\left[y_o^2 \left(\ln y_o\right)^3 - y_i^2 \left(\ln y_i\right)^3\right] \end{aligned}$$

$$+ \frac{1}{6} C_{D121}\left[y_o^6\left(\ln y_o\right)^2 - y_i^6\left(\ln y_i\right)^2\right] + C_{D133}\left[y_o^4\left(\ln y_o\right)^2 - y_i^4\left(\ln y_i\right)^2\right]$$

$$- \frac{2}{3} B_1 B_1 B_2^2\left[y_o^3\left(\ln y_o\right)^2 - y_i^3\left(\ln y_i\right)^2\right] + C_{D134}\left[y_o^2\left(\ln y_o\right)^2 - y_i^2\left(\ln y_i\right)^2\right]$$

$$+ \frac{1}{256} D_{13} D_{14}\left[y_o^8 \ln y_o - y_i^8 \ln y_i\right] + C_{D135}\left[y_o^6 \ln y_o - y_i^6 \ln y_i\right]$$

$$- \frac{1}{10} B_1 B_1 D_{14}\left[y_o^5 \ln y_o - y_i^5 \ln y_i\right] + C_{D136}\left[y_o^4 \ln y_o - y_i^4 \ln y_i\right]$$

$$+ C_{D137}\left[y_o^3 \ln y_o - y_i^3 \ln y_i\right] + C_{D138}\left[y_o^2 \ln y_o - y_i^2 \ln y_i\right] \qquad \text{(B-285)}$$

$$C_{D139} = \frac{1}{4} B_1^4 D_{20} + \frac{1}{16} B_0 B_1^2 D_{13} \qquad \text{(B-286)}$$

$$C_{D140} = \frac{1}{4} B_1^4 D_0 + B_0 B_1^2 D_{20} + \frac{1}{16} B_0^2 D_{13} \qquad \text{(B-287)}$$

$$C_{D141} = B_0 B_1^2 D_0 + B_0^2 D_{20} \qquad \text{(B-288)}$$

$$C_{D142} = B_1^2 B_2^3 + \frac{1}{4} B_2^2 D_{14} \qquad \text{(B-289)}$$

$$C_{D143} = B_2^2 D_{16} + 2B_0 B_2^3 \qquad \text{(B-290)}$$

$$C_{D144} = \frac{1}{4} B_1^4 B_2^2 + \frac{1}{4} B_1^2 B_2 D_{14} + \frac{1}{16} B_2^2 D_{13} \qquad \text{(B-291)}$$

$$C_{D145} = B_1^2 B_2 D_{16} + B_2^2 D_{20} + B_0 B_1^2 B_2^2 + \frac{1}{2} B_0 B_2 D_{14} \qquad \text{(B-292)}$$

$$C_{D146} = B_2^2 D_0 + 2B_0 B_2 D_{16} + B_0^2 B_2^2 \qquad \text{(B-293)}$$

$$C_{D147} = \frac{1}{16} B_1^4 D_{14} + \frac{1}{16} B_1^2 B_2 D_{13} \qquad \text{(B-294)}$$

$$C_{D148} = \frac{1}{4} B_1^4 D_{16} + B_1^2 B_2 D_{20} + \frac{1}{4} B_0 B_1^2 D_{14} + \frac{1}{8} B_0 B_2 D_{13} \qquad \text{(B-295)}$$

$$C_{D149} = B_1^2 B_2 D_0 + B_0 B_1^2 D_{16} + 2B_0 B_2 D_{20} + \frac{1}{4} B_0^2 D_{14} \qquad \text{(B-296)}$$

$$C_{D150} = 2B_0 B_2 D_0 + B_0^2 D_{16} \qquad \text{(B-297)}$$

$$C_{D151} = \frac{1}{8} C_{D139} - \frac{1}{64} C_{D147} \tag{B-298}$$

$$C_{D152} = \frac{1}{6} C_{D140} + \frac{1}{108} C_{D144} - \frac{1}{36} C_{D148} \tag{B-299}$$

$$C_{D153} = \frac{1}{25} \beta_1 B_1^3 B_2 - \frac{1}{5} \beta_1 B_0 B_1^3 \tag{B-300}$$

$$C_{D154} = \frac{1}{4} C_{D141} - \frac{3}{128} C_{D142} + \frac{1}{32} C_{D145} - \frac{1}{16} C_{D149} \tag{B-301}$$

$$C_{D155} = \frac{2}{9} \beta_1 B_0 B_1 B_2 - \frac{1}{3} \beta_1 B_0^2 B_1 - \frac{2}{27} \beta_1 B_1 B_2^2 \tag{B-302}$$

$$C_{D156} = \frac{1}{2} B_0^2 D_0 + \frac{3}{4} B_2^4 - \frac{3}{8} C_{D143} + \frac{1}{4} C_{D146} - \frac{1}{4} C_{D150} \tag{B-303}$$

$$C_{D157} = \frac{1}{2} C_{D143} - B_2^4 \tag{B-304}$$

$$C_{D158} = \frac{1}{4} C_{D145} - \frac{3}{16} C_{D142} \tag{B-305}$$

$$C_{D159} = \frac{3}{2} B_2^4 - \frac{3}{4} C_{D143} + \frac{1}{2} C_{D146} \tag{B-306}$$

$$C_{D160} = \frac{1}{6} C_{D148} - \frac{1}{18} C_{D144} \tag{B-307}$$

$$C_{D161} = \frac{3}{32} C_{D142} - \frac{1}{8} C_{D145} + \frac{1}{4} C_{D149} \tag{B-308}$$

$$C_{D162} = \frac{2}{9} \beta_1 B_1 B_2^2 - \frac{2}{3} \beta_1 B_0 B_1 B_2 \tag{B-309}$$

$$C_{D163} = \frac{3}{4} C_{D143} - \frac{3}{2} B_2^4 - \frac{1}{2} C_{D146} + \frac{1}{2} C_{D150} \tag{B-310}$$

$$\begin{aligned} C_{D34} = (2\gamma-3) \Bigg[& \frac{1}{640} B_1^4 D_{13} \left(y_o^{10} - y_i^{10} \right) + C_{D151} \left(y_o^8 - y_i^8 \right) - \frac{1}{28} \beta_1 B_1^5 \left(y_o^7 - y_i^7 \right) \\ & + C_{D152} \left(y_o^6 - y_i^6 \right) + C_{D153} \left(y_o^5 - y_i^5 \right) + C_{D154} \left(y_o^4 - y_i^4 \right) + C_{D155} \left(y_o^3 - y_i^3 \right) \\ & + C_{D156} \left(y_o^2 - y_i^2 \right) + \frac{1}{2} B_2^4 \left[y_o^2 \left(\ln y_o \right)^4 - y_i^2 \left(\ln y_i \right)^4 \right] \\ & + \frac{1}{4} C_{D142} \left[y_o^4 \left(\ln y_o \right)^3 - y_i^4 \left(\ln y_i \right)^3 \right] + C_{D157} \left[y_o^2 \left(\ln y_o \right)^3 - y_i^2 \left(\ln y_i \right)^3 \right] \end{aligned}$$

$$+ \frac{1}{6} C_{D144}\left[y_o^6\left(\ln y_o\right)^2 - y_i^6\left(\ln y_i\right)^2\right] + C_{D158}\left[y_o^4\left(\ln y_o\right)^2 - y_i^4\left(\ln y_i\right)^2\right]$$

$$- \frac{1}{3} B_1 B_1 B_2^2\left[y_o^3\left(\ln y_o\right)^2 - y_i^3\left(\ln y_i\right)^2\right] + C_{D159}\left[y_o^2\left(\ln y_o\right)^2 - y_i^2\left(\ln y_i\right)^2\right]$$

$$+ \frac{1}{8} C_{D147}\left[y_o^8 \ln y_o - y_i^8 \ln y_i\right] + C_{D160}\left[y_o^6 \ln y_o - y_i^6 \ln y_i\right]$$

$$- \frac{1}{5} B_1 B_1^3 B_2\left[y_o^5 \ln y_o - y_i^5 \ln y_i\right] + C_{D161}\left[y_o^4 \ln y_o - y_i^4 \ln y_i\right]$$

$$+ C_{D162}\left[y_o^3 \ln y_o - y_i^3 \ln y_i\right] + C_{D163}\left[y_o^2 \ln y_o - y_i^2 \ln y_i\right]\Bigg] \qquad \text{(B-311)}$$

$$C_{D164} = \frac{1}{16} B_0 B_1^6 - \frac{1}{128} B_1^6 B_2 \qquad \text{(B-312)}$$

$$C_{D165} = \frac{1}{4} B_0^2 B_1^4 + \frac{1}{72} B_1^4 B_2^2 - \frac{1}{12} B_0 B_1^4 B_2 \qquad \text{(B-313)}$$

$$C_{D166} = \frac{1}{2} B_0^3 B_1^2 - \frac{3}{64} B_1^2 B_2^3 + \frac{3}{16} B_0 B_1^2 B_2^2 - \frac{3}{8} B_0^2 B_1^2 B_2 \qquad \text{(B-314)}$$

$$C_{D167} = \frac{1}{2} B_0^4 + \frac{3}{4} B_2^4 - \frac{3}{2} B_0 B_2^3 + \frac{3}{2} B_0^2 B_2^2 - B_0^3 B_2 \qquad \text{(B-315)}$$

$$C_{D168} = 2B_0 B_2^3 - B_2^4 \qquad \text{(B-316)}$$

$$C_{D169} = \frac{3}{2} B_0 B_1^2 B_2^2 - \frac{3}{8} B_1^2 B_2^3 \qquad \text{(B-317)}$$

$$C_{D170} = \frac{3}{2} B_2^4 - 3B_0 B_2^3 + 3B_0^2 B_2^2 \qquad \text{(B-318)}$$

$$C_{D171} = \frac{1}{2} B_0 B_1^4 B_2 - \frac{1}{12} B_1^4 B_2^2 \qquad \text{(B-319)}$$

$$C_{D172} = \frac{3}{16} B_1^2 B_2^3 - \frac{3}{4} B_0 B_1^2 B_2^2 + \frac{3}{2} B_0^2 B_1^2 B_2 \qquad \text{(B-320)}$$

$$C_{D173} = 3B_0 B_2^3 - \frac{3}{2} B_2^4 - 3B_0^2 B_2^2 + 2B_0^3 B_2 \qquad \text{(B-321)}$$

$$C_{D35} = \left(\frac{2\gamma^2 - 5\gamma + 2}{4}\right)\Bigg[\frac{1}{160} B_1^8\left(y_o^{10} - y_i^{10}\right) + C_{D164}\left(y_o^8 - y_i^8\right) + C_{D165}\left(y_o^6 - y_i^6\right)$$

$$+ C_{D166}\left(y_o^4 - y_i^4\right) + C_{D167}\left(y_o^2 - y_i^2\right) + \frac{1}{2} B_2^4\left[y_o^2\left(\ln y_o\right)^4 - y_i^2\left(\ln y_i\right)^4\right]$$

$$+ \frac{1}{2} B_1^2 B_2^3 \left[y_o^4 \left(\ln y_o \right)^3 - y_i^4 \left(\ln y_i \right)^3 \right] + C_{D168} \left[y_o^2 \left(\ln y_o \right)^3 - y_i^2 \left(\ln y_i \right)^3 \right]$$

$$+ \frac{1}{4} B_1^4 B_2^2 \left[y_o^6 \left(\ln y_o \right)^2 - y_i^6 \left(\ln y_i \right)^2 \right] + C_{D169} \left[y_o^4 \left(\ln y_o \right)^2 - y_i^4 \left(\ln y_i \right)^2 \right]$$

$$+ C_{D170} \left[y_o^2 \left(\ln y_o \right)^2 - y_i^2 \left(\ln y_i \right)^2 \right] + \frac{1}{16} B_1^6 B_2 \left[y_o^6 \ln y_o - y_i^8 \ln y_i \right]$$

$$+ C_{D171} \left[y_o^6 \ln y_o - y_i^6 \ln y_i \right] + C_{D172} \left[y_o^4 \ln y_o - y_i^4 \ln y_i \right]$$

$$+ C_{D173} \left[y_o^2 \ln y_o - y_i^2 \ln y_i \right] \Bigg] \qquad \text{(B-322)}$$

$$C_{D3} = C_{D30} + C_{D31} + C_{D32} + C_{D33} + C_{D34} + C_{D35} \; . \qquad \text{(B-323)}$$

Having determined the (u_1, v_1), (u_2, v_2), and (u_3, v_3) velocity components as well as the discharge coefficient constants C_{D1}, C_{D2}, and C_{D3}, the important flowfield variables may then be evaluated. The series expansions for these quantities are given in Chapter III and are included here for completeness,

$$u(z,y) = 1 + \tilde{u} = 1 + u_1 \varepsilon + u_2 \varepsilon^2 + u_3 \varepsilon^3 + \ldots \qquad \text{(B-324)}$$

$$v(z,y) = \tilde{v} = \left[\frac{\gamma+1}{2} \varepsilon \right]^{1/2} \left[v_1 \varepsilon + v_2 \varepsilon^2 + v_3 \varepsilon^3 + \ldots \right] \qquad \text{(B-325)}$$

$$M^*(z,y) = \left(u^2 + v^2 \right)^{1/2} = 1 + u_1 \varepsilon + u_2 \varepsilon^2 + \left(u_3 + \frac{\gamma+1}{4} v_1^2 \right) \varepsilon^3 + \ldots \qquad \text{(B-326)}$$

$$\theta(z,y) = \tan^{-1}(v/u) = \left[\frac{\gamma+1}{2} \varepsilon \right]^{1/2} \left[v_1 \varepsilon + \left(v_2 - u_1 v_1 \right) \varepsilon^2 + \left(v_3 - u_1 v_2 - u_2 v_1 + u_1^2 v_1 \right) \varepsilon^3 + \ldots \right] \qquad \text{(B-327)}$$

$$M(z,y) = \left[\frac{\frac{2}{\gamma+1} M^{*2}}{1 - \frac{\gamma-1}{\gamma+1} M^{*2}} \right]^{1/2} = 1 + \left(\frac{\gamma+1}{2} \right) \left[u_1 \varepsilon + \left[u_2 + \frac{3}{4} (\gamma-1) u_1^2 \right] \varepsilon^2 + \left[u_3 + \frac{\gamma+1}{4} v_1^2 + \frac{3}{2} (\gamma-1) u_1 u_2 + \frac{\left(5\gamma^2 - 8\gamma + 3 \right)}{8} u_1^3 \right] \varepsilon^3 + \ldots \right] \qquad \text{(B-328)}$$

$$\frac{p}{p_o}(z,y) = \left[1 - \frac{\gamma-1}{\gamma+1} M^{*2}\right]^{\gamma/(\gamma-1)} = \left(\frac{2}{\gamma+1}\right)^{\gamma/(\gamma-1)}\left[1 - \gamma\left[u_1\varepsilon + u_2\varepsilon^2 + \left(u_3 + \frac{\gamma+1}{4} v_1^2 - \frac{\gamma+1}{6} u_1^3\right)\varepsilon^3 + \ldots\right]\right] \quad \text{(B-329)}$$

$$C_D = 1 - \frac{(\gamma+1)\varepsilon^2}{y_o^2 - y_i^2}\left[C_{D1} + C_{D2}\varepsilon + C_{D3}\varepsilon^2 + \ldots\right] . \quad \text{(B-330)}$$

While the preceding list of constants and functions looks quite formidable, it is to be noted that for a given configuration the constants need be evaluated just once. Only z and the functions of y must be determined for each point in the flowfield.

APPENDIX C. SOLUTION SUMMARY FOR THE CONVENTIONAL AXISYMMETRIC CONFIGURATION

For the special case of an axisymmetric nozzle without a centerbody, the parameters which are to be specified are: γ, the ratio of specific heats; R_c, the wall radius of curvature non-dimensionalized with respect to the throat radius; N, the number of terms in the series solution to be employed; and η the parameter in the expansion variable,

$$\varepsilon \equiv \left(R_c+\eta\right)^{-1} , \tag{C-1}$$

With these quantities given, the perturbation velocity components and the discharge coefficient constants for the first three solution orders may be evaluated from,

$$u_1(z,y) = \frac{1}{2}\,y^2 - \frac{1}{4} + z \tag{C-2}$$

$$v_1(z,y) = \frac{1}{4}\,y^3 - \frac{1}{4}\,y + yz \tag{C-3}$$

$$u_2(z,y) = \frac{2\gamma+9}{24}\,y^4 - \frac{4\gamma+15-12\eta}{24}\,y^2 + \frac{10\gamma+57-72\eta}{288} + \left(y^2 + \frac{4\eta-5}{8}\right)z - \left(\frac{2\gamma-3}{6}\right)z^2 \tag{C-4}$$

$$v_2(z,y) = \frac{\gamma+3}{9}\,y^5 - \frac{20\gamma+63-36\eta}{96}\,y^3 + \frac{28\gamma+93-108\eta}{288}\,y + \left(\frac{2\gamma+9}{6}\,y^3 - \frac{4\gamma+15-12\eta}{12}\,y\right)z + yz^2 \tag{C-5}$$

$$u_3(z,y) = \frac{556\gamma^2+1737\gamma+3069}{10,368}\,y^6 - \frac{388\gamma^2+(1161-384\eta)\gamma+(1881-1728\eta)}{2304}\,y^4 + \frac{304\gamma^2+(831-576\eta)\gamma+(1242-2160\eta+864\eta^2)}{1728}\,y^2 - \frac{2708\gamma^2+(7839-5760\eta)\gamma+(14,211-32,832\eta+20,736\eta^2)}{82,944}$$

$$+\left[\frac{52\gamma^2+51\gamma+327}{384}\,y^4-\frac{52\gamma^2+75\gamma+(279-288\eta)}{192}\,y^2\right.$$

$$\left.+\frac{92\gamma^2+180\gamma+(639-1080\eta+432\eta^2)}{1152}\right]z \qquad \text{(C-6)}$$

$$+\left[-\frac{7\gamma-3}{8}\,y^2+\frac{(13-16\eta)\gamma-(27-24\eta)}{48}\right]z^2+\left[\frac{4\gamma^2-57\gamma+27}{144}\right]z^3$$

$$v_3(z,y)=\frac{6836\gamma^2+23{,}031\gamma+30{,}627}{82{,}944}\,y^7$$

$$-\frac{3380\gamma^2+(11{,}391-3840\eta)\gamma+(15{,}291-11{,}520\eta)}{13{,}824}\,y^5$$

$$+\frac{3424\gamma^2+(11{,}271-7200\eta)\gamma+(15{,}228-22{,}680\eta+6480\eta^2)}{13{,}824}\,y^3$$

$$-\frac{7100\gamma^2+(22{,}311-20{,}160\eta)\gamma+(30{,}249-66{,}960\eta+38{,}880\eta^2)}{82{,}944}\,y$$

$$+\left[\frac{556\gamma^2+1737\gamma+3069}{1728}\,y^5-\frac{388\gamma^2+(1161-384\eta)\gamma+(1881-1728\eta)}{576}\,y^3\right.$$

$$\left.+\frac{304\gamma^2+(831-576\eta)\gamma+(1242-2160\eta+864\eta^2)}{864}\,y\right]z \qquad \text{(C-7)}$$

$$+\left[\frac{52\gamma^2+51\gamma+327}{192}\,y^3-\frac{52\gamma^2+75\gamma+(279-288\eta)}{192}\,y\right]z^2+\left[-\frac{7\gamma-3}{12}\,y\right]z^3$$

$$C_{D1}=\frac{1}{96} \qquad \text{(C-8)}$$

$$C_{D2}=-\frac{8\gamma+21-48\eta}{2304} \qquad \text{(C-9)}$$

$$C_{D3}=\frac{754\gamma^2+(1971-2880\eta)\gamma+(2007-7560\eta+8640\eta^2)}{276{,}480}\,. \qquad \text{(C-10)}$$

The quantities u, v, M*, θ, M, p/p_0, and C_D can then be determined from Eqs. (III-73)-(III-78) and (III-80), respectively.

The resulting solution is applicable to axisymmetric nozzles with either circular, parabolic, elliptic, or hyperbolic arc wall contours. It should also be noted that the expansion parameter employed here is not the one obtained by simplifying the definition of ε used in the general solution, Eq. (III-22), for the case of a straight inner wall. The latter procedure results in the definition given in Eq. (III-82) which, because of the presence of the coefficient 2, is somewhat less meaningful for the present case than the one used in this appendix, Eq. (C-1). For general use, and particularly for nozzles with a small wall radius of curvature, the value $\eta = 1$ is recommended for the solution given above.

APPENDIX D. TABLES OF DATA, FIGS IV.11-IV.15

COMPARISON OF FULL- AND HALF-SECTION WALL PRESSURE MEASUREMENTS FOR AXISYMMETRIC NOZZLE, FIG. IV.11

FULL-SECTION MODEL

$\overline{p}_0$ = 350.3 kPa = 50.80 psia $\overline{T}_0$ = 288.9 K = 520.0°R γ = 1.4 (air)

$\overline{p}_{chamber}$ = 69.3 kPa = 10.06 psia $\overline{Re}_{2d}$ = 2.68 x 10^6 d = 25.4 mm = 1.00 in.

Wall Pressure Ratios:

Tap No.	1	2	3	4	5	6	7	8
Z	-0.6	-0.45	-0.3	-0.15	0.0	0.15	0.3	0.45
R	1.2	1.107	1.046	1.011	1.000	1.011	1.046	1.107
p/p_0	0.8756	0.7695	0.6565	0.5345	0.4104	0.2884	0.1848	0.1217

HALF-SECTION MODEL

$\overline{p}_0$ = 402.8 kPa = 58.42 psia $\overline{T}_0$ = 288.9 K = 520.0°R γ = 1.4 (air)

$\overline{p}_{chamber}$ = 80.0 kPa = 11.60 psia $\overline{Re}_{2d}$ = 3.09 x 10^6 d = 25.4 mm = 1.00 in.

Wall Pressure Ratios:

Tap No.	1	2	3	4	5	6	7	8
Z	-0.6	-0.45	-0.3	-0.15	0.0	0.15	0.3	0.45
R	1.2	1.107	1.046	1.011	1.000	1.011	1.046	1.107
p/p_0	0.8735	0.7666	0.6572	0.5360	0.4087	0.2839	0.1811	0.1186

FLOWFIELD PRESSURE TAP MEASUREMENTS FOR CONVENTIONAL,
AXISYMMETRIC NOZZLE, FIG. IV.12

$\bar{p}_0$ = 397.9 kPa = 57.71 psia $\bar{T}_0$ = 288.9 K = 520.0°R γ = 1.4 (air)

$\bar{p}_{chamber}$ = 80.9 kPa = 11.73 psia $\overline{Re}_{2d}$ = 3.04×10^6 d = 25.4 mm = 1.00 in.

Flowfield Pressure Ratios:

R \ Z	-0.6	-0.45	-0.3	-0.15	0.0	0.15	0.3	0.45	0.6	0.75	0.9	1.05
0.0	0.8464	0.8054	0.7564	0.6981	0.6346	0.5669	0.4979	0.4299	0.3679	0.3124	0.2610	0.2173
0.15	0.8468	0.8050	0.7551	0.6965	0.6320	0.5626	0.4950	0.4259	0.3631	0.3085	0.2584	---
0.3	0.8469	0.8047	0.7517	0.6910	0.6232	0.5519	0.4816	0.4128	0.3509	0.2934	0.2456	---
0.45	0.8468	0.8018	0.7448	0.6793	0.6073	0.5342	0.4592	0.3905	0.3278	0.2741	---	---
0.6	0.8454	0.7959	0.7337	0.6605	0.5822	0.5007	0.4256	0.3526	0.2939	0.2435	---	---
0.75	0.8463	0.7911	0.7192	0.6329	0.5432	0.4499	0.3721	0.2998	0.2484	---	---	---
0.9	0.8496	0.7836	0.6951	0.5877	0.4793	0.3742	0.2965	0.2333	---	---	---	---

Outer Wall Pressure Ratios:

Z	-0.6	-0.45	-0.3	-0.15	0.0	0.15	0.3	0.45
R	1.2	1.107	1.046	1.011	1.000	1.011	1.046	1.107
p/p_0	0.8726	0.7661	0.6562	0.5358	0.4089	0.2846	0.1825	0.1249

INTERPOLATED CONSTANT MACH NUMBER CONTOURS FOR
CONVENTIONAL, AXISYMMETRIC NOZZLE, FIG. IV. 12

$\overline{p}_0$ = 397.9 kPa = 57.71 psia $\overline{T}_0$ = 288.9 K = 520.0°R γ = 1.4 (air)

$\overline{p}_{chamber}$ = 80.9 kPa = 11.73 psia $\overline{Re}_{2d}$ = 3.04×10^6 d = 25.4 mm = 1.00 in.

M = 0.6	Z	-0.3810	-0.3836	-0.3882	-0.4003	-0.4190	-0.4337	-0.4508	-0.4746
	R	0.0	0.15	0.3	0.45	0.6	0.75	0.9	1.1198
M = 0.8	Z	-0.0494	-0.0539	-0.0711	-0.1008	-0.1413	-0.1892	-0.2443	-0.2998
	R	0.0	0.15	0.3	0.45	0.6	0.75	0.9	1.0460
M = 1.0	Z	0.2345	0.2268	0.2003	0.1614	0.0982	0.0240	-0.0685	-0.1410
	R	0.0	0.15	0.3	0.45	0.6	0.75	0.9	1.0100
M = 1.2	Z	0.4909	0.4809	0.4510	0.4006	0.3268	0.2199	0.0911	-0.0039
	R	0.0	0.15	0.3	0.45	0.6	0.75	0.9	1.0000
M = 1.4	Z	0.7447	0.7335	0.6934	0.6355	0.5453	0.4172	0.2628	0.1120
	R	0.0	0.15	0.3	0.45	0.6	0.75	0.9	1.0063

FLOWFIELD PRESSURE TAP MEASUREMENTS FOR ANNULAR NOZZLE
WITH CENTERBODY CENTER OF CURVATURE ALONG Z = 0 PLANE, FIG. IV.13

$\bar{p}_0$ = 409.5 kPa = 59.38 psia $\bar{T}_0$ = 288.9 K = 520.0°R γ = 1.4 (air)

$\bar{p}_{chamber}$ = 80.6 kPa = 11.70 psia $\overline{Re}_{2d}$ = 1.96 x 10^6 d = 15.88 mm = 0.625 in.

Flowfield Pressure Ratios:

R \ Z	-0.5	-0.375	-0.25	-0.125	0.0	0.125	0.25	0.375	0.5	0.625
0.4375	0.8543	0.8070	0.7360	0.6581	0.5717	0.4834	0.4043	0.3321	0.2730	0.2251
0.5625	0.8498	0.8037	0.7387	0.6656	0.5835	0.5001	0.4193	0.3427	0.2821	0.2285
0.6875	0.8446	0.7960	0.7297	0.6575	0.5725	0.4863	0.4050	0.3302	0.2685	0.2171
0.8125	0.8400	0.7858	0.7146	0.6319	0.5422	0.4503	0.3663	0.2930	0.2385	0.1913
0.9375	0.8369	0.7730	0.6903	0.5905	0.4833	0.3821	0.3013	0.2352	0.1909	0.1543

Inner Wall Pressure Ratios:

Z	-0.5	-0.375	-0.25	-0.125	0.0	0.125	0.25	0.375	0.5
R	0.311	0.340	0.359	0.371	0.375	0.371	0.359	0.340	0.311
p/p_0	0.8631	0.8035	0.7338	0.6496	0.5587	0.4666	0.3776	0.3008	0.2361

Outer Wall Pressure Ratios:

Z	-0.6	-0.45	-0.3	-0.15	0.0	0.15	0.3	0.45
R	1.2	1.107	1.046	1.011	1.000	1.011	1.046	1.107
p/p_0	0.8907	0.7990	0.6970	0.5756	0.4404	0.3030	0.1876	0.1133

INTERPOLATED CONSTANT MACH NUMBER CONTOURS FOR ANNULAR NOZZLE
WITH CENTERBODY CENTER OF CURVATURE ALONG Z = 0 PLANE, FIG. IV.13

$\overline{p}_0$ = 409.5 kPa = 59.38 psia $\overline{T}_0$ = 288.9 K = 520.0°R γ = 1.4 (air)

$\overline{p}_{chamber}$ = 80.6 kPa = 11.70 psia $\overline{Re}_{2d}$ = 1.96×10^6 d = 15.88 mm = 0.625 in.

M = 0.6	Z	-0.3377	-0.3323	-0.3348	-0.3511	-0.3715	-0.3941	-0.4270
	R	0.3463	0.4375	0.5625	0.6875	0.8125	0.9375	1.0957
M = 0.8	Z	-0.1340	-0.1219	-0.1099	-0.1226	-0.1600	-0.2053	-0.2456
	R	0.3705	0.4375	0.5625	0.6875	0.8125	0.9375	1.0306
M = 1.0	Z	0.0414	0.0603	0.0825	0.0635	0.0185	-0.0527	-0.0963
	R	0.3746	0.4375	0.5625	0.6875	0.8125	0.9375	1.0047
M = 1.2	Z	0.1992	0.2367	0.2610	0.2383	0.1794	0.0847	0.0296
	R	0.3651	0.4375	0.5625	0.6875	0.8125	0.9375	1.0004
M = 1.4	Z	0.3515	0.4100	0.4312	0.4054	0.3360	0.2284	0.1374
	R	0.3439	0.4375	0.5625	0.6875	0.8125	0.9375	1.0095

FLOWFIELD PRESSURE TAP MEASUREMENTS FOR ANNULAR NOZZLE
WITH CENTERBODY CENTER OF CURVATURE ALONG Z = 0.5 PLANE, FIG. IV.14

$\overline{p}_0$ = 409.0 kPa = 59.31 psia $\overline{T}_0$ = 288.9 K = 520.0°R γ = 1.4 (air)

$\overline{p}_{chamber}$ = 79.9 kPa = 11.58 psia $\overline{Re}_{2d}$ = 2.08×10^6 d = 16.90 mm = 0.665 in.

Flowfield Pressure Ratios:

R \ Z	-0.5	-0.375	-0.25	-0.125	0.0	0.125	0.25	0.375	0.5	0.625
0.4375	0.8507	0.8229	0.7922	0.7512	0.6771	0.5936	0.4995	0.4080	0.3236	0.2550
0.5625	0.8475	0.8126	0.7707	0.7205	0.6538	0.5791	0.4950	0.4110	0.3362	0.2691
0.6875	0.8414	0.8005	0.7492	0.6955	0.6223	0.5474	0.4677	0.3914	0.3210	0.2590
0.8125	0.8373	0.7879	0.7257	0.6545	0.5790	0.4984	0.4199	0.3461	0.2865	0.2330
0.9375	0.8335	0.7737	0.6964	0.6075	0.5170	0.4240	0.3463	0.2804	0.2320	0.1918

Inner Wall Pressure Ratios:

Z	0.0	0.125	0.25	0.375	0.5	0.625	0.75	0.875	1.0
R	0.311	0.340	0.359	0.371	0.375	0.371	0.359	0.340	0.311
p/p_o	0.6906	0.5892	0.4893	0.3917	0.3068	0.2348	0.1770	0.1337	0.1027

Outer Wall Pressure Ratios:

Z	-0.6	-0.45	-0.3	-0.15	0.0	0.15	0.3	0.45
R	1.2	1.107	1.046	1.011	1.000	1.011	1.046	1.107
p/p_o	0.8885	0.7956	0.6984	0.5888	0.4722	0.3440	0.2276	0.1338

INTERPOLATED CONSTANT MACH NUMBER CONTOURS FOR ANNULAR NOZZLE
WITH CENTERBODY CENTER OF CURVATURE ALONG Z = 0.5 PLANE, FIG. IV.14

$\overline{p}_0$ = 409.0 kPa = 59.31 psia $\overline{T}_0$ = 288.9 K = 520.0 R γ = 1.4 (air)

$\overline{p}_{chamber}$ = 79.9 kPa = 11.58 psia $\overline{Re}_{2d}$ = 2.08×10^6 d = 16.90 mm = 0.665 in.

M = 0.6	Z	-0.1217	-0.2191	-0.2876	-0.3339	-0.3665	-0.3939	-0.4320
	R	0.2759	0.4375	0.5625	0.6875	0.8125	0.9375	1.0981
M = 0.8	Z	0.0427	0.0323	-0.0039	-0.0533	-0.1275	-0.1926	-0.2389
	R	0.3220	0.4375	0.5625	0.6875	0.8125	0.9375	1.0290
M = 1.0	Z	0.2013	0.2121	0.2017	0.1554	0.0788	-0.0153	-0.0702
	R	0.3526	0.4375	0.5625	0.6875	0.8125	0.9375	1.0025
M = 1.2	Z	0.3473	0.3690	0.3728	0.3398	0.2623	0.1425	0.0704
	R	0.3692	0.4375	0.5625	0.6875	0.8125	0.9375	1.0025
M = 1.4	Z	0.4883	0.5155	0.5395	0.5128	0.4395	0.3072	0.1857
	R	0.3750	0.4375	0.5625	0.6875	0.8125	0.9375	1.0174

FLOWFIELD PRESSURE TAP MEASUREMENTS FOR ANNULAR NOZZLE
WITH CENTERBODY CENTER OF CURVATURE ALONG Z = - 0.5 PLANE, FIG. IV.15

$\bar{p}_0$ = 408.2 kPa = 59.20 psia $\bar{T}_0$ = 288.9 K = 520.0°R γ = 1.4 (air)

$\bar{p}_{chamber}$ = 76.4 kPa = 11.08 psia $\overline{Re}_{2d}$ = 2.08 x 10^6 d = 16.90 mm = 0.665 in.

Flowfield Pressure Ratios:

R \ Z	-0.5	-0.375	-0.25	-0.125	0.0	0.125	0.25	0.375	0.5	0.625
0.4375	0.7934	0.7322	0.6590	0.5842	0.5153	0.4465	0.4701†	0.4598†	0.3925†	0.3305†
0.5625	0.8041	0.7470	0.6764	0.6022	0.5273	0.4511	0.3845	0.3941†	0.3570†	0.3030†
0.6875	0.8105	0.7524	0.6785	0.6019	0.5201	0.4367	0.3645	0.3011	0.3018†	0.2618†
0.8125	0.8133	0.7495	0.6698	0.5817	0.4905	0.3993	0.3230	0.2590	0.2166	0.2097†
0.9375	0.8145	0.7410	0.6477	0.5413	0.4295	0.3318	0.2588	0.2016	0.1651	0.1396

†These measurements were affected by the presence of an oblique shock wave and were not used in the interpolations for the constant Mach number contours

Inner Wall Pressure Ratios:

Z	-1.0	-0.875	-0.75	-0.625	-0.5	-0.375	-0.25	-0.125	0.0
R	0.311	0.340	0.359	0.371	0.375	0.371	0.359	0.340	0.311
p/p_0	0.9390	0.9143	0.8815	0.8389	0.7836	0.7176	0.6398	0.5566	0.4737

Outer Wall Pressure Ratios:

Z	-0.6	-0.45	-0.3	-0.15	0.0	0.15	0.3	0.45
R	1.2	1.107	1.046	1.011	1.000	1.011	1.046	1.107
p/p_0	0.8826	0.7749	0.6582	0.5270	0.3859	0.2546	0.1530	0.1687[†]

[†]This measurement was affected by the presence of an oblique shock wave and was not used in the interpolations for the constant Mach number contours

INTERPOLATED CONSTANT MACH NUMBER CONTOURS FOR ANNULAR NOZZLE
WITH CENTERBODY CENTER OF CURVATURE ALONG Z = - 0.5 PLANE, FIG. IV.15

$\overline{p}_0$ = 408.2 kPa = 59.20 psia $\overline{T}_0$ = 288.9 K = 520.0°R γ = 1.4 (air)

$\overline{p}_{chamber}$ = 76.4 kPa = 11.08 psia $\overline{Re}_{2d}$ = 2.08×10^6 d = 16.90 mm = 0.665 in.

M = 0.6	Z	-0.5008	-0.4791	-0.4524	-0.4383	-0.4387	-0.4441	-0.4622
	R	0.3750	0.4375	0.5625	0.6875	0.8125	0.9375	1.1132
M = 0.8	Z	-0.2749	-0.2451	-0.2156	-0.2131	-0.2301	-0.2602	-0.2973
	R	0.3623	0.4375	0.5625	0.6875	0.8125	0.9375	1.0452
M = 1.0	Z	-0.0827	-0.0237	-0.0016	-0.0121	-0.0513	-0.1110	-0.1513
	R	0.3310	0.4375	0.5625	0.6875	0.8125	0.9375	1.0115
M = 1.2	Z	0.0944	0.1882	0.1955	0.1654	0.1056	0.0204	-0.0277
	R	0.2846	0.4375	0.5625	0.6875	0.8125	0.9375	1.0004